Supporting Information

BODIPYs α-appended with distyryl-linked aryl bisboronic acids: single-step cell staining and turn-on fluorescence binding with D-glucose

Adil Alkaş,[a] Josh M. Kofsky,[b] Em C. Sullivan,[a] Daisy Nebel,[b] Katherine N. Robertson,[c] Chantelle Capicciotti,[b] David L. Jakeman,[a,d] Erin R. Johnson,[a] and Alison Thompson[a*]

[a]Department of Chemistry, Dalhousie University, Halifax, Nova Scotia, B3H 4J3, Canada

[b]Department of Chemistry, Queen's University, Kingston, Ontario, K7L 3N6, Canada

[c]Department of Chemistry, Saint Mary's University, Halifax, Nova Scotia, B3H 3C3, Canada

[d]College of Pharmacy, Dalhousie University, Halifax, Nova Scotia, B3H 4R2, Canada

Table of Contents

Table of Figures

Table of Tables

Experimental Procedures

General Remarks

All starting materials and solvents were used as received from commercial sources unless otherwise noted. Anhydrous solvents were used only where indicated. Column chromatography was carried out on silica gel (grade 60, mesh size 230-400). TLC was performed on silica gel-covered aluminium sheets and visualized using UV light (254 and/or 365 nm). NMR spectra were recorded using 300 or 500 MHz spectrometers as indicated. All ^{1}H NMR chemical shifts are expressed in parts per million (ppm) using the solvent signal [$CDCl_3$ (^{1}H 7.26 ppm; ^{13}C 77.16 ppm); CD_2Cl_2 (^{1}H 5.32 ppm; ^{13}C 53.84 ppm); DMSO-d_6 (^{1}H 2.50 ppm; ^{13}C 39.52 ppm)] as the internal reference. ^{11}B chemical shifts are reported in ppm, externally referenced to boron trifluoride diethyl etherate (δ = 0.00 ppm). ^{19}F chemical shifts are reported in ppm, externally referenced to $CFCl_3$ (δ = 0.00 ppm). ^{1}H NMR splitting patterns are indicated as follows: s, singlet; d, doublet; t, triplet; q, quartet; m, multiplet. All coupling constants (*J*) are reported in Hertz (Hz). Mass spectra were recorded using ion trap (ESI or APCI) instruments. Microwave-promoted reactions were carried out using a Biotage Initiator 8 microwave with 0–100 W power at 2.45 GHz. Absorption and emission spectra were recorded in an appropriate solvent (DCM, DMSO or DMSO/phosphate buffer) using a Horiba Duetta spectrometer and a quartz cuvette.

2,6-Diethyl-4,4-difluoro-1,3,5,7-tetramethyl-8-H-4-bora-3a,4a-diaza-s-indacene (**4**) was synthesized according to a literature procedures.[1,2]

Table S1: Reaction conditions for the synthesis of **5.**

	1	Aldehyde	Piperidine	Acetic acid	MS 3Å	Solvent	Temp.	Time	Yield
a	0.1 mmol	3.3 eq.	30 eq.	21 eq.	-	MeCN	100 °C	10 min.	-
b	0.1 mmol	3.3 eq.	30 eq.	-	-	MeCN	100 °C	10 min.	-
c	0.1 mmol	3.3 eq.	30 eq.	21 eq.	-	DMF	150 °C	10 min.	-
d	0.1 mmol	3.3 eq.	30 eq	-	-	DMF	150 °C	10 min.	-
e	0.1 mmol	3.3 eq.	30 eq.	48 eq.	-	MeCN	100 °C	10 min.	-
f	0.1 mmol	3.3 eq.	30 eq.	21 eq.	-	MeCN	100 °C	1 h	22%
g	0.1 mmol	3.3 eq.	30 eq.	21 eq.	-	MeCN	100 °C	1+1+1 h	-
h	0.3 mmol	4 eq.	30 eq.	24 eq.	-	MeCN	100 °C	1 h	33%
i	0.3 mmol	4 eq.	30 eq.	24 eq.	1 g	MeCN	100 °C	1 h	17%

1,3-Di((E)-4-bromostyryl)-2,6-diethyl-4,4-difluoro-5,7-dimethyl-8-H-4-bora-3a,4a-diaza-s-indacene (5)

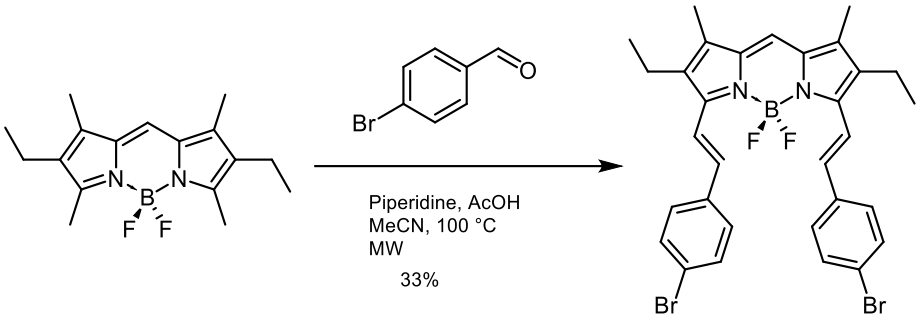

Compound **4** (100 mg, 0.33 mmol) and 4-bromobenzaldehyde (243 mg, 1.31 mmol) were dissolved in anhydrous MeCN (10 mL) in a 20 mL microwave vial. After addition of piperidine (900 µL, 9.11 mmol) and acetic acid (450 µL, 7.87 mmol), the vial was sealed using a manual cap crimper and placed in the microwave reactor. The reaction mixture was irradiated at 75 W power until the temperature reached 100 °C (0.5-1 minute). The reaction mixture was kept under microwave irradiation to maintain this temperature for 1 hour. The reaction mixture was then allowed to cool to 50 °C (2-3 minutes) in the air-cooled microwave reactor. The reaction mixture was diluted with ethyl acetate (30 mL) and washed with water (30 mL) and brine (30 mL). The organic phase was dried over magnesium sulfate and dried under vacuum. The mixture was then purified over silica using gradient hexane:EtOAc (v:v; 9:1) as eluent to give **5** as a brown solid (69 mg, 33%). **^{1}H NMR** (500 MHz; CD_2Cl_2) δ: 7.68 (d, *J* = 16.8 Hz, 2H), 7.61-7.53 (m, 8H), 7.33 (d, *J* = 16.8 Hz, 2H), 7.14 (s, 1H), 2.76 (q, *J* = 7.6 Hz, 4H), 2.29 (s, 6H), 1.28 (t, *J* = 7.6 Hz, 6H) ppm; **^{13}C NMR** (125 MHz; CD_2Cl_2) δ: 150.6, 138.2, 136.2, 135.1, 134.5, 133.8, 131.9, 128.6, 122.6, 120.2, 117,4, 18.5, 13.7, 8.9 ppm; **^{11}B NMR** (160 MHz; CD_2Cl_2) δ: 1.3 (t, *J* = 35 Hz) ppm; **^{19}F NMR** (470 MHz; CD_2Cl_2) δ: -139.2 (dd, *J* = 69, 34 Hz) ppm. HRMS: $(M+Na)^+$; 659.0660 found, 659.0650 calculated for $C_{31}H_{29}B^{79}Br_2F_2N_2Na$.

2,6-Diethyl-4,4-difluoro-5,7-dimethyl-1,3-di((E)-4-styrylboronic acid pinacol ester)-8-H-4-bora-3a,4a-diaza-s-indacene (6)

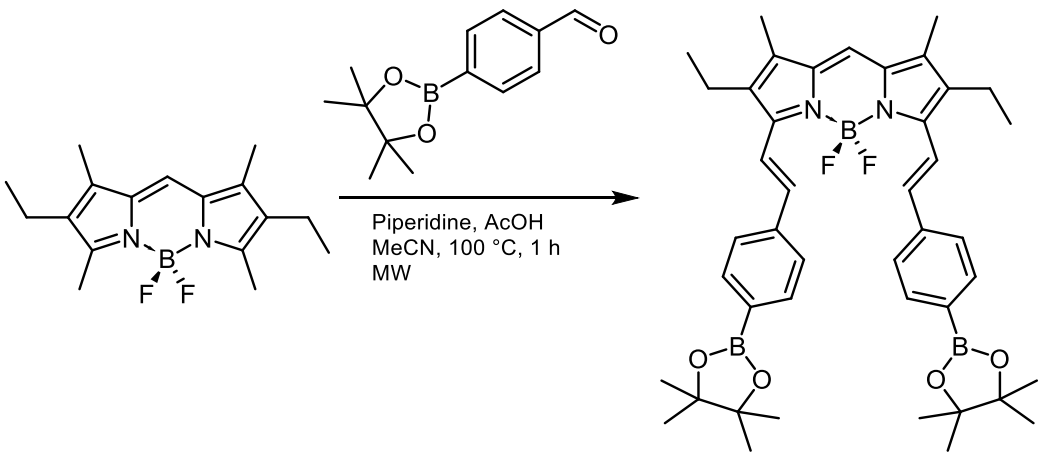

***Microwave heating method*:** Compound **4** (100 mg, 0.33 mmol) and 4-formylphenylboronic acid pinacol ester (304 mg, 1.31 mmol) were dissolved in anhydrous MeCN (10 mL) in a 20 mL microwave vial. After addition of piperidine (900 µL, 9.11 mmol) and acetic acid (450 µL, 7.87 mmol), the vial was sealed using a manual cap crimper and placed in the microwave reactor. The reaction mixture was irradiated at 75 W power until the temperature reached 100 °C (0.5-1 minute). The reaction mixture was kept under microwave irradiation to maintain this temperature for 1 hour. The reaction mixture was then allowed to cool to 50 °C (2-3 minutes) in the air-cooled microwave reactor. The reaction mixture was diluted with ethyl acetate (30 mL) and washed with water (30 mL) and brine (30 mL). The organic phase was dried over magnesium sulfate, concentrated, and dried under vacuum. The crude material was purified over silica using gradient hexane:EtOAc (v:v; 95:5→80:20) as eluent. The semi-pure product was washed with pentane to give **6** as a blue solid (46 mg, 19%).

***Conventional heating method*:** Compound **4** (500 mg, 1.64 mmol) and 4-formylphenylboronic acid pinacol ester (1.153 g, 4.96 mmol) were dissolved in anhydrous MeCN (36 mL) in a thick-walled 75 mL glass pressure vessel. After addition of piperidine (4.5 mL, 45.55 mmol) and acetic acid (2.3 mL, 40.22 mmol), the reaction mixture was heated at 100 °C for 1 hour. The reaction mixture was allowed to cool to room temperature, then diluted with ethyl acetate (70 mL) and washed with water (70 mL) and brine (70 mL). The organic phase was dried over sodium sulfate, concentrated, and dried under vacuum. The crude material was then purified over silica using gradient hexane:acetone (v:v; 95:5→90:10) as eluent. The semi-pure product was washed with pentane to give **6** as a blue solid (401 mg, 33%). **^{1}H NMR** (500 MHz; $CDCl_3$) δ: 7.83 (d, *J* = 8.0 Hz, 4H), 7.76 (d, *J* = 16.7 Hz, 2H), 7.61 (d, *J* = 8.0 Hz, 4H), 7.33 (d, *J* = 16.8 Hz, 2H), 6.98 (s, 1H), 2.71 (q, *J* = 7.5 Hz, 4H), 2.22 (s, 6H), 1.37 (s, 24H), 1.24 (t, *J* = 7.5 Hz, 6H) ppm; **^{13}C NMR** (125 MHz; $CDCl_3$) δ: 151.0, 139.9, 137.2, 135.9, 135.2, 135.1, 133.3, 129.3, 126.6, 120.7, 116.9, 83.8, 24.9, 18.7, 13.9, 9.2 ppm; **^{11}B NMR** (160 MHz; $CDCl_3$) δ: 31.5, 1.4 (t, *J* = 34 Hz) ppm; **^{19}F NMR** (471 MHz; $CDCl_3$) δ: -139.4 (dd, *J* = 68, 33 Hz) ppm. HRMS: $(M+Na)^+$; 755.4174 found, 755.4144 calculated for $C_{43}H_{53}B_3F_2N_2NaO_4$.

1,3-Di((E)-4-diethanolemine-styrylboronate)-2,6-diethyl-4,4-difluoro-5,7-dimethyl-8-H-4-bora-3a,4a-diaza-s-indacene (8)

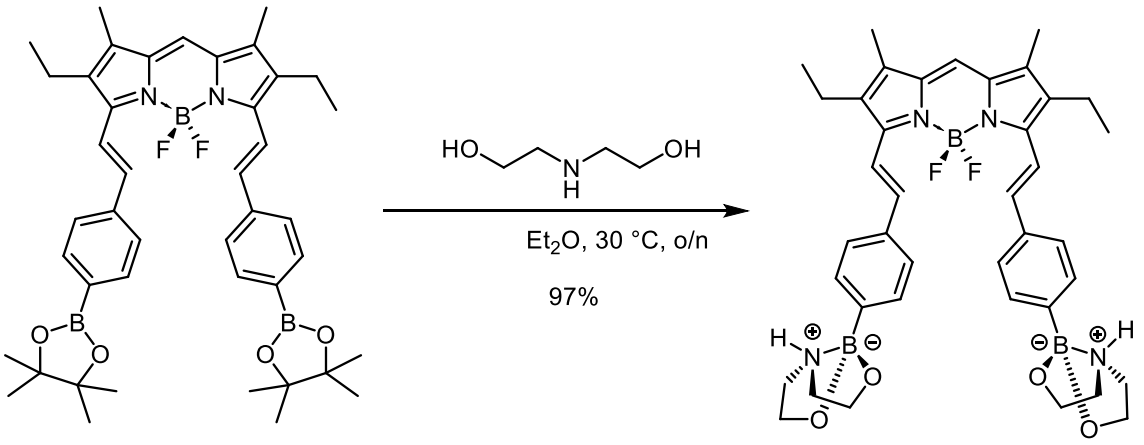

Compound **6** (227 mg, 0.39 mmol) and diethanolamine (422 mg, 4.00 mmol) were combined in diethyl ether (60 mL). The mixture was stirred at 30 °C overnight. The precipitate was then isolated via filtration, washed with ether, and dried under vacuum to afford the desired product as a dark blue solid (211 mg, 97%). **^{1}H NMR** (500 MHz; DMSO-d_6) δ: 7.58 (m, 1H), 7.56-7.50 (m, 6H), 7.46 (d, *J* = 7.9 Hz, 4H), 7.36 (d, *J* = 16.9 Hz, 2H), 6.90-6.87 (m, 2H), 3.94-3.89 (m, 4H), 3.85-3.81 (m, 4H), 3.17-3.10 (m, 4H), 2.91-2.86 (m, 4H), 2.72 (q, *J* = 7.4 Hz, 4H), 2.29 (s, 6H), 1.20 (t, *J* = 7.5 Hz, 6H) ppm. **^{13}C NMR** (125 MHz; DMSO-d_6) δ: 150.1, 138.1, 136.7, 134.9, 134.4, 133.3, 132.4, 125.5, 118.4, 117.7, 63.0, 50.7, 18.0, 13.7, 8.9 ppm (one signal missing); **^{11}B NMR** (160 MHz; DMSO-d_6) δ: 10.8, 1.2 (t, *J* = 36 Hz) ppm; **^{19}F NMR** (470 MHz; DMSO-d_6) δ: -137.3 (dd, *J* = 69, 31 Hz) ppm; HRMS: $(M+H)^+$; 707.3917 found, 707.3914 calculated for $C_{39}H_{48}B_3F_2N_4O_4$.

2,6-Diethyl-4,4-difluoro-5,7-dimethyl-1,3-di((E)-4-styrylboronic acid)-8-H-4-bora-3a,4a-diaza-s-indacene (2)

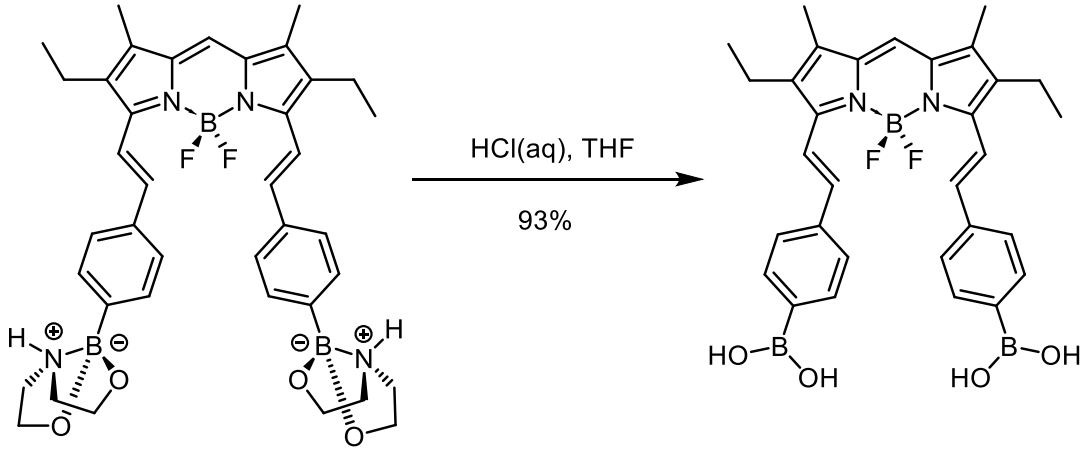

To a suspension of compound **8** (211 mg, 0.30 mmol) in THF (50 mL) was added aqueous HCl (0.1 M, 50 mL). The mixture was stirred at room temperature for 1 hour. After removal of THF under reduced pressure, the precipitate was then isolated via filtration, washed with water, and dried under vacuum to afford the desired product as a brown solid (152 mg, 93%). **^{1}H NMR** (500 MHz; DMSO-d_6) δ: 8.09 (s, 4H), 7.87 (d, *J* = 7.7 Hz 4H), 7.66 (s, 1H), 7.60-7.56 (m, 6H), 7.39 (d, J = 16.8 Hz, 2H), 2.72 (q, *J* = 7.5 Hz, 4H), 2.29 (s, 6H), 1.19 (t, *J* = 7.5 Hz, 6H) ppm. **^{13}C NMR** (125 MHz; DMSO-d_6) δ: 150.5, 139.0, 138.6, 136.4, 135.2, 135.1, 133.4, 126.5, 119.8, 18.4, 14.2, 9.4 ppm (two signals missing); **^{11}B NMR** (160 MHz; DMSO-d_6) δ: 1.3 (t, *J* = 37 Hz) ppm; **^{19}F NMR** (470 MHz; DMSO-d_6) δ: -137.0 (dd, *J* = 68, 31 Hz) ppm; HRMS: $(M)^-$; 567.2635 found, 567.2614 calculated for $C_{31}H_{32}B_3F_2N_2O_4$.

2,6-Diethyl-4,4-difluoro-5,7-dimethyl-1,3-di((E)-3-styrylboronic acid pinacol ester)-8-H-4-bora-3a,4a-diaza-s-indacene (7)

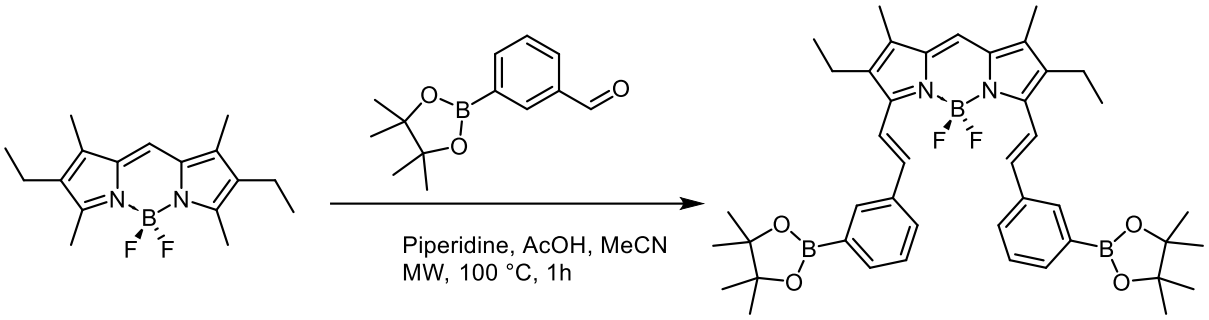

***Microwave heating method*:** Compound **4** (91 mg, 0.3 mmol) and 3-formylphenylboronic acid pinacol ester (210 mg, 0.9 mmol) were dissolved in anhydrous MeCN (9 mL) in a 20 mL microwave vial. After addition of piperidine (900 µL, 9.11 mmol) and acetic acid (450 µL, 7.87 mmol), the vial was sealed using a manual cap crimper and placed in the microwave reactor. The reaction mixture was irradiated at 75 W power until the temperature reached 100 °C (0.5-1 minute). The reaction mixture was kept under microwave irradiation to maintain this temperature for 1 hour. The reaction mixture was then allowed to cool to 50 °C (2-3 minutes) in the air-cooled microwave reactor. The reaction mixture was diluted with ethyl acetate (30 mL) and washed with water (30 mL) and brine (30 mL). The organic phase was dried over magnesium sulfate, concentrated, and dried under vacuum. The crude material was then purified over silica using gradient hexane:acetone (v:v; 95:5→85:15) as eluent. The semi-pure product was washed with pentane to give **7** as a blue solid (62 mg, 28%).

***Conventional heating method*:** Compound **4** (500 mg, 1.64 mmol) and 3-formylphenylboronic acid pinacol ester (1.153 g, 4.96 mmol) were dissolved in anhydrous MeCN (36 mL) in a thick-walled 75 mL glass pressure vessel. After addition of piperidine (4.5 mL, 45.55 mmol) and acetic acid (2.3 mL, 40.22 mmol), the reaction mixture was heated at 100 °C for 1 hour. The reaction mixture was allowed to cool to room temperature, then diluted with ethyl acetate (70 mL) and washed with water (70 mL) and brine (70 mL). The organic phase was dried over magnesium sulfate, concentrated, and dried under vacuum. The crude material was then purified over silica using gradient hexane:acetone (v:v; 95:5→85:15) as eluent. The semi-pure product was washed with pentane to give **7** as a blue solid (548 mg, 45%). **^{1}H NMR** (500 MHz; $CDCl_3$) δ: 7.90 (d, *J* = 8.0 Hz, 2H), 7.87 (s, 2H), 7.78-7.73 (m, 4H), 7.43 (t, *J* = 7.6 Hz, 2H), 7.34 (d, *J* = 16.8 Hz, 2H), 6.97 (s, 1H), 2.71 (q, *J* = 7.6 Hz, 4H), 2.22 (s, 6H), 1.38 (s, 24H), 1.25 (t, *J* = 7.5 Hz, 6H) ppm; **^{13}C NMR** (125 MHz; $CDCl_3$) δ: 151.2, 137.1, 136.7, 136.0, 135.2, 135.1, 134.9, 133.0, 128.7, 128.2, 120.0, 116.7, 83.9, 24.9, 18.7, 14.0, 9.2 ppm (one signal missing); **^{11}B NMR** (160 MHz; $CDCl_3$) δ: 31.3, 1.35 (t, *J* = 34 Hz) ppm; **^{19}F NMR** (471 MHz; $CDCl_3$) δ: -139.4 (dd, *J* = 68, 34 Hz) ppm. HRMS: $(M+Na)^+$; 755.4164 found, 755.4145 calculated for $C_{43}H_{53}B_3F_2N_2NaO_4$.

1,3-Di((E)-3-diethanolemine-styrylboronate)-2,6-diethyl-4,4-difluoro-5,7-dimethyl-8-H-4-bora-3a,4a-diaza-s-indacene (9)

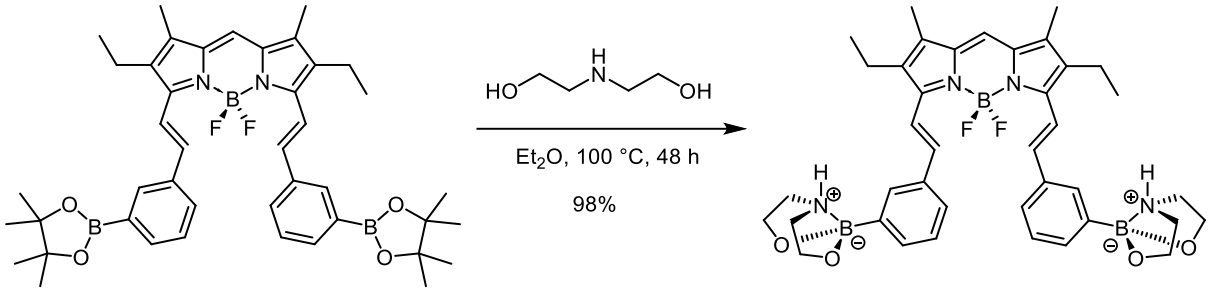

Compound **7** (225 mg,0.32 mmol) and diethanolamine (443 mg, 4.21 mmol) were combined in diethyl ether (60 mL) in a 100 mL glass pressure vessel. The mixture was stirred at 100 °C for 2 days. The precipitate was then filtered, washed with ether (100 mL), and dried under vacuum to afford the desired product as a dark blue solid (212 mg, 98%). **^{1}H NMR** (500 MHz; DMSO-d_6) δ: 7.68 (s, 2H), 7.60 (s, 1H), 7.55 (d, *J* = 16.8 Hz, 2H), 7.47-7.45 (m, 4H), 7.38 (d, *J* = 16.8 Hz, 2H), 7.29 (t, *J* = 7.4 Hz, 2H), 7.01-6.98 (m, 2H), 3.96-3.91 (m, 4H), 3.86-3.82 (m, 4H), 3.17-3.11 (m, 4H) 2.93-2.88 (m, 4H), 2.73 (q, *J* = 7.5 Hz, 4H), 2.29 (s, 6H), 1.21 (t, *J* = 7.5 Hz, 6H) ppm; **^{13}C NMR** (125 MHz; DMSO-d_6) δ: 150.6, 138.6, 137.6, 135.5, 134.8, 134.4, 132.9, 132.6, 127.8, 125.2, 119.0, 118.4, 63.5, 51.2, 18.5, 14.2, 9.4 ppm (one signal missing); **^{11}B NMR** (160 MHz; DMSO-d_6) δ: 10.1, 0.7 (t, *J* = 36 Hz) ppm; **^{19}F NMR** (470 MHz; DMSO-d_6) δ: -137.6 (dd, *J* = 70, 30 Hz) ppm; HRMS: $(M+H)^+$; 707.3922 found, 707.3917 calculated for $C_{39}H_{48}B_3F_2N_4O_4$.

2,6-Diethyl-4,4-difluoro-5,7-dimethyl-1,3-di((E)-3-styrylboronic acid)-8-H-4-bora-3a,4a-diaza-s-indacene (3)

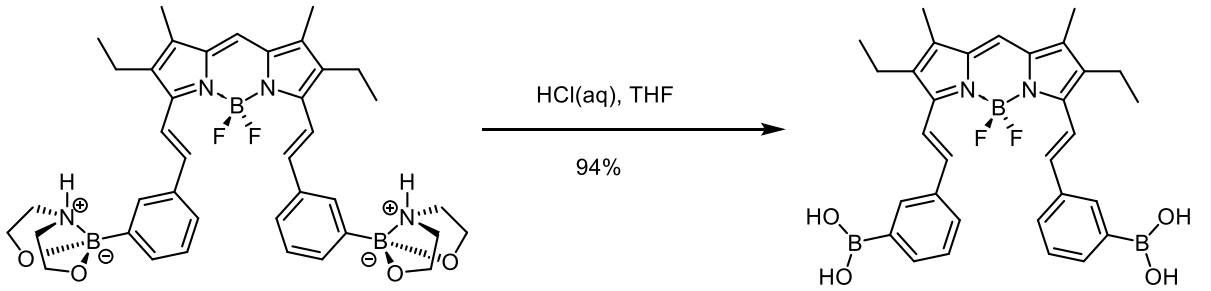

To a suspension of compound **9** (206 mg, 0.29 mmol) in THF (50 mL) was added aqueous HCl (0.1 M, 50 mL). The mixture was stirred at room temperature for 1 hour. After removal of THF under reduced pressure, the precipitate was then isolated via filtration, washed with water, and dried under vacuum to afford the desired product as a brown solid (157 mg, 94%). **^{1}H NMR** (500 MHz; DMSO-d_6) δ: 8.18 (s, 4H), 8.02 (s, 2H), 7.79 (d, *J* = 7.3 Hz, 2H), 7.67 (d, *J* = 7.7 Hz, 2H), 7.64 (s, 1H), 7.54 (d, *J* = 16.8 Hz, 2H), 7.44 (t, *J* = 7.5 Hz, 2H), 7.38 (d, *J* = 16.8 Hz, 2H), 2.72 (q, *J* = 7.4 Hz, 4H), 2.29 (s, 6H), 1.20 (t, *J* = 7.5 Hz, 6H) ppm; **^{13}C NMR** (125 MHz; DMSO-d_6) δ: 150.2, 138.5,136.4, 135.6, 134.9, 134.5, 133.4, 132.7, 128.3, 128.1, 119.1, 118.5, 18.0, 13.8, 8.9 ppm (one signal missing); **^{11}B NMR** (160 MHz; DMSO-d_6) δ: 1.2 (t, *J* = 36 Hz) ppm;

^{19}F NMR (470 MHz; DMSO-d_6) δ: -137.0 (dd, *J* = 69, 31 Hz) ppm. HRMS: $(M+Na)^+$; 591.2607 found, 591.2580 calculated for $C_{31}H_{33}B_3F_2N_2NaO_4$.

Photophysical Characterization

Photophysical properties of synthesized compounds were determined in dichloromethane (**4**, **5**, **6** and **7**) and DMSO (**2**, **3**, **8**, and **9**) solutions at room temperature. Molar absorptivity values were recorded at the peak maximum in the visible area for each compound. Fluorescence spectra were determined by exciting at the wavelength where the absorption maximum was observed for each compound. Relative fluorescence quantum yields were obtained by comparing the area under the emission spectrum of the compound of interest to that of the standard, rhodamine B (ϕ = 0.70 in ethanol).[3] Relative quantum yields were determined using equation:[4] $\Phi_{unk} = (\Phi_{std})(\eta/\eta_{std})^2(I_{unk}/I_{std})(A_{std}/A_{unk})$ where Φ_{std} is the reported quantum yield of the standard, I is the area of the integrated emission spectra, A is the absorbance at the excitation wavelength and η is the refractive index of the solvent used. The subscripts "unk" and "std" denote the unknown and standard, respectively.

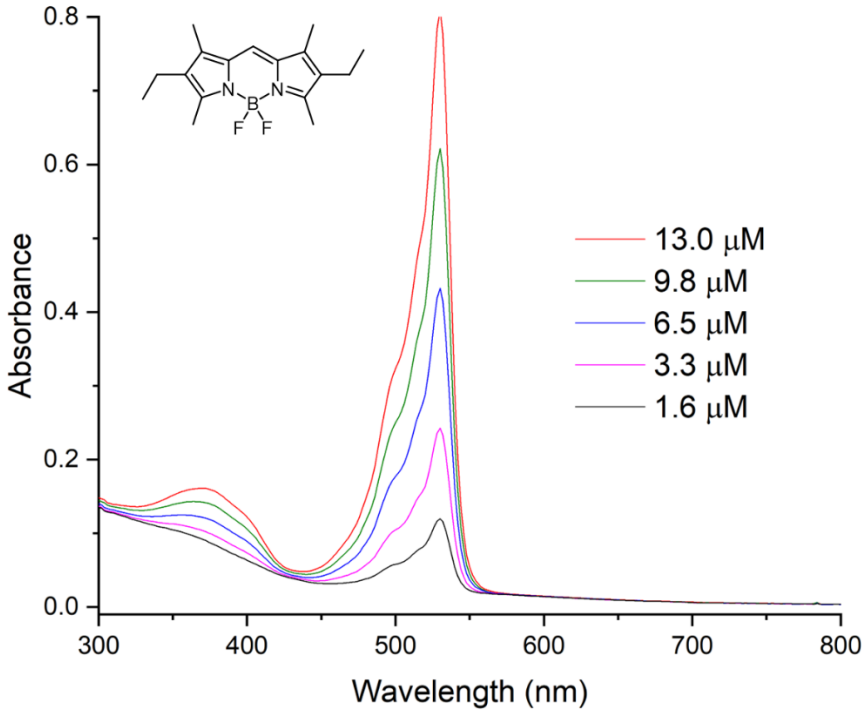

Figure S1: Absorption spectra of compound of **4** in dichloromethane at varying concentrations.

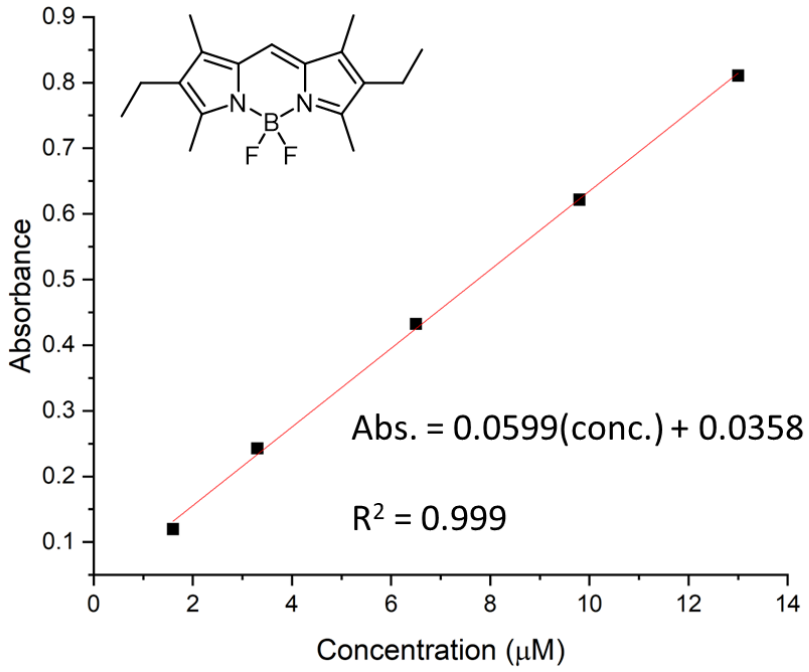

Figure S2: Calibration curve for determination of molar extinction coefficient of compound **4** in dichloromethane.

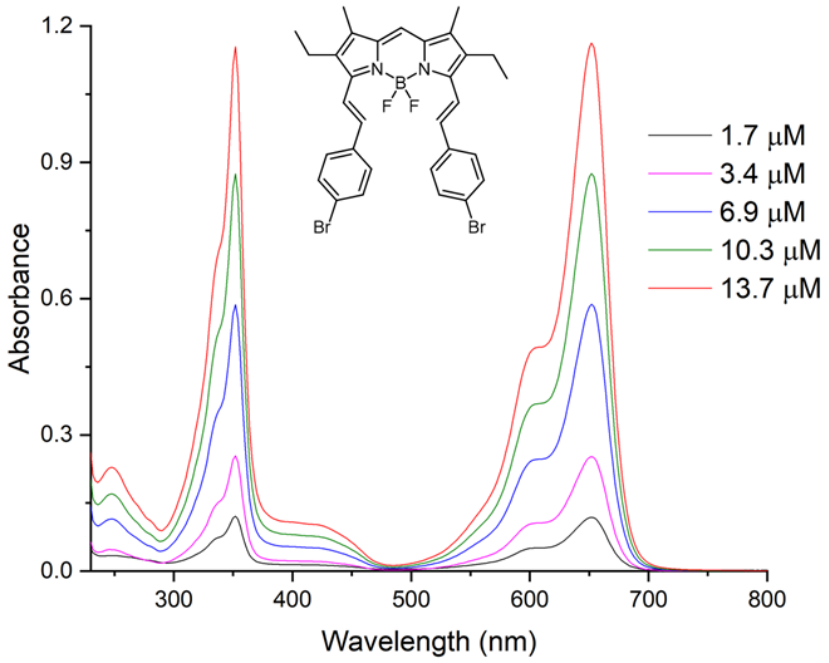

Figure S3: Absorption spectra of compound of **5** in dichloromethane at varying concentrations.

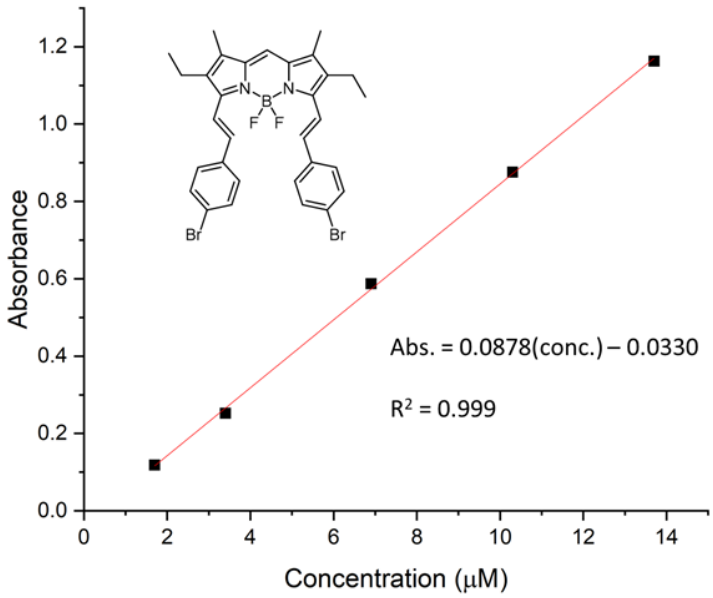

Figure S4: Calibration curve for determination of molar extinction coefficient of compound **5** in dichloromethane.

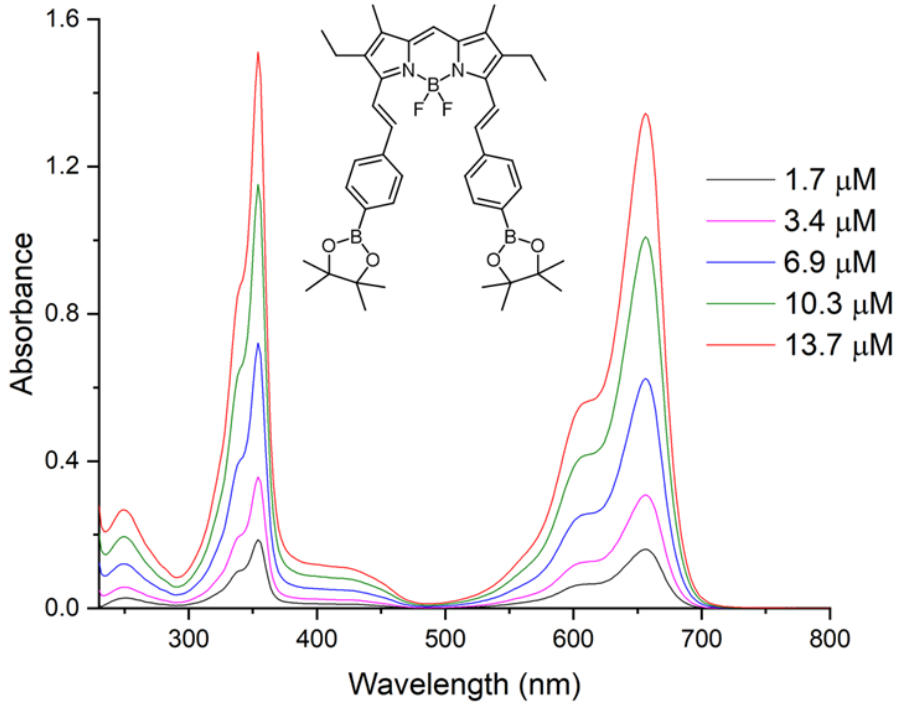

Figure S5: Absorption spectra of compound **6** in dichloromethane at varying concentrations.

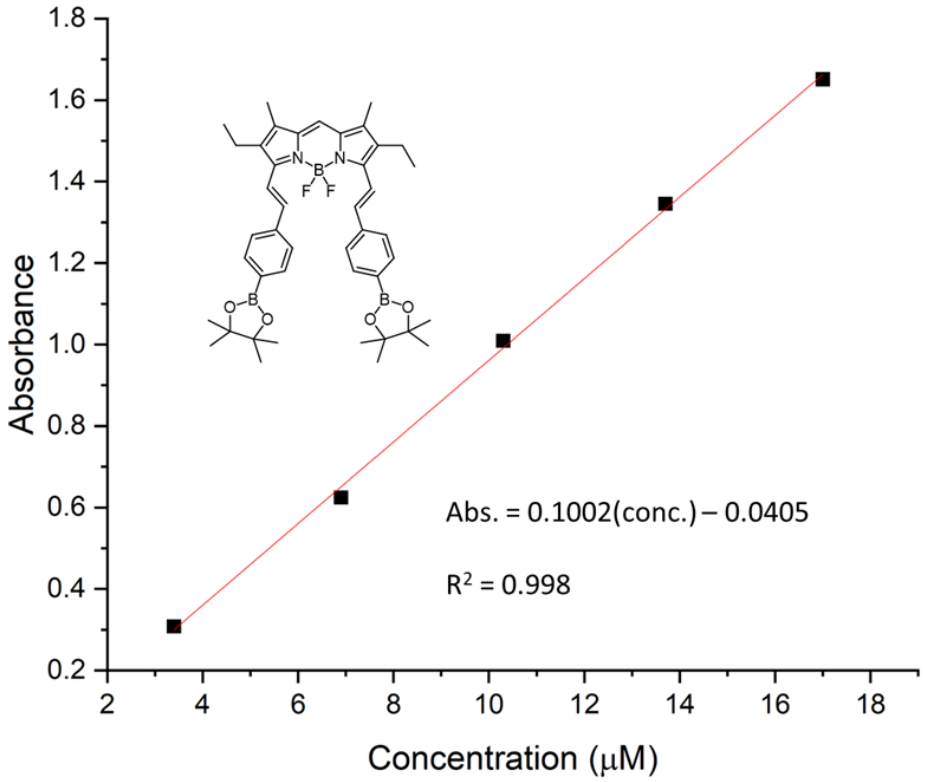

Figure S6: Calibration curve for determination of molar extinction coefficient of compound **6** in dichloromethane.

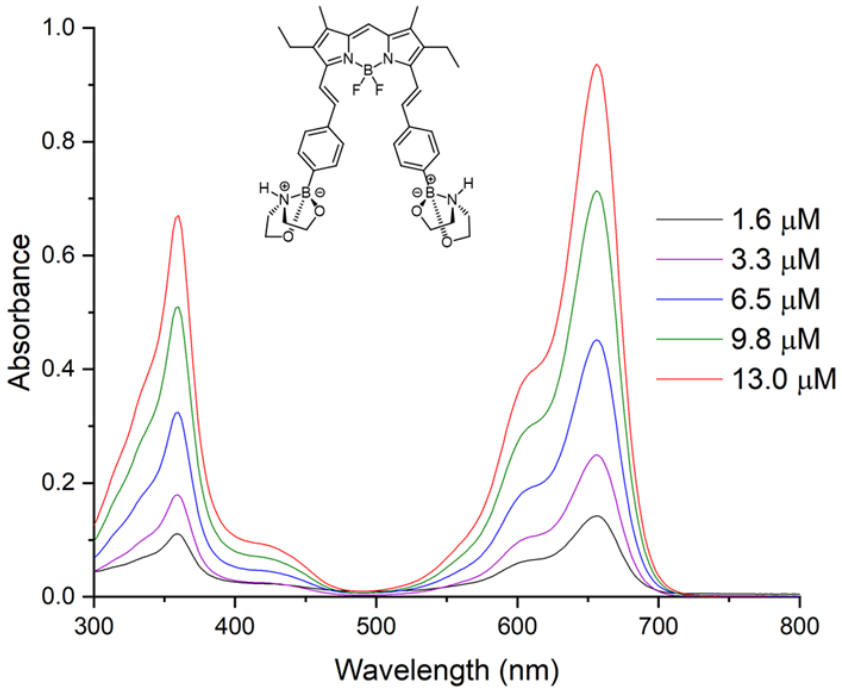

Figure S7: Absorption spectra of compound **8** in DMSO at varying concentrations.

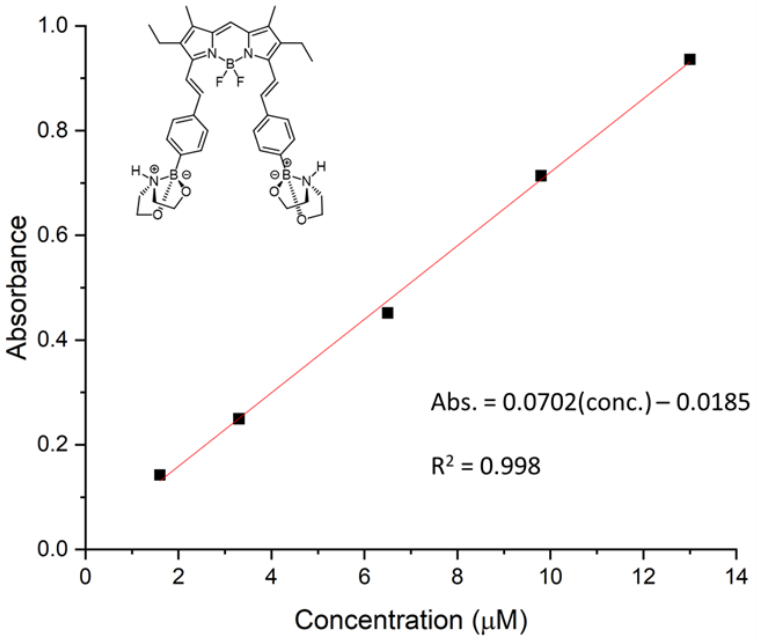

Figure S8: Calibration curve for determination of molar extinction coefficient of compound **8** in DMSO.

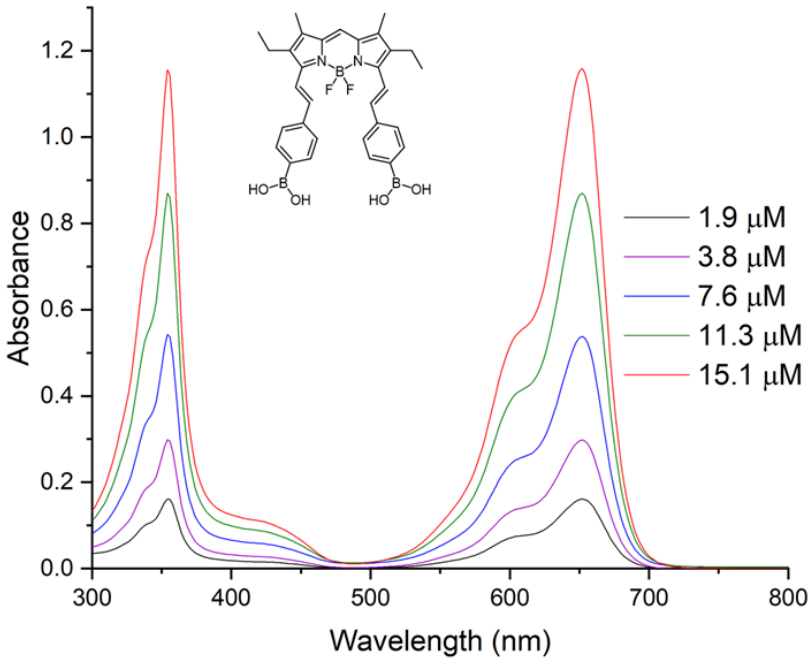

Figure S9: Absorption spectra of compound **2** in DMSO at varying concentrations.

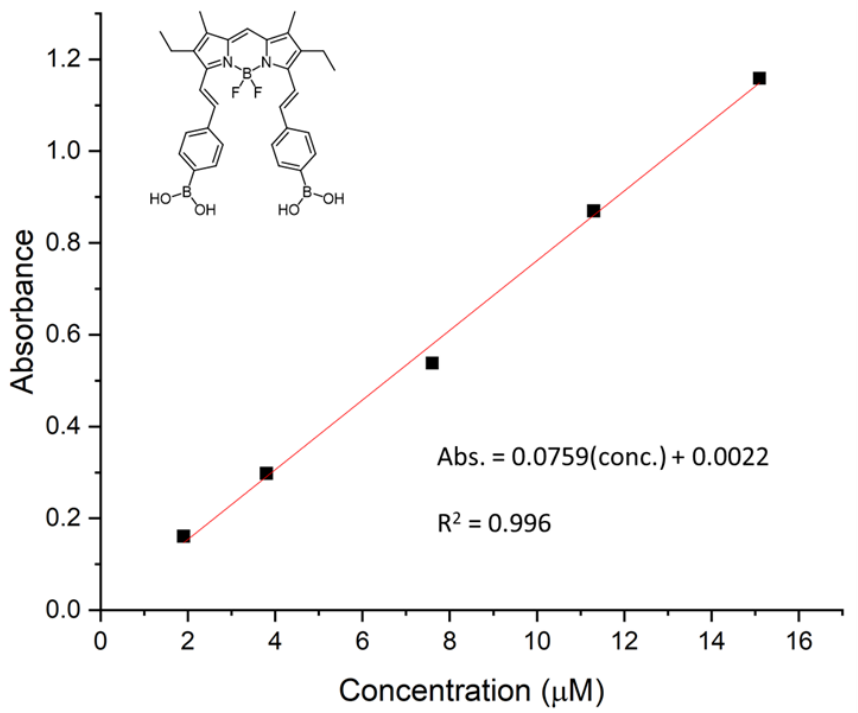

Figure S10: Calibration curve for determination of molar extinction coefficient of compound **2** in DMSO.

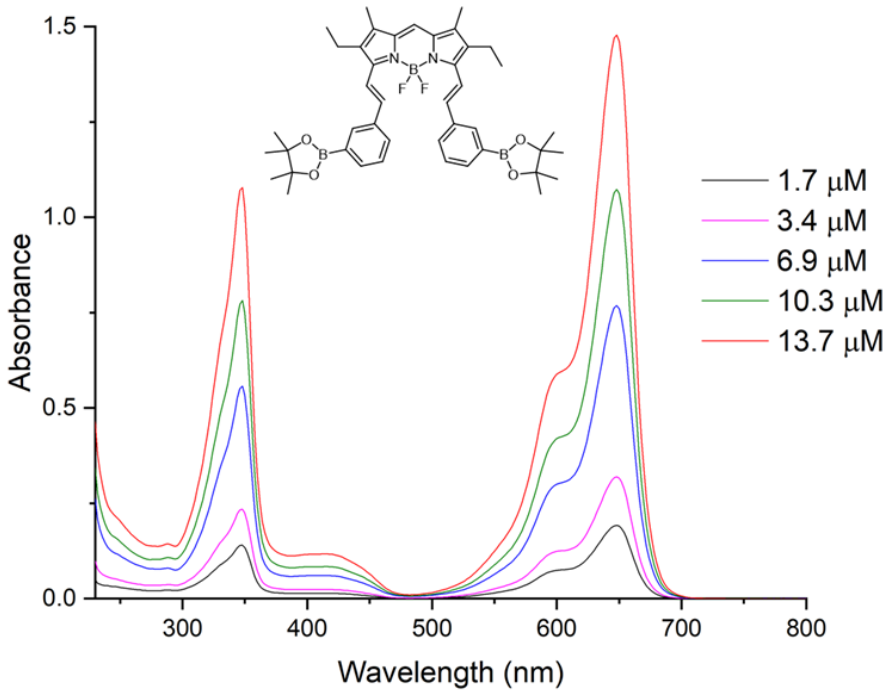

Figure S11: Absorption spectra of compound **7** in dichloromethane at varying concentrations.

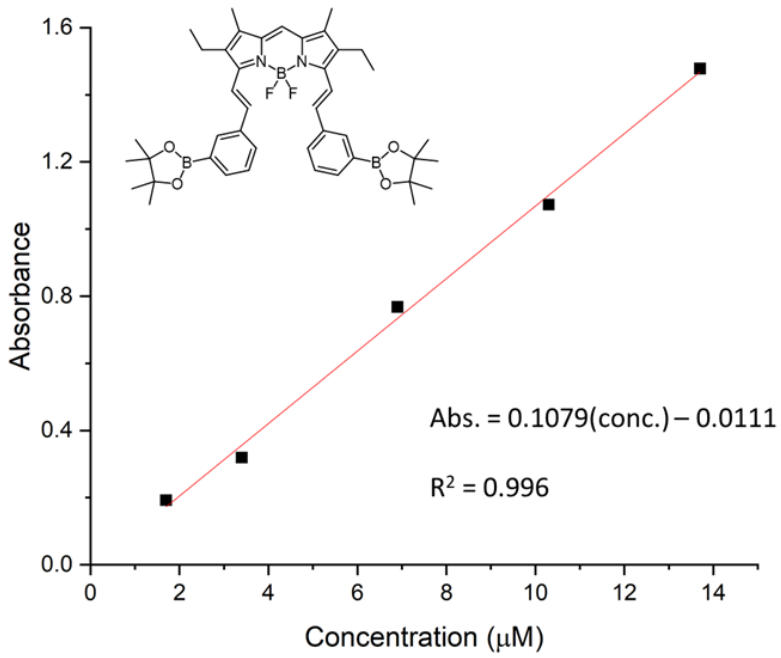

Figure S12: Calibration curve for determination of molar extinction coefficient of compound **7** in dichloromethane.

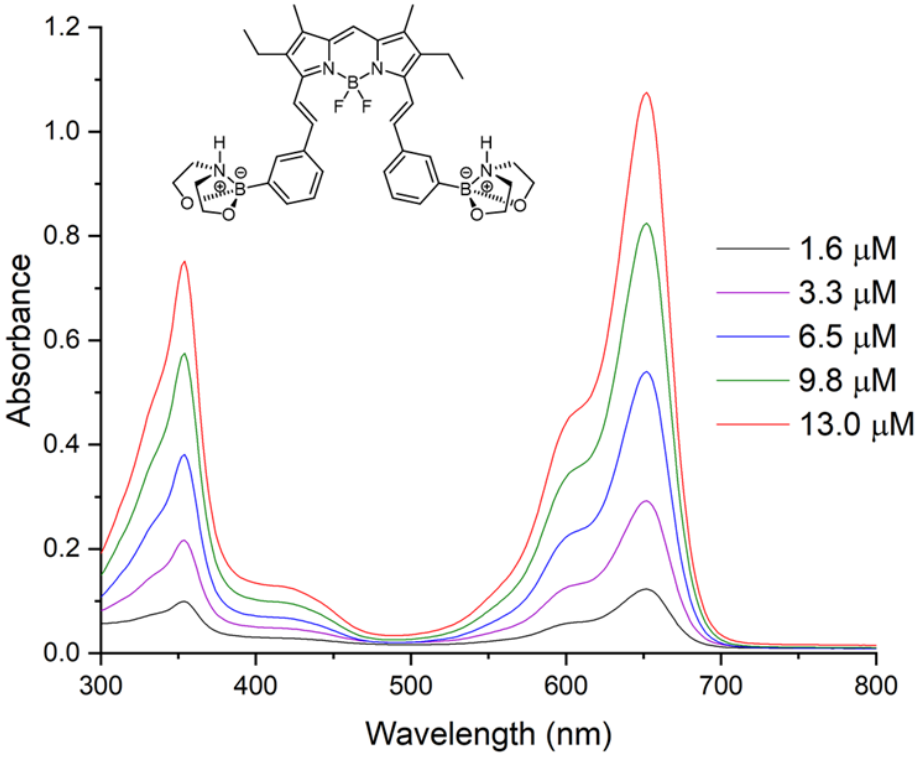

Figure S13: Absorption spectra of compound **9** in DMSO at varying concentrations.

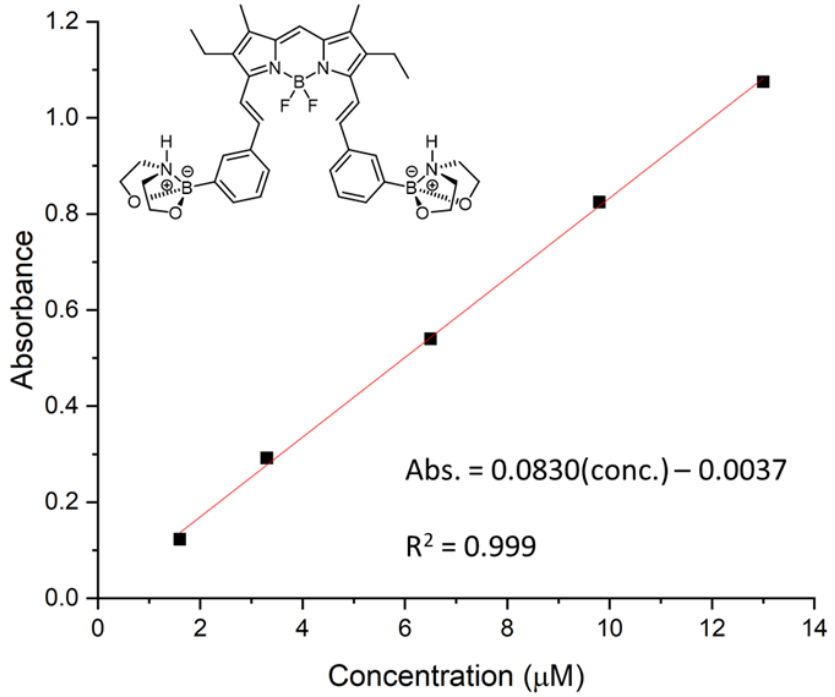

Figure S14: Calibration curve for determination of molar extinction coefficient of compound **9** in DMSO.

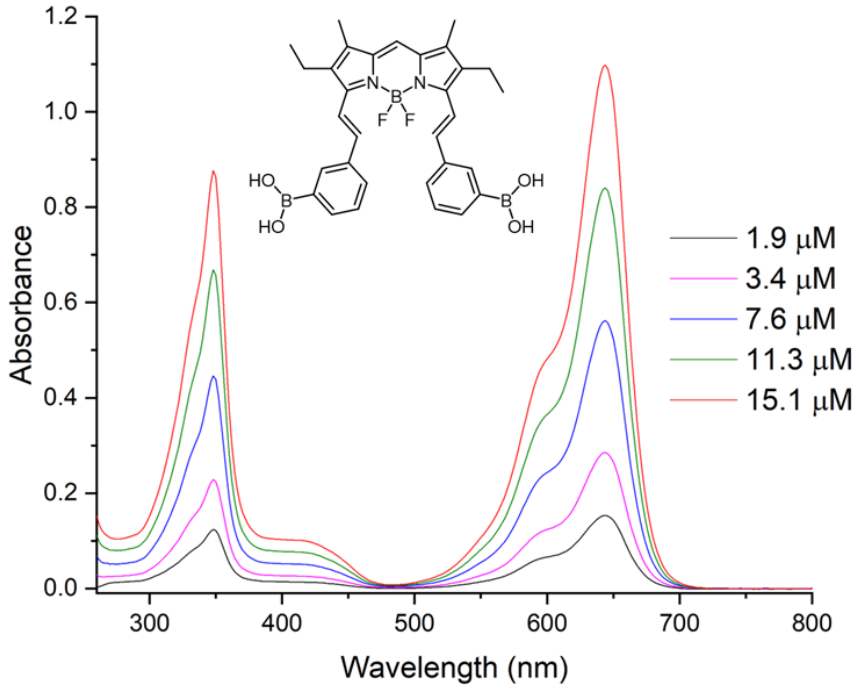

Figure S15: Absorption spectra of compound **3** in DMSO at varying concentrations.

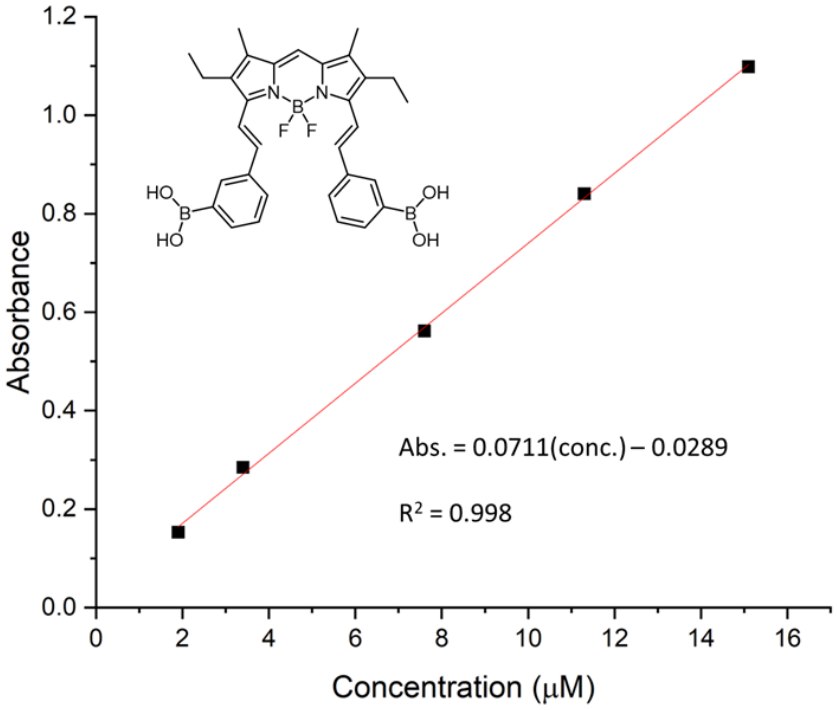

Figure S16: Calibration curve for determination of molar extinction coefficient of compound **3** in DMSO.

DFT Calculations

Methods

Geometry optimizations were performed using the range-separated LC-ωPBE density functional[5] with the XDM dispersion correction[6–8] and a mixed basis set consisting of 6-31G* for H, B, C and 6-31+G* for N, O, and F. The overlays were generated by minimizing the root-mean-square deviation in position of the nonhydrogen atoms of the glucose and adjacent phenyl moieties. To evaluate binding energies, single-point energy calculations were performed on the optimized geometries using LC-ωPBE-XDM/6-311+G(2d,2p) with the PCM[9] model of aqueous solvent. Binding energies are reported relative to the electronic energy difference for the following reaction involving the Drueckhammer reference compound:

1 + glucose + 2 OH^- -> **complex-1** + 4 H_2O

Optimised structures

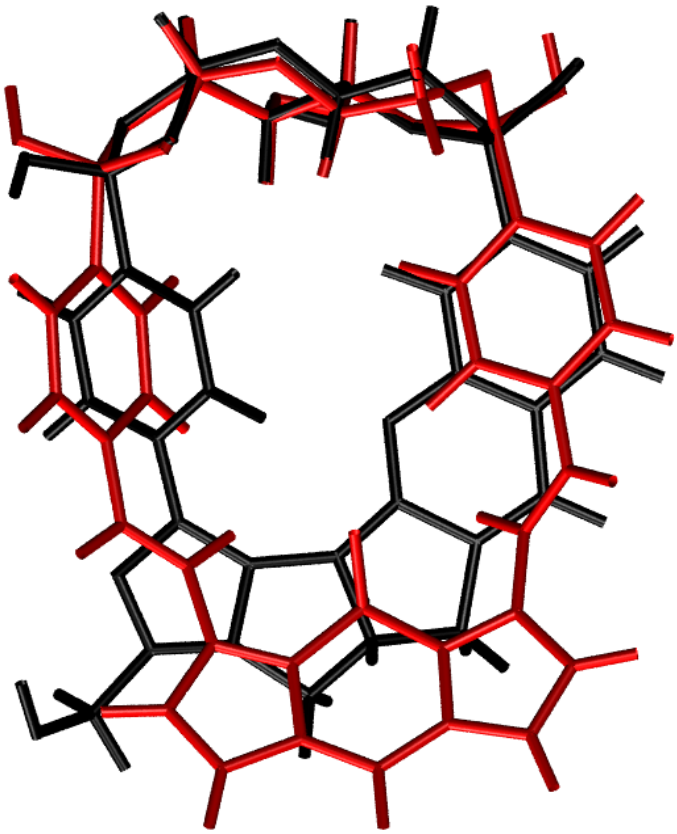

Figure S17: Optimised and overlayed structures of complex-**2'** (red) and with the Drueckhammer reference complex-**1** (black).

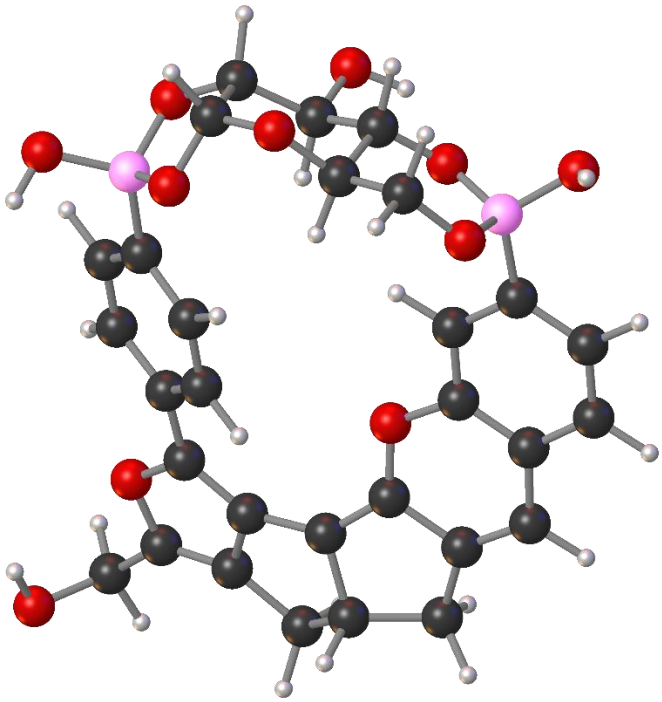

Figure S18: Optimised structure of the Drueckhammer reference complex-**1**.

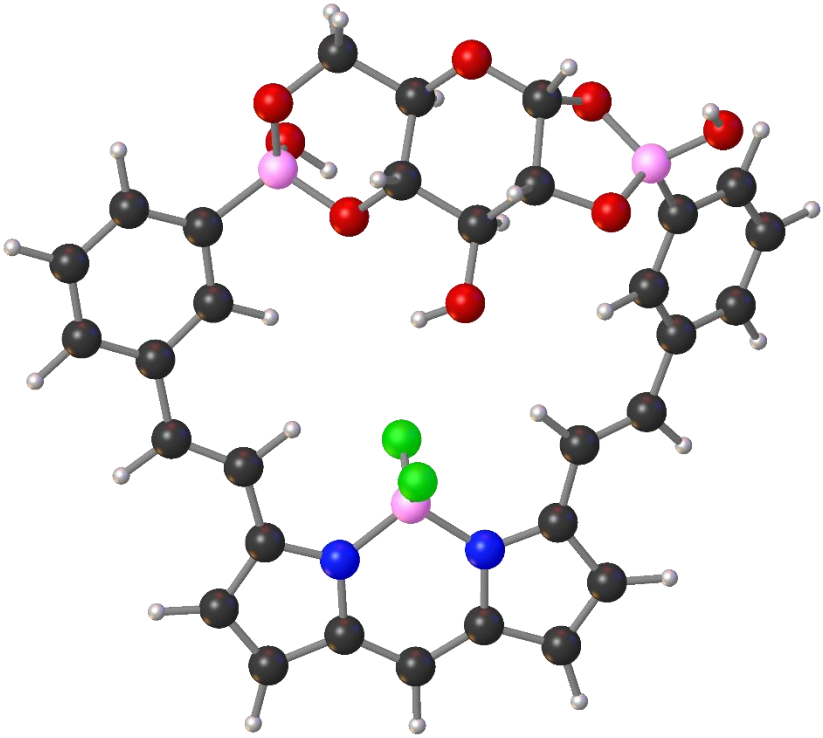

Figure S19: Optimised structure of complex-**P46b**.

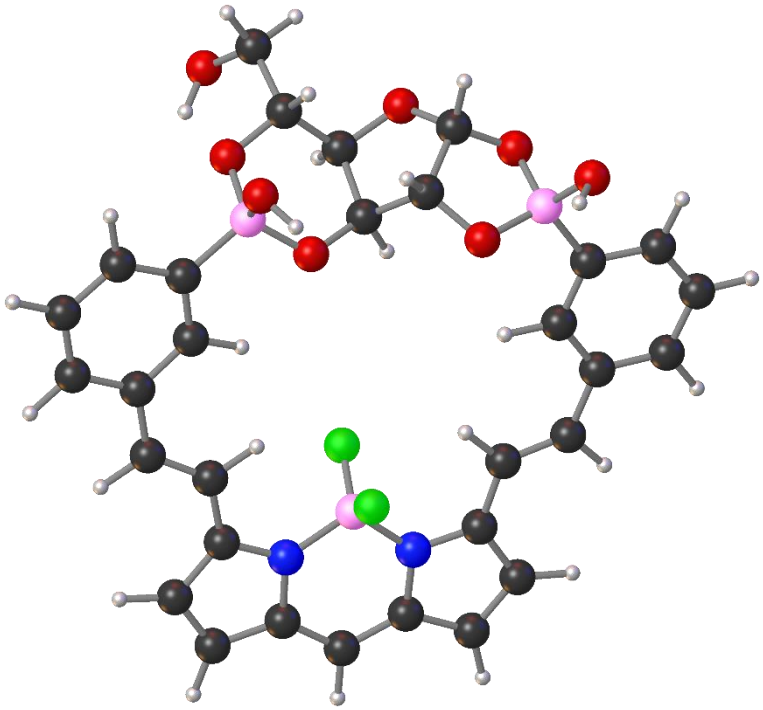

Figure S20: Optimised structure of complex-**F35a**.

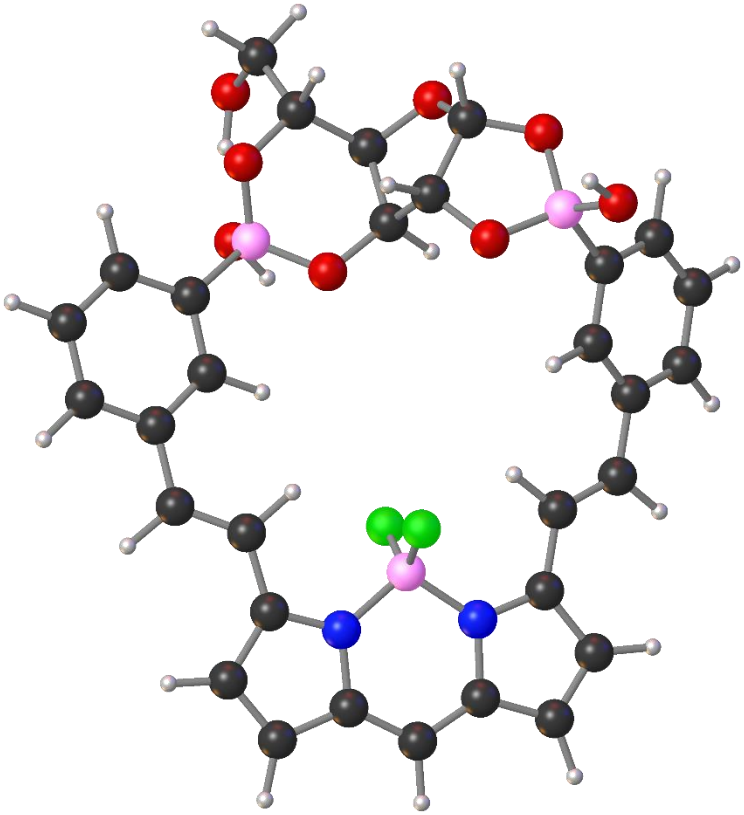

Figure S21: Optimised structure of complex-**F35b**.

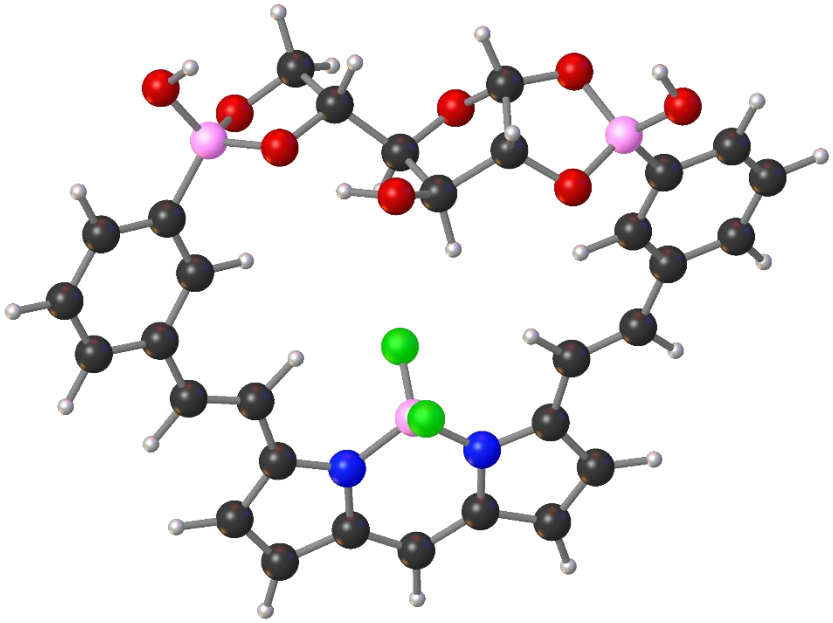

Figure S22: Optimised structure of complex-**F56a**.

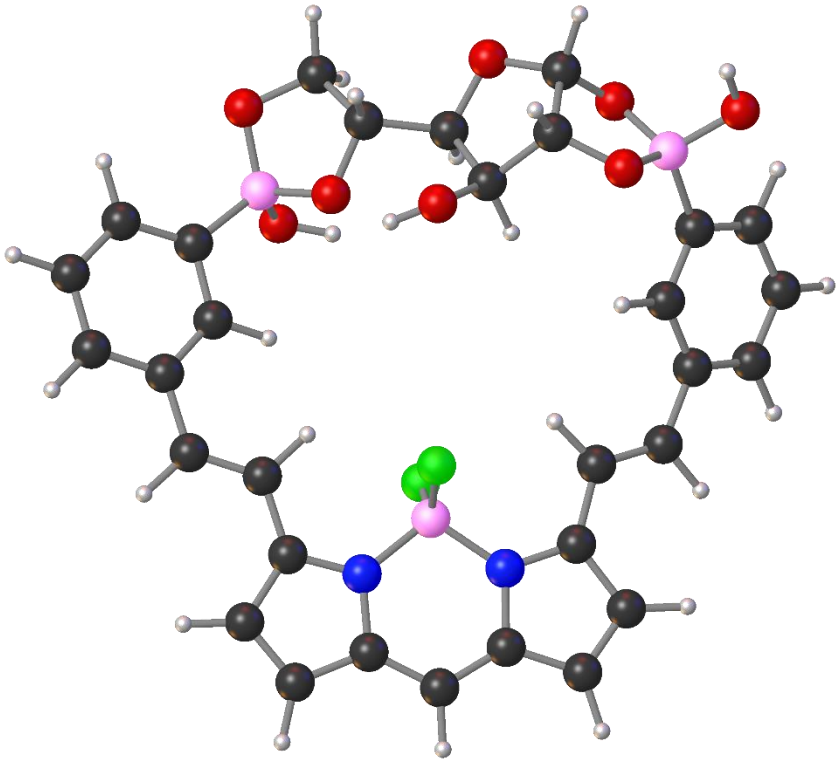

Figure S23: Optimised structure of complex-**F56b**.

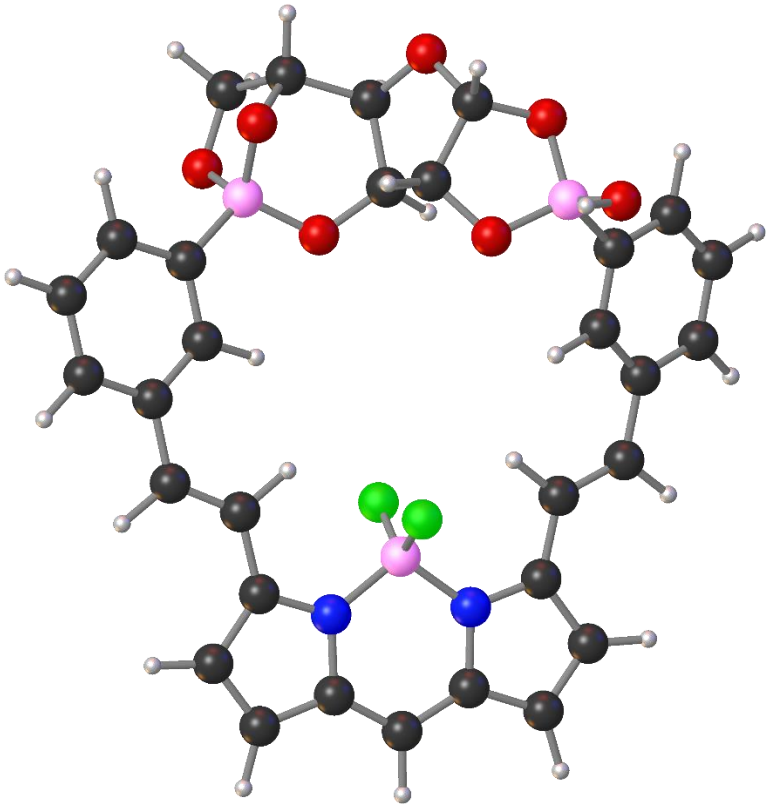

Figure S24: Optimised structure of complex-**F356b**.

Glucose Binding Studies

Studies on stability of buffer solutions of 2 and 3

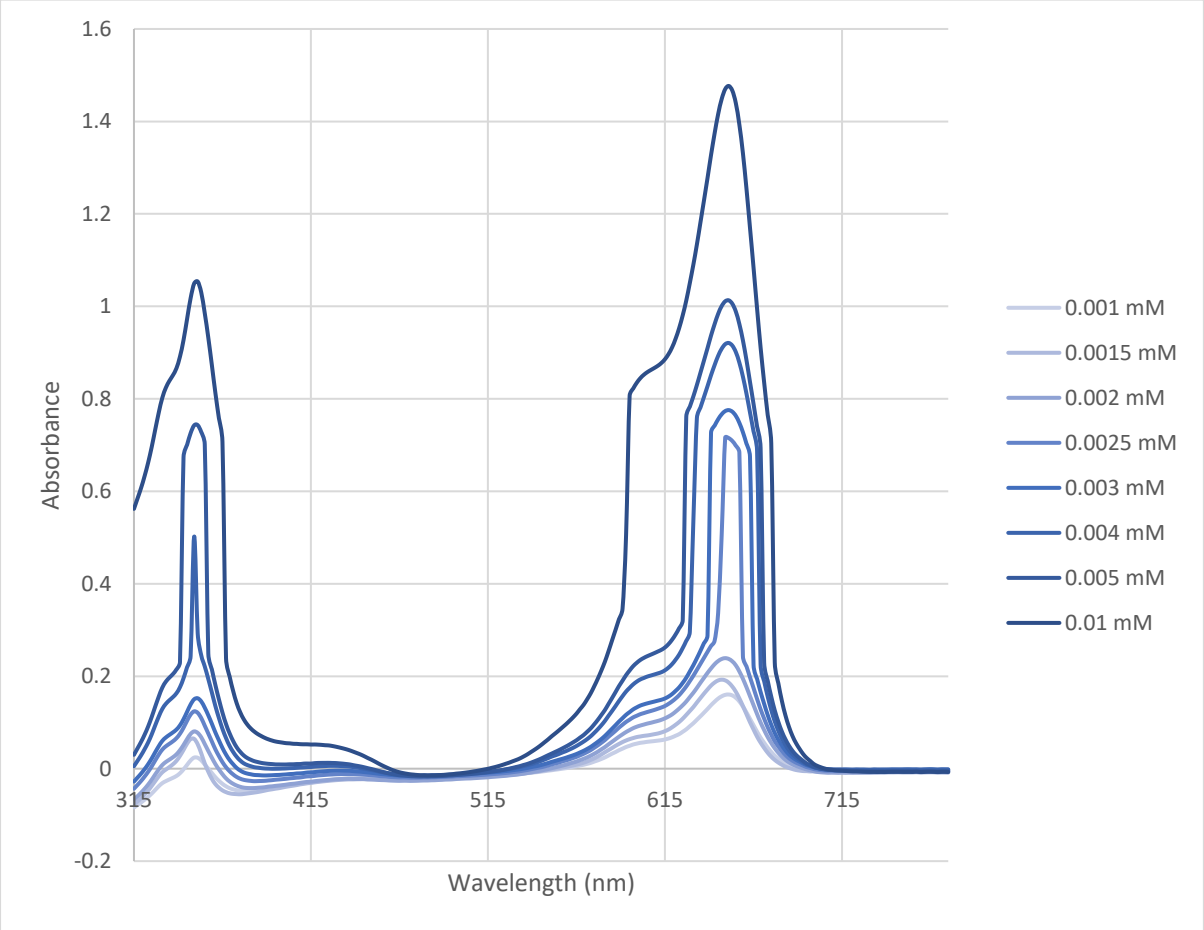

Figure S25: Absorption spectra of **2** at varying concentrations in 80% MeOH/phosphate buffer (0.012 M) at pH 7.5.

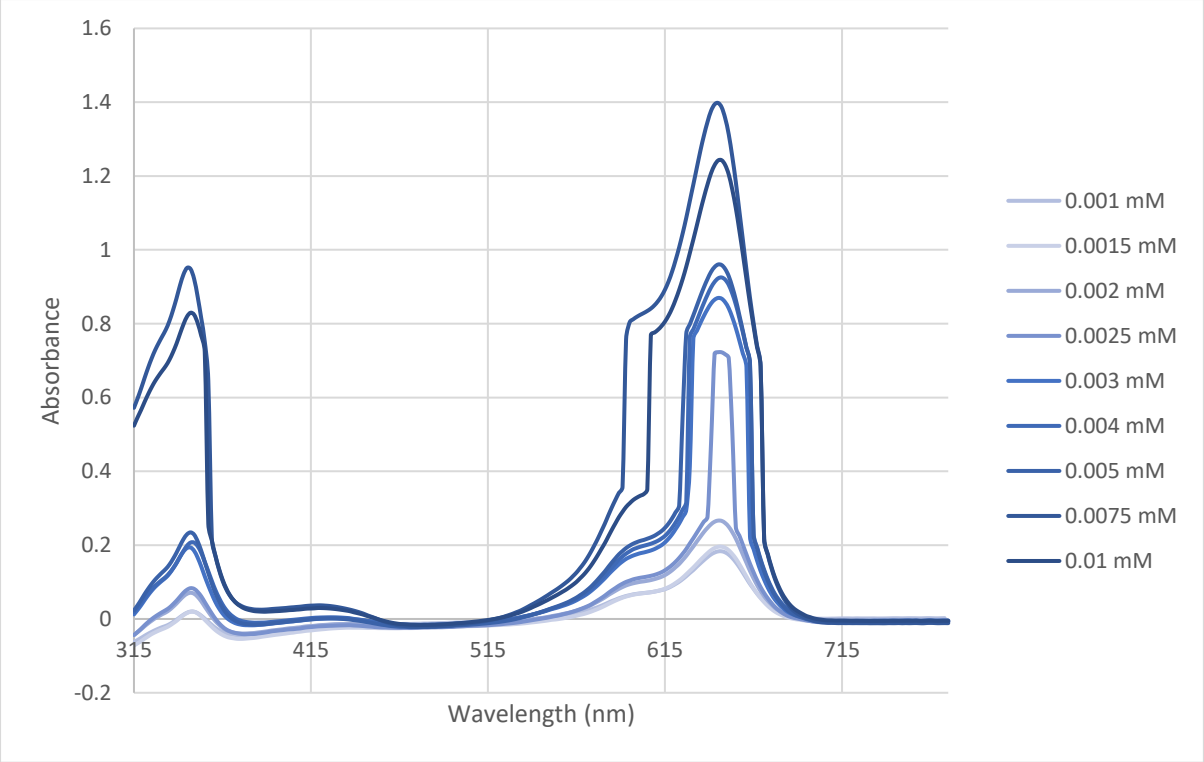

Figure S26: Absorption spectra of **3** at varying concentrations in 80% MeOH/phosphate buffer (0.012 M) at pH 7.5.

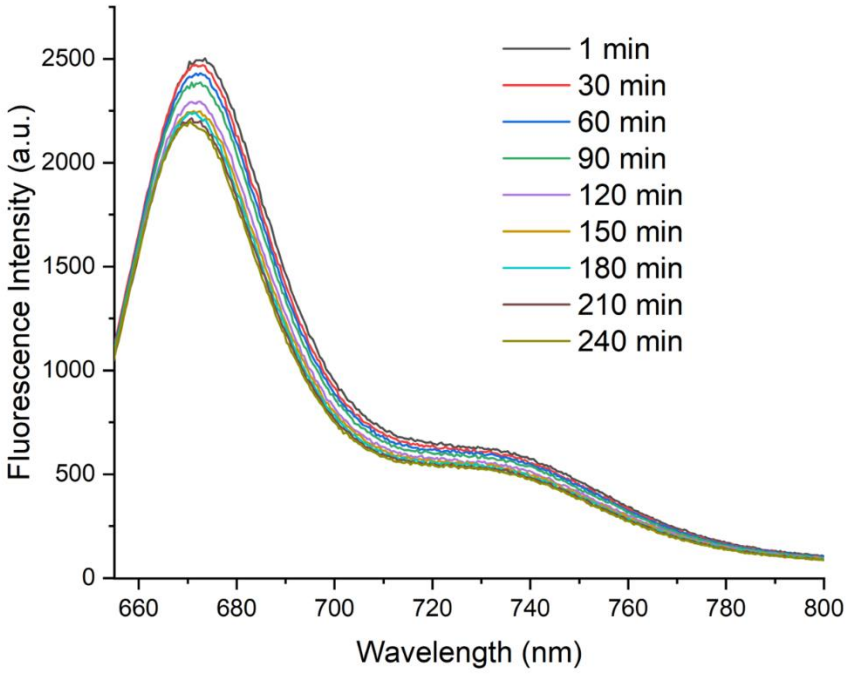

Figure S27: Fluorescence spectra of compound **2** (3.3 µM) measured over a period of 4 hours in 35% DMSO/phosphate buffer (0.012 M) at pH 10 when excited at 650 nm.

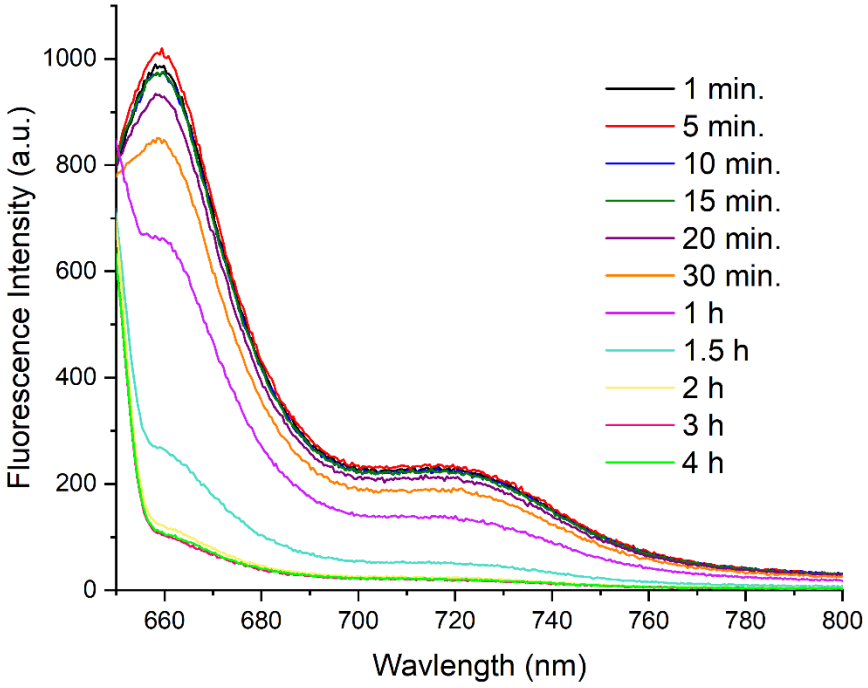

Figure S28: Fluorescence spectra of compound **3** (6.7 µM) measured over a period of 4 hours in 20% DMSO/phosphate buffer (0.012 M) at pH 7.5 when excited at 645 nm.

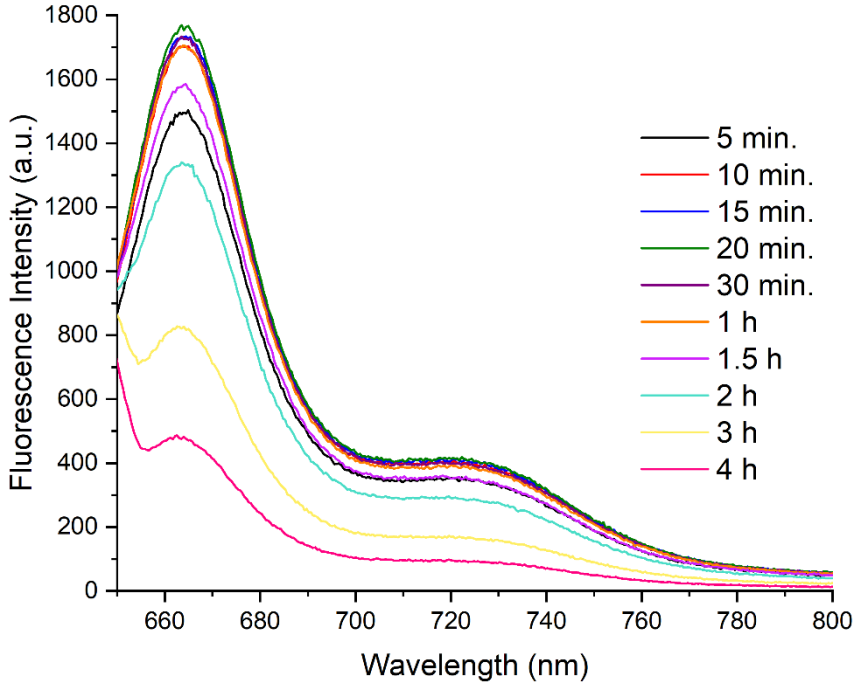

Figure S29: Fluorescence spectra of compound **3** (6.7 µM) with D-glucose (3.3 mM) measured over a period of 4 hours in 20% DMSO/phosphate buffer (0.012 M) at pH 7.5 when excited at 645 nm.

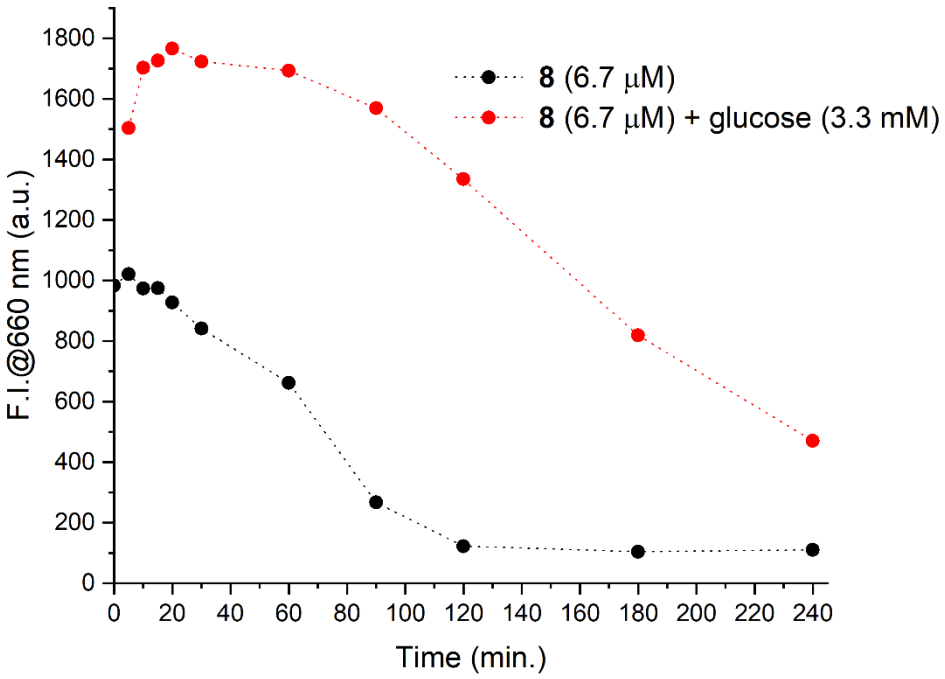

Figure S30: The change in the fluorescence intensities at 660 nm for compound **3** with and without D-glucose over a period of 4 hours in 20% DMSO/phosphate buffer (0.012 M) at pH 7.5.

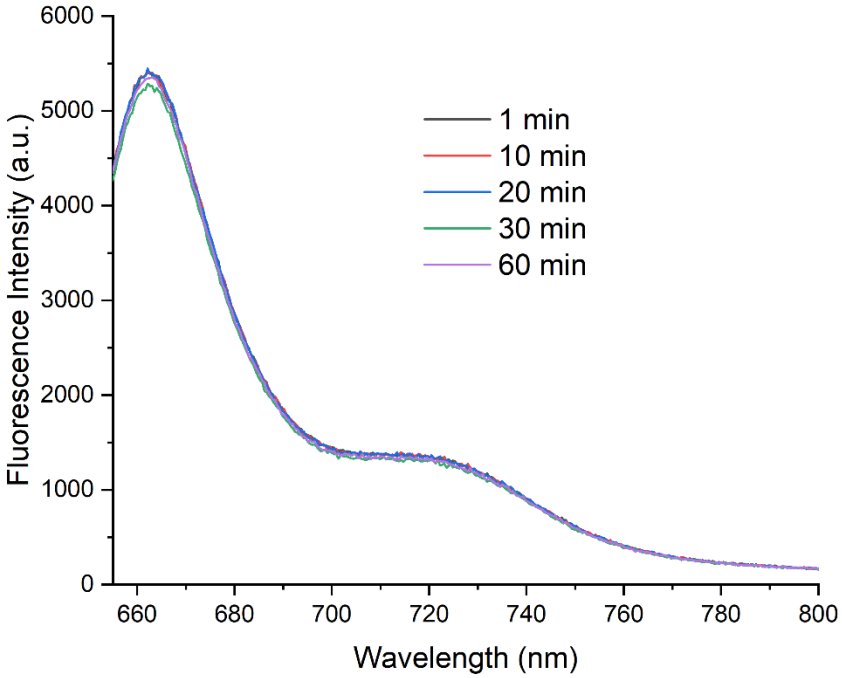

Figure S31: Fluorescence spectra of compound **3** (6.7 μM) measured over a period of 60 minutes in 35% DMSO/phosphate buffer (0.012 M) at pH 7.5 when excited at 645 nm.

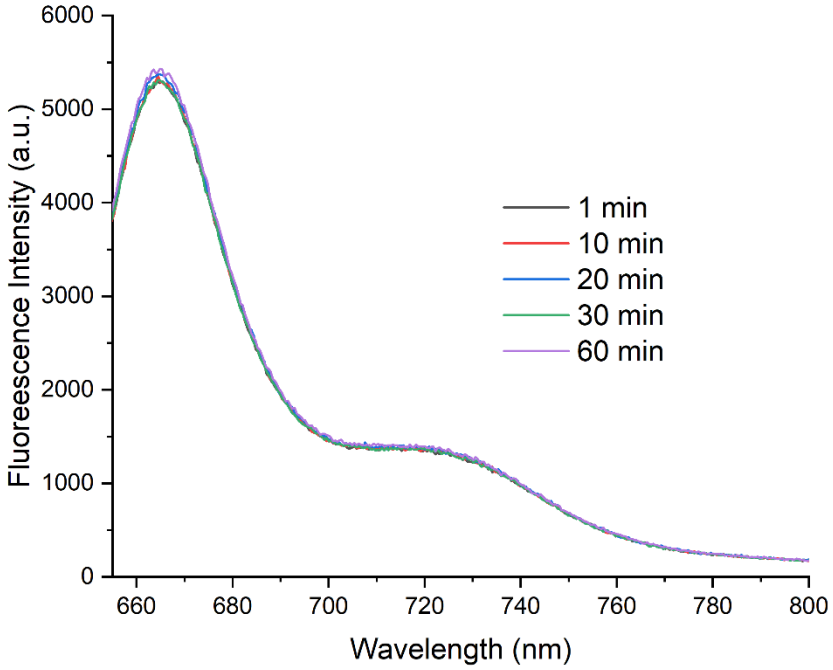

Figure S32: Fluorescence spectra of compound **3** (6.7 µM) with D-glucose (3.3 mM) measured over a period of 60 minutes in 35% DMSO/phosphate buffer (0.012 M) at pH 7.5 when excited at 645 nm.

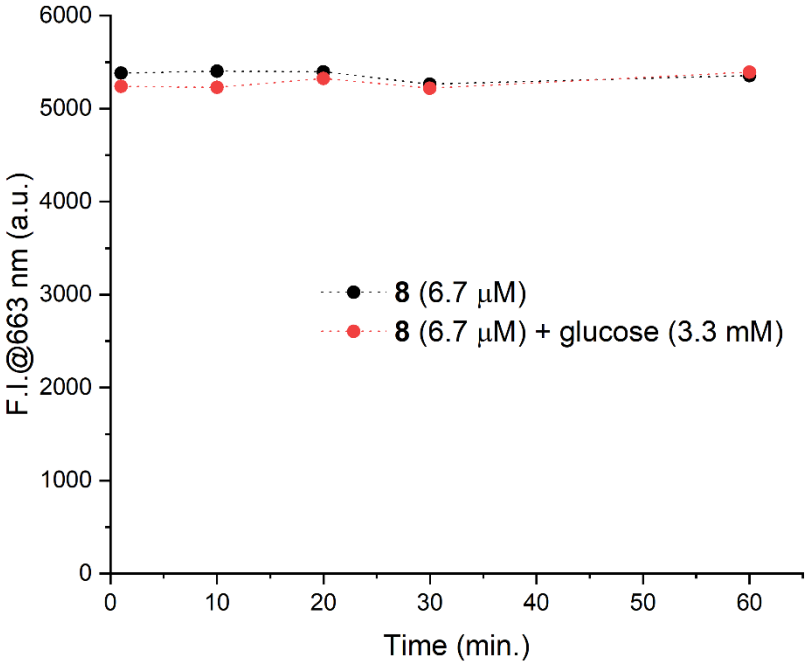

Figure S33: The change in the fluorescence intensities at 663 nm for compound **3** with and without D-glucose over a period of 60 minutes in 35% DMSO/phosphate buffer (0.012 M) at pH 7.5.

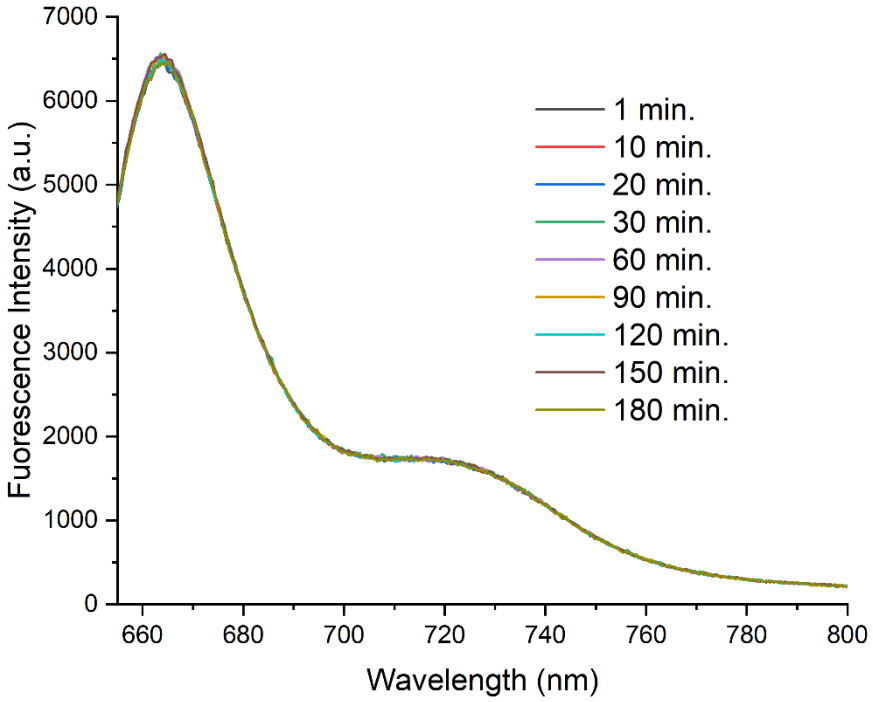

Figure S34: Fluorescence spectra of compound **3** (6.7 µM) measured over a period of 3 hours in 50% DMSO/phosphate buffer (0.012 M) at pH 7.5 when excited at 645 nm.

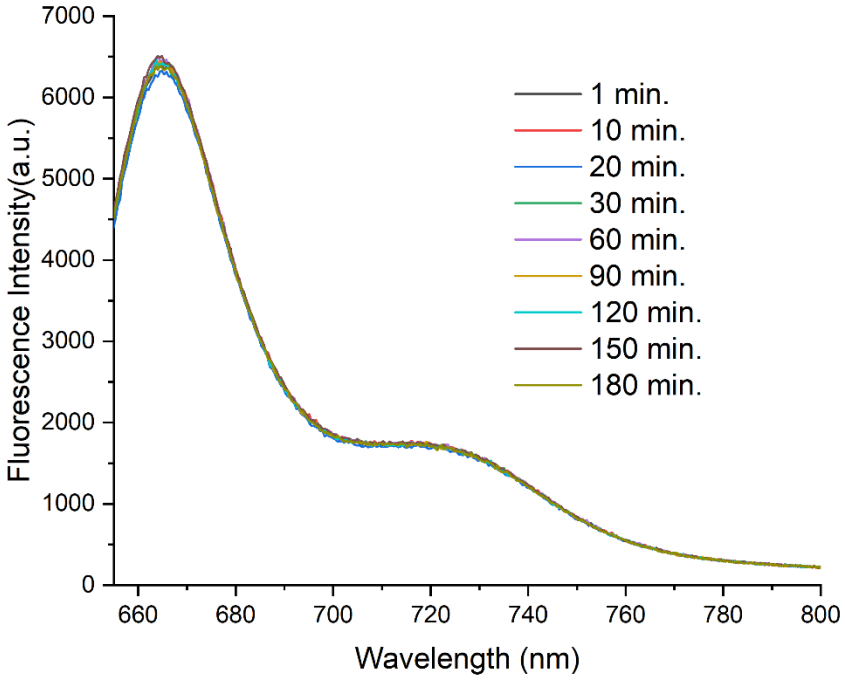

Figure S35: Fluorescence spectra of compound **3** (6.7 µM) with D-glucose (3.3 mM) measured over a period of 3 hours in 50% DMSO/phosphate buffer (0.012 M) at pH 7.5 when excited at 645 nm.

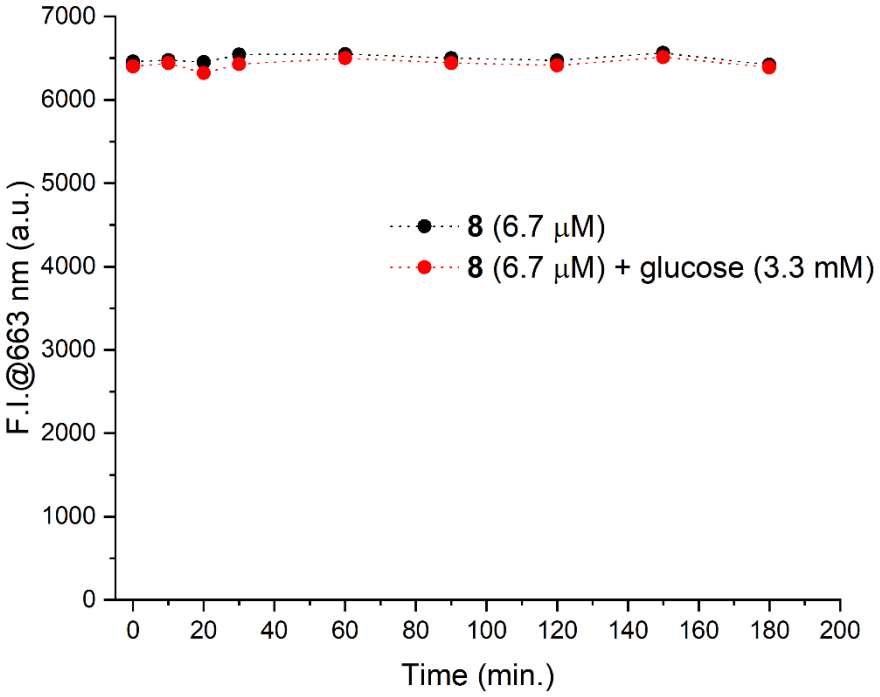

Figure S36: The change in the fluorescence intensities at 663 nm for compound **3** with and without D-glucose over a period of 3 hours in 50% DMSO/phosphate buffer (0.012 M) at pH 7.5.

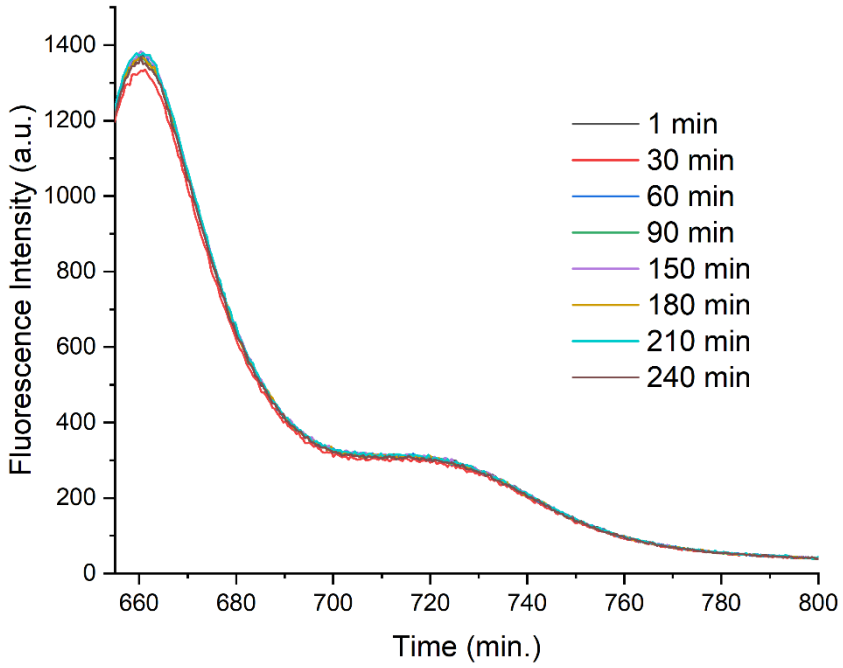

Figure S37: Fluorescence spectra of compound **3** (3.3 μM) measured over a period of 4 hours in 35% DMSO/phosphate buffer (0.012 M) at pH 8.5 when excited at 645 nm.

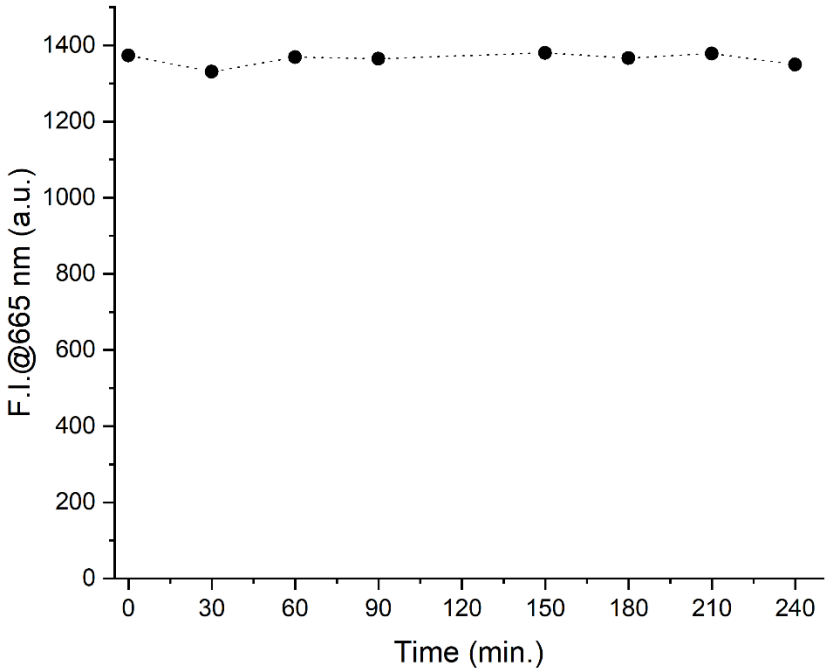

Figure S38: The change in the fluorescence intensities at 665 nm for compound **3** over a period of 4 hours in 35% DMSO/phosphate buffer (0.012 M) at pH 8.5.

pKa determination for diboronic acid 3

The pKa of diboronic acid **3** was determined using UV-vis spectroscopy. Initially, a stock solution of **3** (1 mM) was prepared in DMSO. The stock solution was then diluted by 35% DMSO/sodium phosphate buffer (0.012 M). Samples with desired pH values were prepared by titration with dilute HCl or NaOH. The absorption spectra were measured between the range of pH 7 to 13, and the absorbance maximum was plotted as a function of pH, and the pKa was taken as the mid-point of the titration curve.[10]

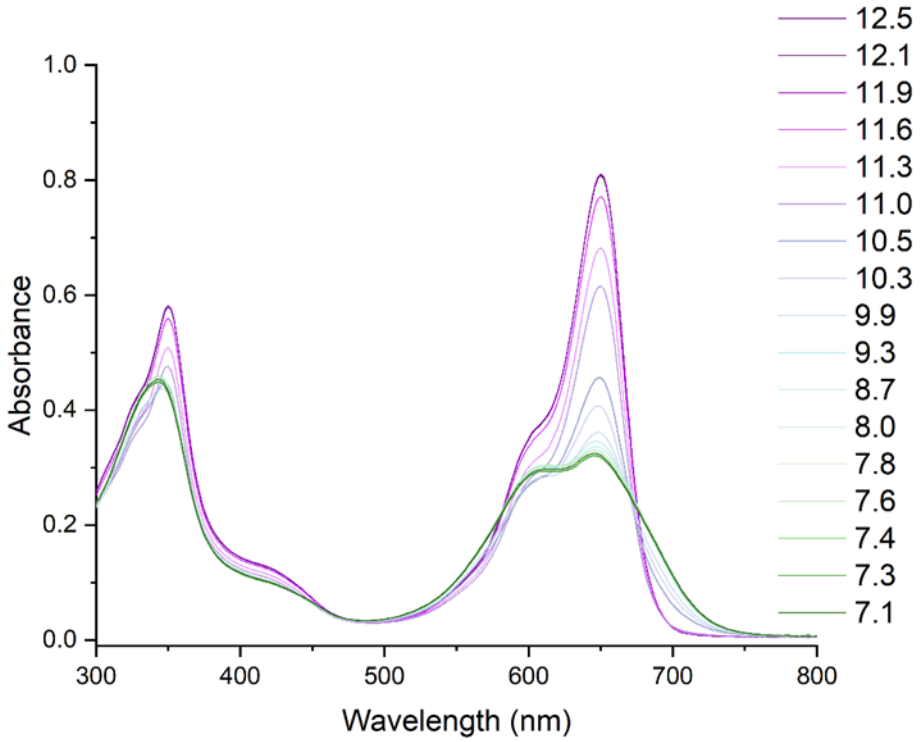

Figure S39: Absorption spectra of compound **3** at varying pH values.

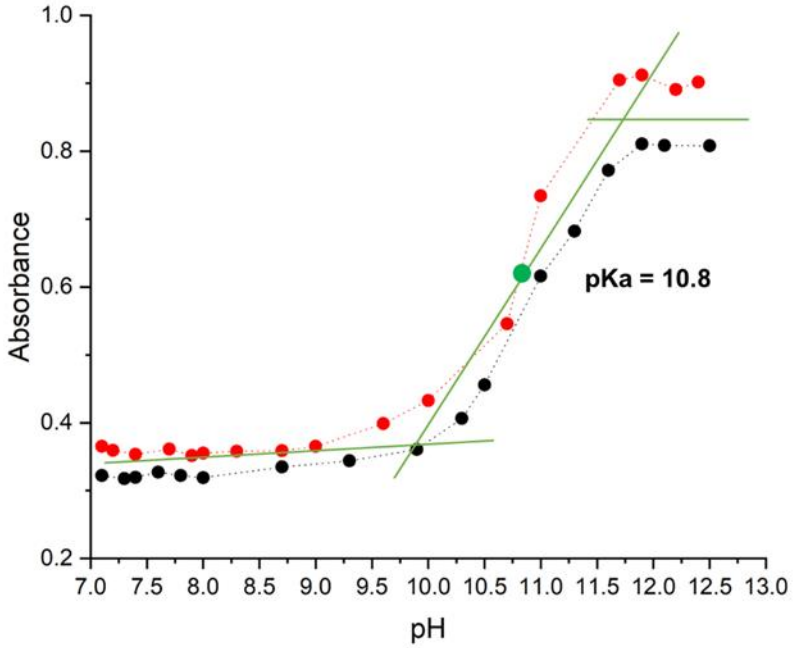

Figure S40: pH titration curve for compound **3** (6.7 µM) in 35% DMSO/sodium phosphate buffer (0.012 M); absorbance measured at 650 nm.

Titration studies of 2 and 3 with carbohydrates

A stock solution of the diboronic acid was prepared in DMSO/ phosphate buffer (0.012 M) (35:65, v:v, pH 7.5). Similarly, a stock solution of D-glucose in phosphate buffer solution (0.25 M, pH 7.5) was prepared. The pH of each solution was adjusted to a desired value by addition of 2 M NaOH aqueous solution, and the solutions were allowed to cool to room temperature (mixing DMSO with phosphate buffer solution generates heat). For each absorption and fluorescence measurement a separate sample was prepared, 1 mL of D-glucose solution with desired concentration was added to 2 mL of diboronic acid solution for keeping the concentration of the diboronic acid constant throughout the experiment. The excitation wavelength was fixed at 650 nm for compound **2** and 645 nm for compound **3**, and the emission spectrum recorded between 655 – 800 nm. The absorption spectrum was recorded between 300 – 800 nm. The binding constants,[11,12] alongside their standard deviation were calculated by a non-linear least square fitting using the online tool Bindfit (http://app.supramolecular.org/bindfit/). All absorption and fluorescence titration experiments were carried out two times.

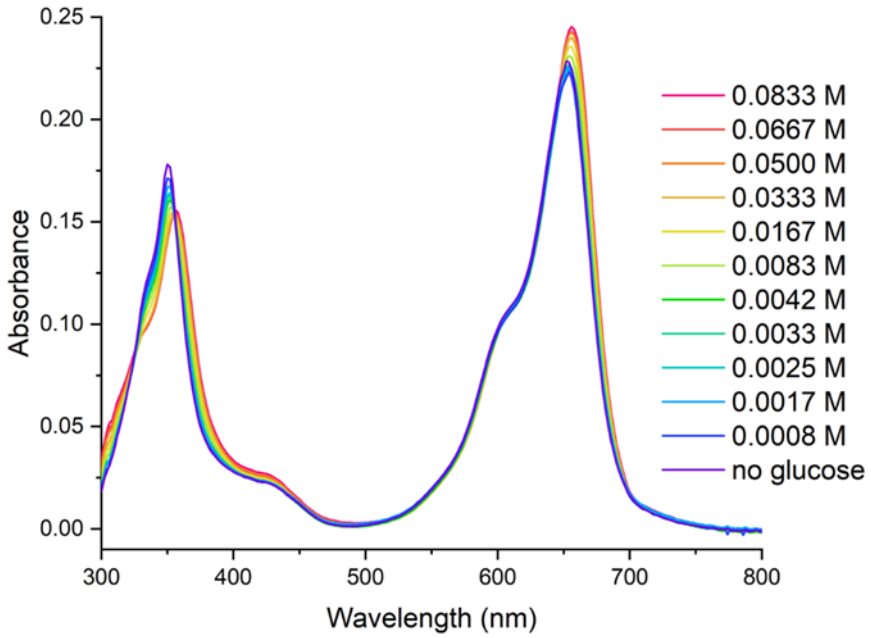

Figure S41: Absorbance spectra of compound **2** (3.3 µM) with varying concentrations of D-glucose in 35% DMSO/ sodium phosphate buffer at pH 10.

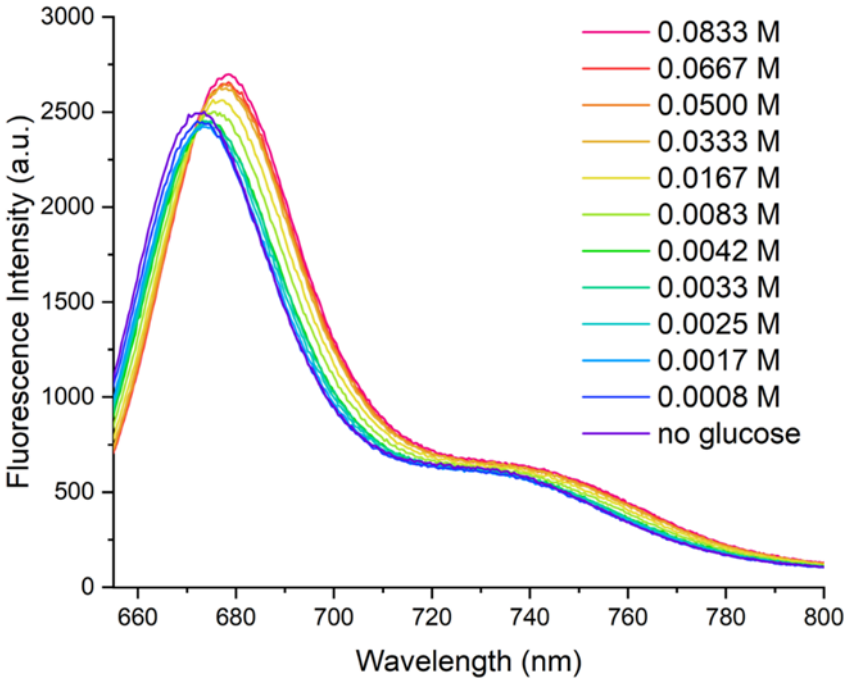

Figure S42: Fluorescence spectra of compound **2** with varying concentrations of D-glucose in 35% DMSO/ sodium phosphate buffer at pH 10 when excited at 650 nm.

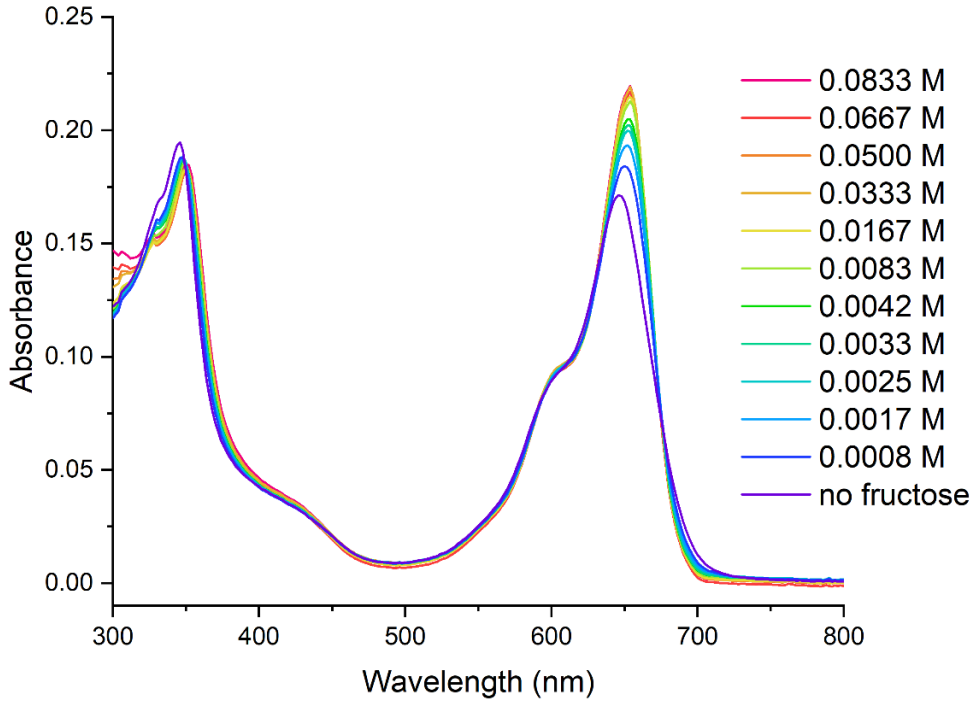

Figure S43: Absorbance spectra of compound **2** (3.3 µM) with varying concentrations of D-fructose in 35% DMSO/ sodium phosphate buffer at pH 8.5.

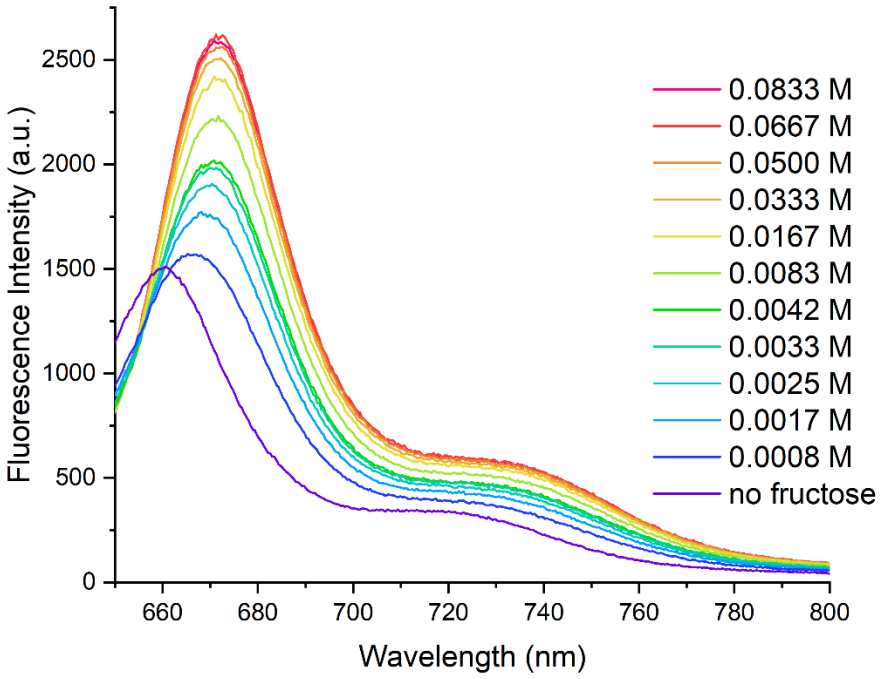

Figure S44: Fluorescence spectra of compound **3** (3.3 µM) with varying concentrations of D-fructose in 35% DMSO/ sodium phosphate buffer at pH 8.5 when excited at 645 nm.

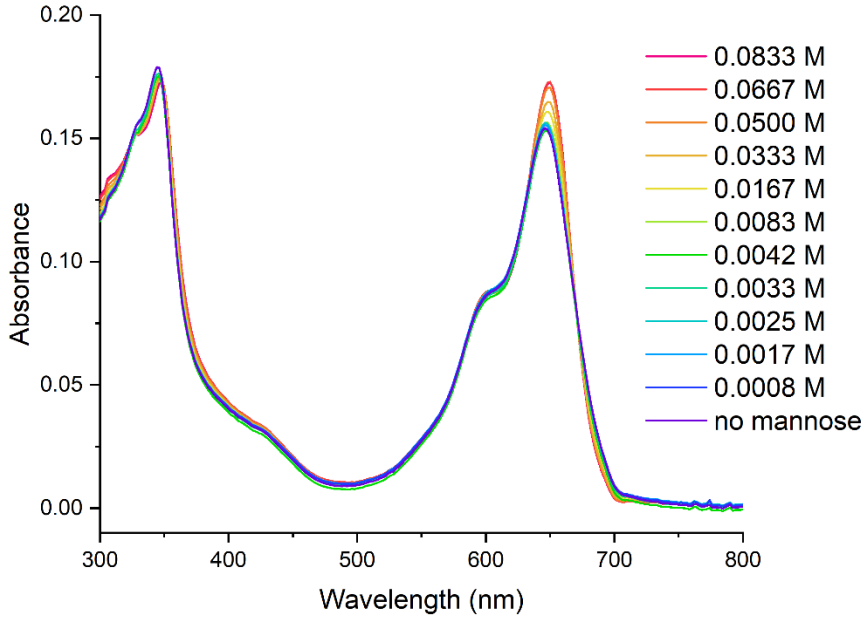

Figure S45: Absorbance spectra of compound **3** (3.3 µM) without D-mannose and with varying concentrations of D-mannose added in 35% DMSO/ sodium phosphate buffer at pH 8.5.

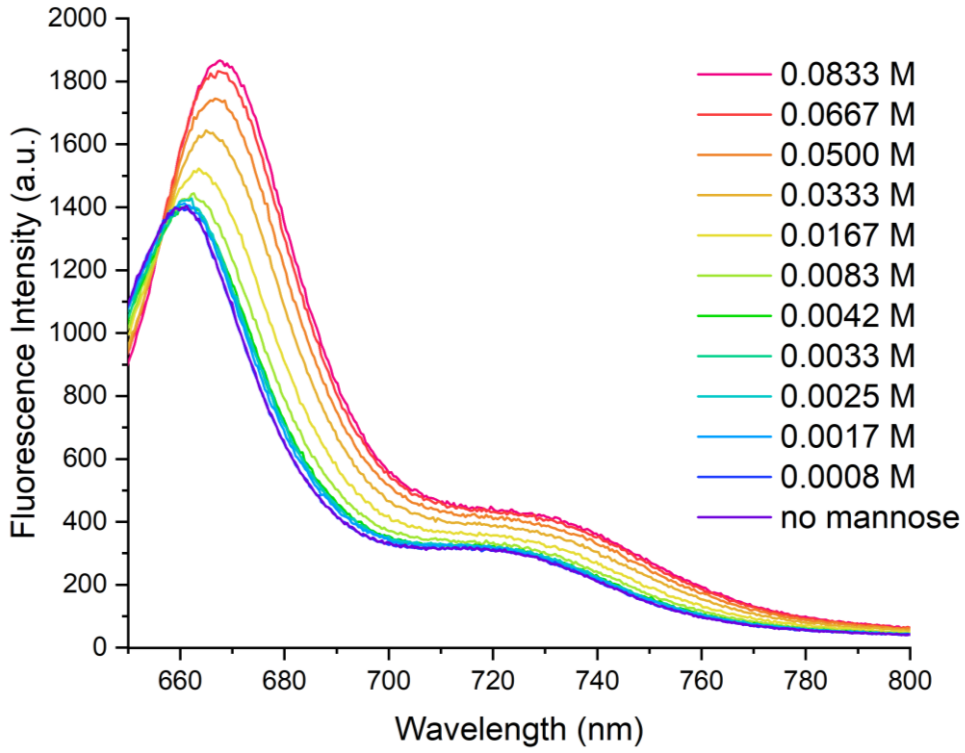

Figure S46: Fluorescence spectra of compound **3** (3.3 µM) with varying concentrations of D-mannose in 35% DMSO/ sodium phosphate buffer at pH 8.5 when excited at 645 nm.

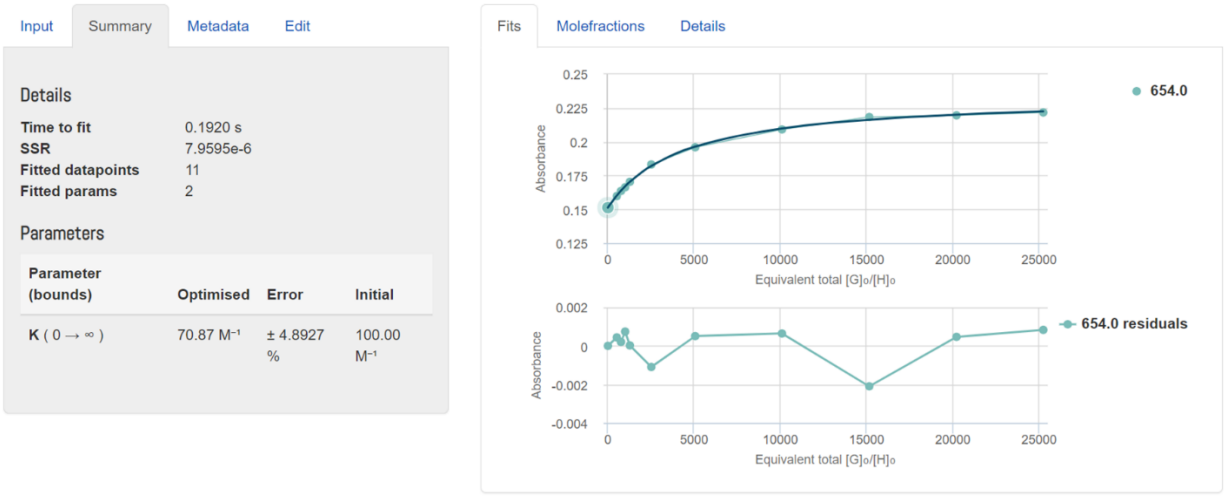

Figure S47: Least-squares nonlinear fitting of the normalized change in absorbance at 654 nm obtained as a function of concentration based on the UV-vis titration of **3** with D-glucose. The solid lines were obtained from nonlinear curve-fitting to a 1:1 binding model using the www.supramolecular.org web applet. (http://app.supramolecular.org/bindfit/view/ff3c3d9c-3365-44df-b382-700fe46d2a2c).

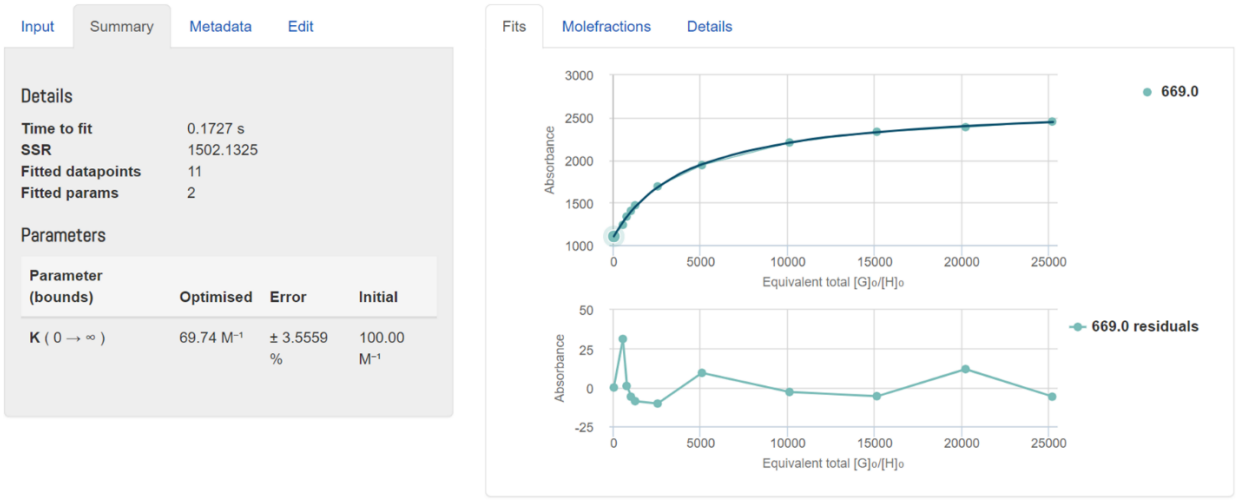

Figure S48: Least-squares nonlinear fitting of the normalized change in fluorescence at 669 nm obtained as a function of concentration based on the fluorescence titration of **3** with D-glucose. The solid lines were obtained from nonlinear curve-fitting to a 1:1 binding model using the www.supramolecular.org web applet. (http://app.supramolecular.org/bindfit/view/bfa4673a-b18d-4dee-a31e-7941b86997aa).

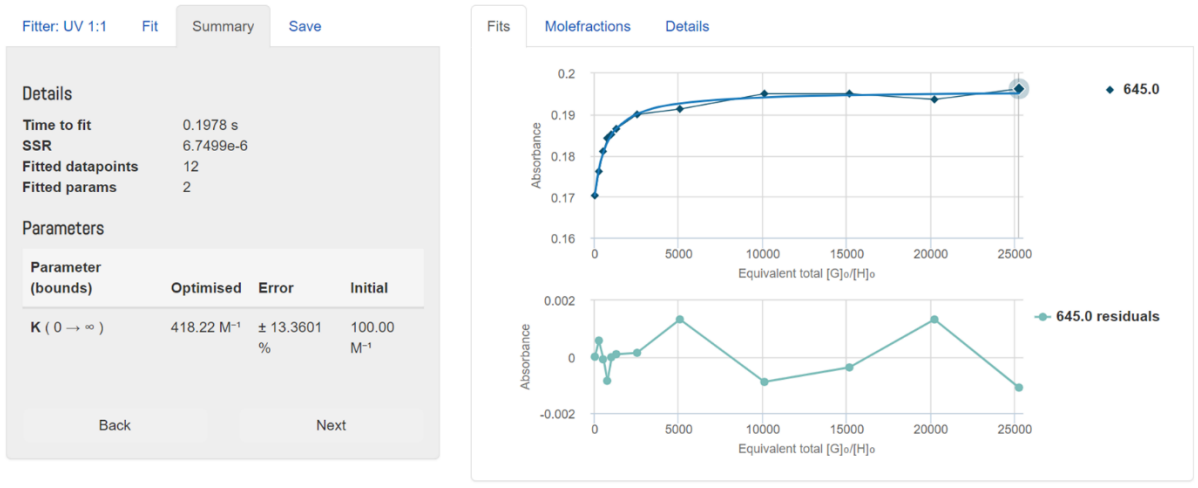

Figure S49: Least-squares nonlinear fitting of the normalized change in absorbance at 645 nm obtained as a function of concentration based on the UV-vis titration of **3** with D-fructose. The solid lines were obtained from nonlinear curve-fitting to a 1:1 binding model using the www.supramolecular.org web applet. (http://app.supramolecular.org/bindfit/view/2abde538-6aee-4a67-9556-950826c38a1d).

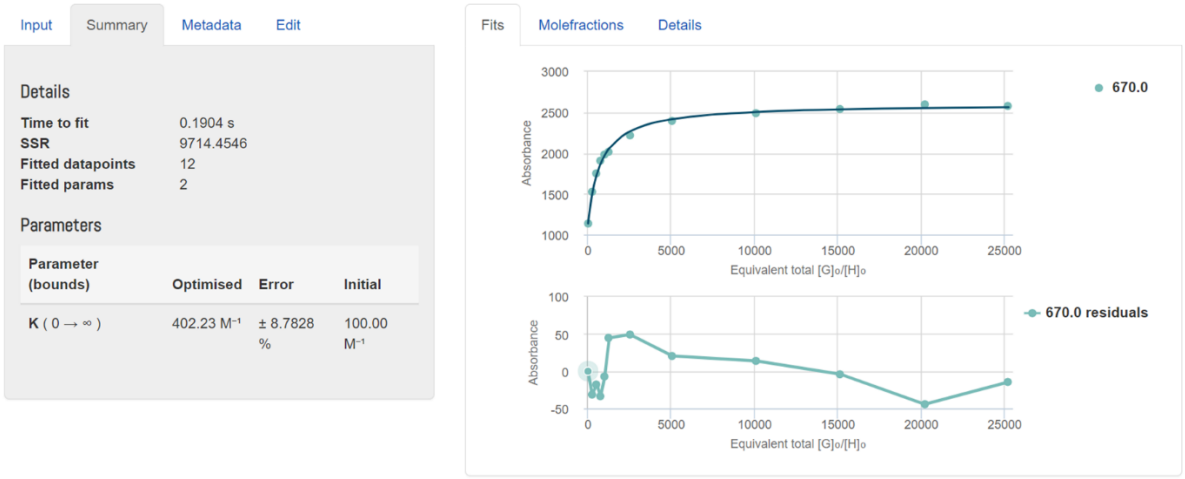

Figure S50: Least-squares nonlinear fitting of the normalized change in fluorescence at 670 nm obtained as a function of concentration based on the fluorescence titration of **3** with D-fructose. The solid lines were obtained from nonlinear curve-fitting to a 1:1 binding model using the www.supramolecular.org web applet. (http://app.supramolecular.org/bindfit/view/9f2ef8d1-b99f-4fd2-aa6f-09fc3cce2faf).

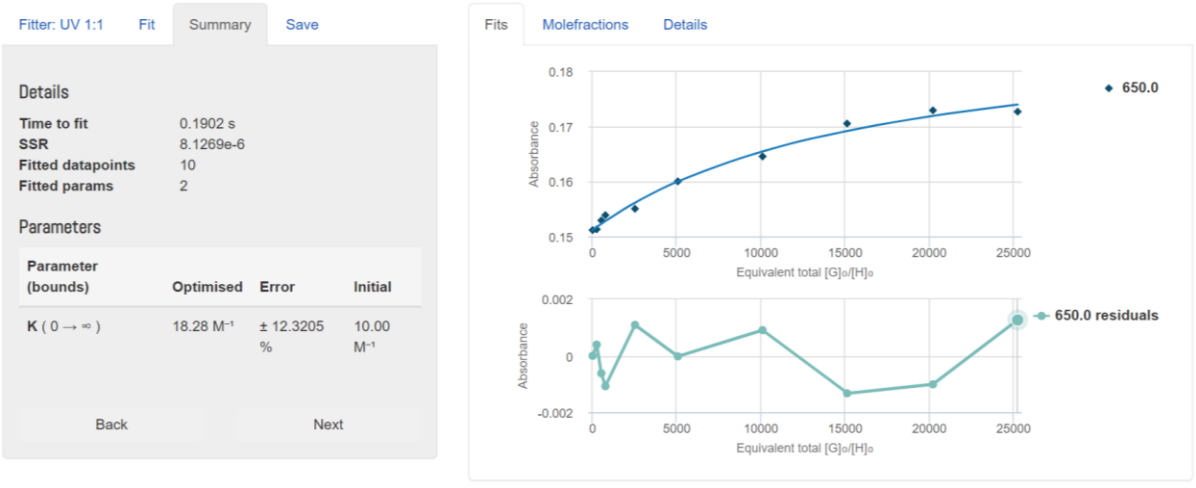

Figure S51: Least-squares nonlinear fitting of the normalized change in absorbance at 650 nm obtained as a function of concentration based on the UV-vis titration of **3** with D-mannose. The solid lines were obtained from nonlinear curve-fitting to a 1:1 binding model using the www.supramolecular.org web applet. (http://app.supramolecular.org/bindfit/view/9347ed7b-bd0e-4954-9dbf-d3ce12bfcb90).

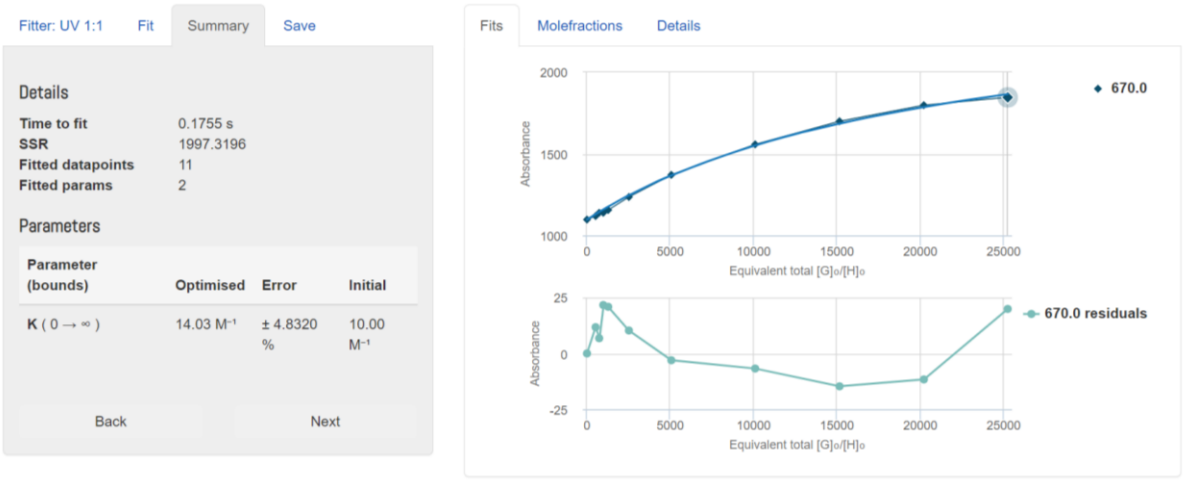

Figure S52: Least-squares nonlinear fitting of the normalized change in fluorescence at 670 nm obtained as a function of concentration based on the fluorescence titration of **3** with D-mannose. The solid lines were obtained from nonlinear curve-fitting to a 1:1 binding model using the www.supramolecular.org web applet. (http://app.supramolecular.org/bindfit/view/4f750f11-d773-456b-a576-752094b1dff7).

NMR Studies

Preparation of NMR samples

A 10 mL stock solution of 1 mM of boronic acid (phenylboronic acid, **2** or **3**) was prepared in a 10 mL volumetric flask. 8 mL of methanol is first added to dissolve the substrate, then 2 mL of sodium phosphate buffer is slowly added, the pH is then carefully adjusted to 7.5 with 4M NaOH. This solution is then divided into 6 different samples, with 0.9 mL of the stock solution in each sample. In each sample, 0.1 mL of glucose solution is added with varying concentrations from 0-2 mM. The ^{1}H NMR spectrum is then measured on a 500 MHz spectrometer, with proton suppression settings suppressing peaks from water and methanol.

Calculation of glucose binding constant (K_a)

If a boronic acid (B) and a saccharide are assumed to bind in one modality, B•S, the equilibrium equation is as follows, where $[B_T]$ is the concentration of boronic acid titrated and $[S_T]$ is the concentration of sugar titrated.[13]

$$B + S \rightleftharpoons B{\bullet}S$$

$$K_a = \frac{[B{\bullet}S]}{[B]+[S]}$$

$$[B{\bullet}S] + [B] = [B_T]$$

$$[B{\bullet}S] + [S] = [S_T]$$

$$\frac{[B\bullet S]}{[B]} + 1 = \frac{[B_T]}{[B]}$$

Equations **1** through **3** are used to determine the equilibrium concentrations of the boronic acid, [B], the sugar, [S] and the complex [B•S]. The ratio [B•S]/[B] is determined from the ratio of the integrals of the peaks corresponding to bound boronic acid, and the peaks corresponding to free boronic acid.[13]

1) $$[B] = \frac{[B_T]}{\frac{[B\cdot S]}{[B]} + 1}$$

2) $$[B\bullet S] = \frac{[B\bullet S]}{[B]}[B]$$

3) $$[S] = [S_T] - [B\bullet S]$$

Equation 4 and 5 represent a modified version of the Benesi-Hildebrand equation,[14] and can be used to determine K_a graphically. From a plot of 1/[S] v.s. 1/[θ], K_a can be found by taking the reciprocal of the slope.

4) $$\theta = \frac{[B\cdot S]}{[B\cdot S] + [B]}$$

5) $$\frac{1}{\theta} = \frac{1}{K_a}\left(\frac{1}{[S]}\right) + 1$$

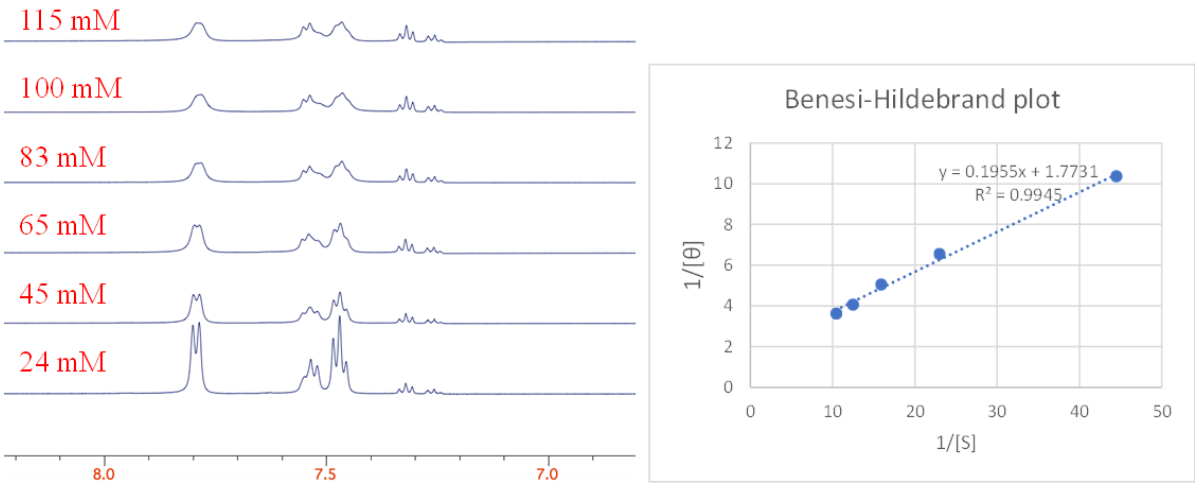

Figure S53: ^{1}H NMR spectra of phenylboronic acid (1 mM) samples with varying amount of d-glucose added in 80% Methanol, 20% phosphate buffer, pH=7.5 (right) and the corresponding Benesi-Hildebrand plot (left).

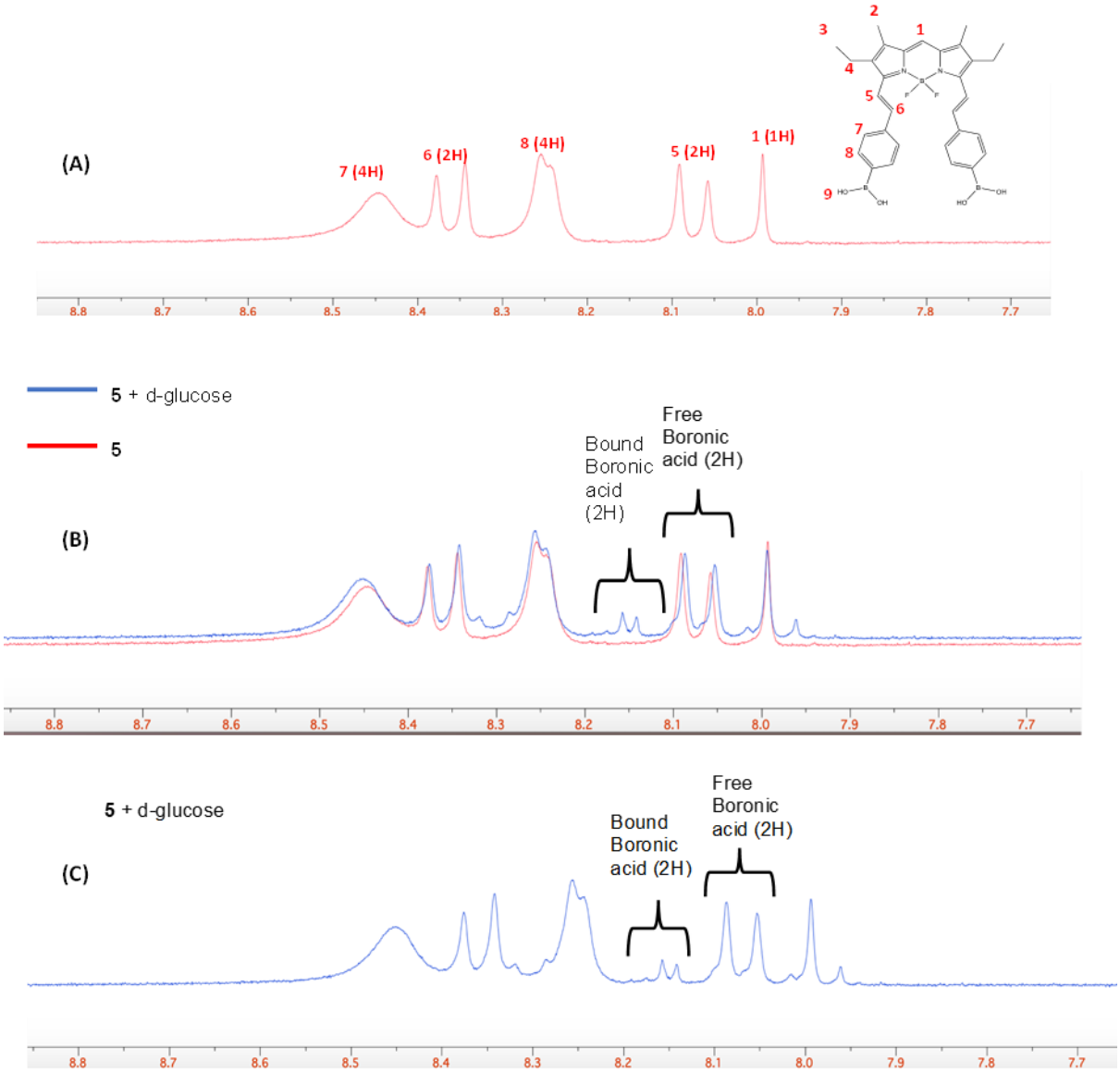

Figure S54: (A) ^{1}H NMR spectrum of **2** (1 mM) in 80% Methanol, 20% phosphate buffer, pH = 7.5, with peaks in aromatic region assigned. (B) Overlay of (A) and (C), indicating new peaks formed after d-glucose addition. (C) ^{1}H NMR spectrum of **2** (1 mM) and d-glucose (2 mM) in 80% Methanol, 20% phosphate buffer, pH=7.5.

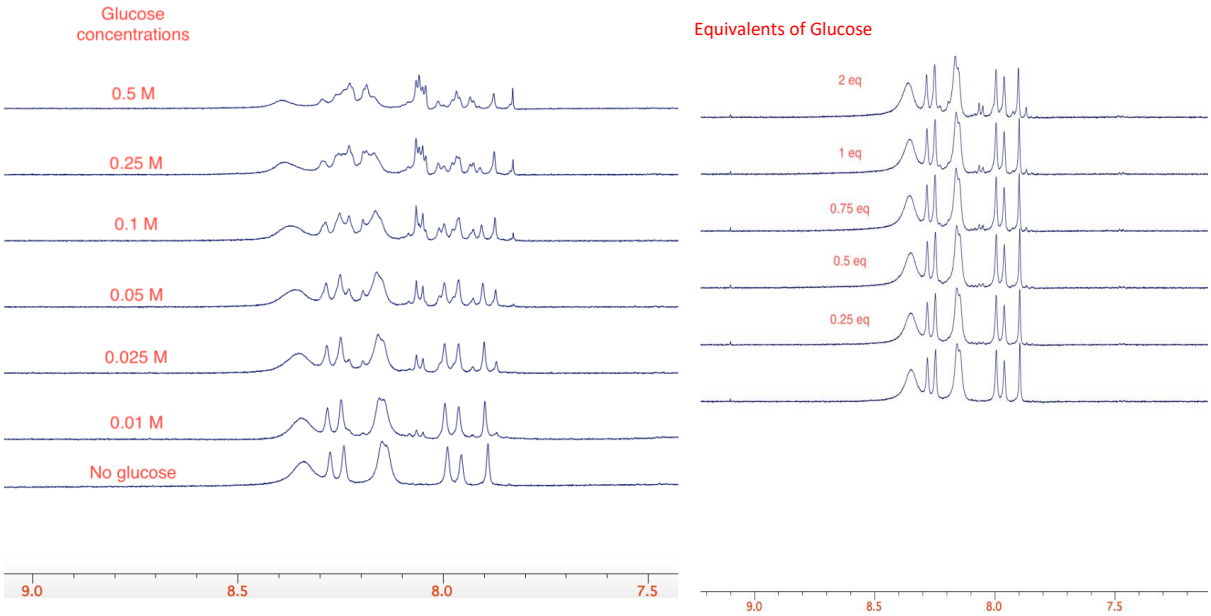

Figure S55: Aromatic area of ^{1}H NMR spectra of **2** (1 mM) samples without and with varying amount of d-glucose added in 80% Methanol, 20% phosphate buffer, pH = 7.5.

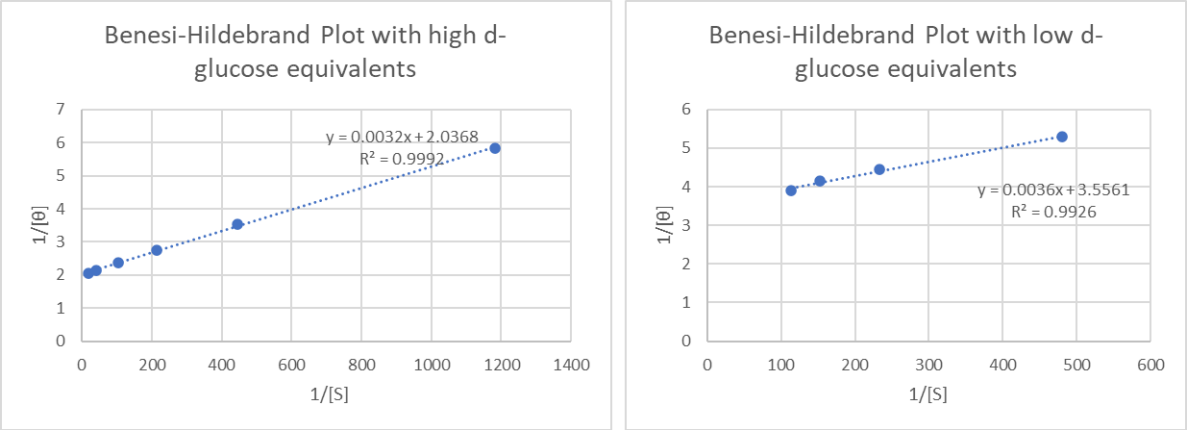

Figure S56: Benesi-Hildebrand plots generated from samples of **2** with high (right plot) and low (left plot) equivalents of d-glucose added.

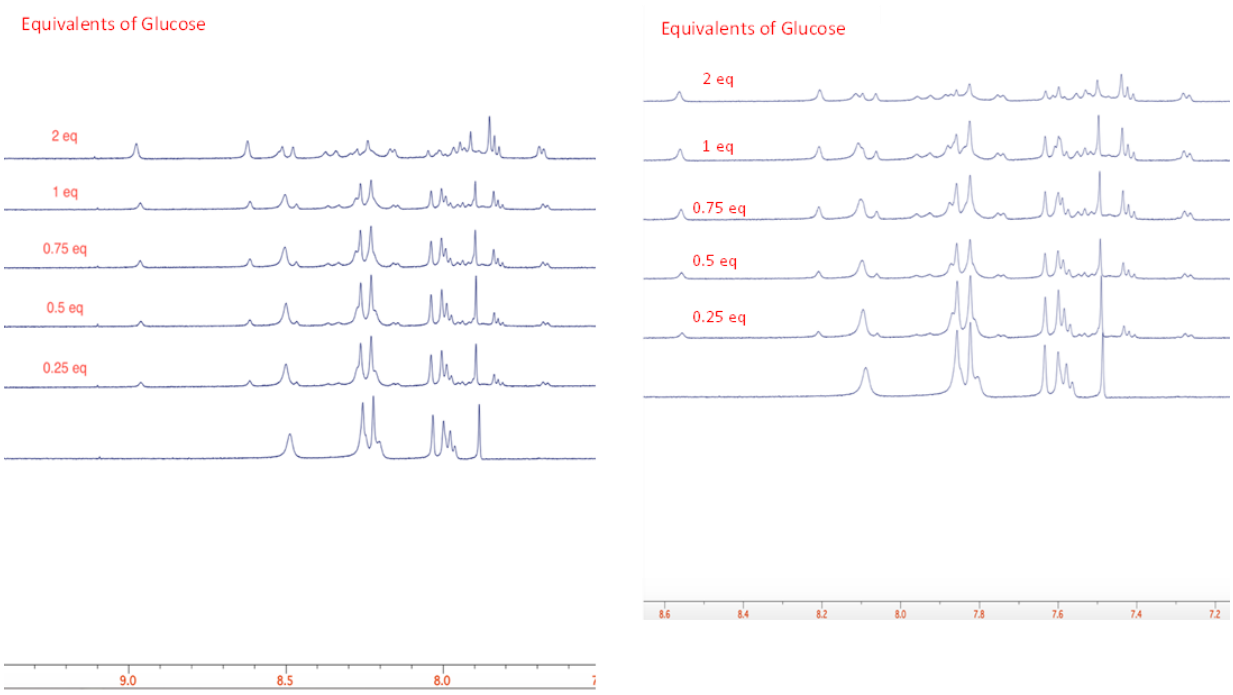

Figure S57: Aromatic area of ^{1}H NMR spectra of **3** (1 mM) samples without and with varying amount of d-glucose added in 80% Methanol, 20% phosphate buffer, pH = 7.5.

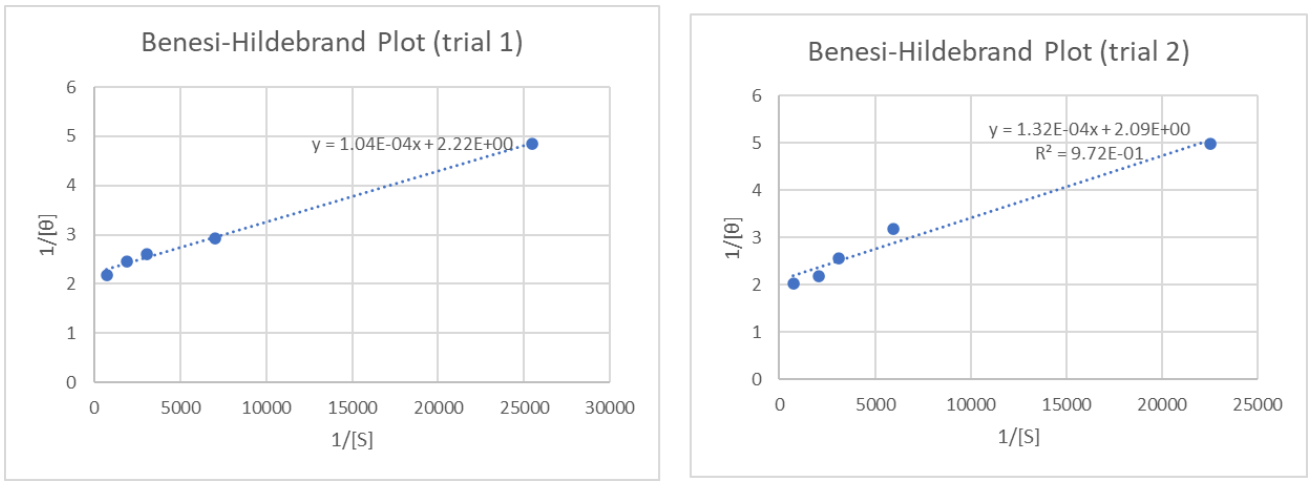

Figure S58: Benesi-Hildebrand plots generated from samples of **3** of d-glucose added for two independent trials.

Table S2: Glucose binding constants calculated for phenylboronic acid, **2** and **3**.

Boronic acid	Binding constant, K_a (M^{-1})
Phenylboronic acid	5
2, trial 1	278
2, trial 2	313
3, trial 1	9615
3, trial 2	7576

Cell Staining Studies

Cell Culture

HS578T cells were cultured in high-glucose Dulbecco's Modified Eagle's Medium (DMEM) with L-glutamine supplemented with 10% fetal bovine serum (FBS) and 1X penicillin/streptomycin (P/S). Cells were passaged after reaching 80-85% confluency. Cells were maintained in a humid 5% CO_2 atmosphere at 37°C.

Cell Staining

HS578T cells were seeded on 22x22 mm cover slips in 6-well plates (100 000 cells/cover slip; for microscopy) or in 24-well plates (100 000 cells/well; for flow cytometry) and incubated in a humid 5% CO_2 atmosphere at 37°C in high-glucose DMEM with 10% FBS and 1X P/S for 24-48 hours until the cells reached 80% confluency. Staining solutions of **2-5** at 0.1-100 µM in PBS (with Ca/Mg) with 1% bovine serum albumin (BSA) were prepared from a solution of **2-5** at 10 mM in DMSO. Cells were washed three times with 1% BSA in PBS and incubated with 0.1-100 µM **2-5** in 1% BSA in PBS for 2 hr in the dark at 37°C. Cells were then subjected to fluorescence confocal microscopy or flow cytometry analysis.

Fluorescence confocal microscopy

After staining with **2-5** for 2 hr, cells were washed with 1% BSA in PBS, fixed (3.7% formaldehyde in PBS, 15 min, room temperature), and permeabilized (0.1% Triton X-100 in PBS, 10 min, room temperature). Cover slips with fixed and permeabilized cells were mounted on glass slides with Prolong™ Diamond Antifade Mountant with DAPI (ThermoFisher Scientific Canada, Cat. P36966). Slides were imaged with a Leica Mica fluorescence confocal microscope using a 20x air objective.

Flow cytometry

After staining with **2-5** for 2 hr, cells were sequentially washed with 1% BSA in PBS and PBS without Ca/Mg. Cells were detached using 10 mM EDTA for 5 min at 37°C.

Cells were then suspended in 1% BSA in PBS, transferred to a 96-well plate, centrifuged gently (500 rcf for 5 min), and resuspended in 280 µL FACS buffer (PBS without Ca/Mg supplemented with 2 mM EDTA and 0.5% BSA) for flow cytometric analysis (Beckman Coulter, Cytoflex S). Staining with **2-5** was assessed using the ECD channel (561 nm ex excitation, 610/20 BP filter). Statistical significance of differences in median fluorescence intensity was assessed by one-way ANOVA (Brown-Forsythe and Welch tests).

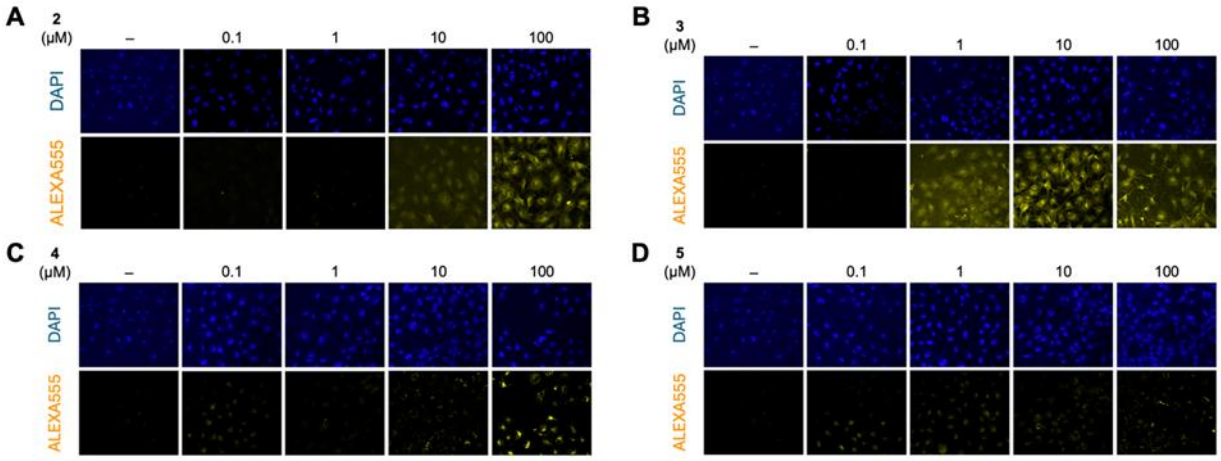

Figure S59: Fluorescence microscopy images of HS578T cells incubated with **2** (A), **3** (B), **4** (C), and **5** (D) at 0.1-100 µM. DAPI = 358 nm excitation, 461 nm emission. ALEXA555 = 555 nm excitation, 565 nm emission.

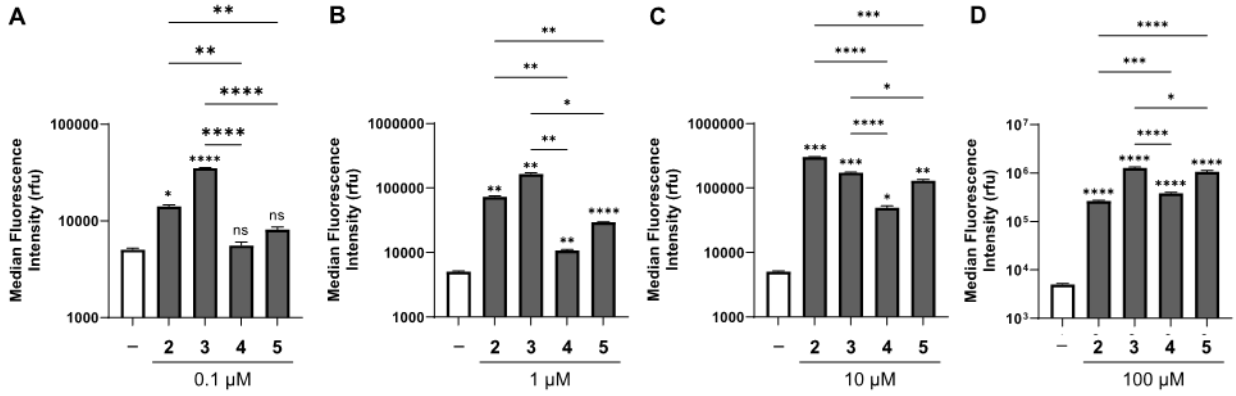

Figure S60: Median fluorescence intensities of HS578T cells stained with **2-5** (0.1-100 µM in 1% BSA in PBS, 2 hr, 37°C). Flow cytometry fluorescence data collected with the ECD channel (excitation 561 nm, emission 610 nm, N=3). Statistics above columns are relative to the blank control. ns = not significant $p \geq 0.05$; * $p < 0.05$; ** $p < 0.01$; *** $p < 0.001$; **** $p < 0.0001$.

X-ray Crystallography

The crystal chosen was attached to the tip of a MicroLoop with paratone-N oil. Measurements were made on a Bruker D8 VENTURE diffractometer equipped with a PHOTON III CMOS detector using monochromated Mo Kα radiation (λ = 0.71073 Å) from an Incoatec microfocus sealed tube at 125 K.[15] Most of the crystals used in this study were very thin and difficult to center in the X-ray beam; they also did not diffract well so long frame times were often necessary. The initial orientation and unit cell were indexed using a least-squares analysis of the reflections collected from a complete 180° phi-scan, generally with 5 seconds per frame and 1° per frame. For data collection, a strategy was calculated to maximize data completeness and multiplicity, in a reasonable amount of time, and then implemented using the Bruker Apex 4 software suite.[15] The data were collected with the frame times indicated below for each crystal. The crystal to detector distance was set to 4 cm. Cell refinement and data reduction were performed with the Bruker SAINT software,[16] which corrects for beam inhomogeneity, possible crystal decay, and Lorentz and polarisation effects. A multi-scan absorption correction was applied (SADABS[17]). The structure was solved using SHELXT-2014[18,19] and was refined using a full-matrix least-squares method on F^2 with SHELXL-2018.[18,19] The non-hydrogen atoms were refined anisotropically. The hydrogen atoms bonded to carbon were included at geometrically idealized positions and were allowed to ride on the atom to which they were bonded. The isotropic thermal parameters of these hydrogen atoms were fixed at 1.2U_{eq} of the parent carbon atom or 1.5U_{eq} for methyl hydrogens. The positions of the hydrogen atoms bonded to oxygen (if present) were located in a near final difference Fourier map. They were added to the atom list and refined with U_{iso}H equal to -1.5 U_{eq}O and with weak restraints placed on their geometries to keep them similar and reasonable.

All diagrams were prepared using the program Mercury CSD 4.3.[20,21] The crystallographic data has been deposited with the Cambridge Crystallographic Data Centre. CCDC 2328988-2328992 contain the supplementary crystallographic data for this paper. The individual number for each structure is given in Table S4. The data can be obtained free of charge via www.ccdc.cam.ac.uk/data_request/cif, or by emailing data_request@ccdc.cam.ac.uk.

Compound 5, 20 sec frames (0.75° per frame)

Data was integrated to a maximum resolution of 0.65 Å (θ_{max} = 33.14°) and all of this data was used in the refinement. The initial structure refinement suggested the presence of a small twin component. The program Cell_Now[22] was used to identify the main crystal domain and the frames were re-integrated at the same resolution using this domain only.

The compound crystallized in the centrosymmetric Triclinic space group *P*-1 with one complete molecule in the asymmetric unit. The crystal is solvated with dichloromethane, the solvent which had been used for recrystallization. There is one molecule of solvent present for each molecule of compound. The solvent was found

to be disordered and a model was developed which split each of its atoms over three positions. The occupancy of each part was refined but restrained so that the total occupancy of the solvent was one. The geometry of each part was restrained to be similar and the heavy atoms of each type in the solvent were restrained to have similar thermal parameters. The occupancies of the three parts refined to 0.57(2), 0.28(2) and 0.15(1), for parts 1, 2 and 3, respectively.

Compound 6, 75 sec frames (0.5° per frame)

Data was collected and integrated to a maximum resolution of 0.80 Å (θ_{max} = 26.39°). In this experiment the crystal to detector distance was increased to 5 cm. Six reflections were removed from the final refinement because of poor agreement between F_{obs}^2 and F_{calc}^2.

The compound crystallized in the non-centrosymmetric Orthorhombic space group $Pca2_1$ with two complete molecules in the asymmetric unit. The crystal proved to be an inversion twin, so BASF was refined but gave an ambiguous result of 0.4(1.2). The program Platon[23] was used to calculate a Hooft parameter of 0.7(3) but the structure was not inverted as even this value is not definitive.

The structure was found to be quite disordered. In both of the molecules, the tetramethyl dioxaborolanyl rings are both disordered, as is one of the ethyl side groups in one of the molecules. These disorders were each defined using two part models, with the total occupancy set to one in each case. In every model, the geometries of each part were restrained to be similar, and the atoms of the same type involved in each disordered group were restrained to have similar thermal parameters. Bonds from disordered parts to ordered parts of the molecules were restrained to be similar. Finally, a rigid bond restraint was placed over all of the atoms in both of the molecules.

For the two tetramethyl dioxaborolanyl rings in molecule 1, the occupancies of the first ring (containing B2) refined to 85.4(6) % and 14.6%, for parts one and two, respectively, while the second ring (containing B3) had occupancies of 93.8(5) % and 6.2%. In molecule 2, the first ring (containing B4) gave occupancies of 82.8(5) % and 17.2% and the values for the second ring (containing B5) refined to 92.4(5) % and 7.6 %. Refinement of the occupancies of the atoms of the ethyl group in molecule 1 gave 63(1) % and 37% for parts 1 and 2, respectively.

The final Fourier difference map showed more visible disorder that could have been modelled. The disorder works its way back up the chains from the dioxaborolanyl rings with the most residual electron density evident in the phenyl rings next to these rings. The phenyl disorder was easily modelled and gave stable results. However, the statistics of the refinement improved only slightly and the data to parameter ratio (which was already low) decreased even further. For this reason, the results for the model with only the 4 rings (and one ethyl group) split are reported here.

Compound 2, 40 sec frames (0.75° per frame)

Data was collected and integrated to a maximum resolution of 0.80 Å (θ_{max} = 26.37°). All of this data was included in the refinement. One reflection (0 -1 1) was removed from the final refinement because it was partially obscured by the beam stop resulting in poor agreement between F_{obs}^2 and F_{calc}^2.

The compound crystallized in the centrosymmetric Triclinic space group *P-1* with one complete molecule in the asymmetric unit. There was also determined to be one molecule of disordered acetonitrile solvent present in the asymmetric unit. The acetonitrile was found to be disordered over 3 sets of positions. The occupancies of the atoms at the original set of positions refined to a value of 0.50, so they were given this fixed occupation and were no longer refined. The other two, more minor sets of positions, were located in a Fourier difference map. The occupancies of the atoms in these two sets were refined to total the remaining 50% of one acetonitrile molecule. The refined values came out to 44.9(8) and 5.1% respectively. In the refinement, the geometries of the solvent molecules were restrained to be similar, and they were restrained to have similar anisotropic displacement parameters. The atoms N3B and N3C were constrained to occupy the same position.

The positions of the hydrogen atoms bonded to oxygen were clearly visible in the Fourier difference map prior to their being added to the refinement. Each oxygen was found to have two hydrogen atoms bonded to it, with each of those hydrogens having an occupancy of 50%, which was then set and not refined. The positions of those hydrogens could be freely refined with only a few weak restraints added to keep the geometries similar. This resulted in two distinct hydrogen bonding systems being present in the solid-state structure. Based on the O..O and O…N distances in the unit cell, the OH hydrogen atoms were separated into two groups (A and B) based on which hydrogen bonding pattern they belonged to (see the figures provided). Each oxygen atom correctly ended up with one A atom and one B hydrogen atom bonded to it.

The hydrogen bonding pattern and the positions of the hydrogen atoms participating in each pattern was quite clear (see the provided Table of hydrogen bond geometries) except for that of H1A, which proved somewhat problematic. The hydrogen position that H1A would be expected to take involves the closed ring of HBs “O4...O1...O4...O1” of two different molecules. Instead, it moves away from closing this ring and makes a new contact with a second O1 atom in a completely different molecule. The problem with this contact is 2-fold: (1) it is out of the plane of the molecule and out of the plane of the hydrogen bonded ring just mentioned., and (2) more importantly, this new hydrogen bond would have a geometry of O1-H1A...H1A-O1. It is unlikely that these two H1A atoms would occupy the same space at the same time. It is perhaps more reasonable that H1A forms a bifurcated interaction where it lies somewhere between O4 and O1 so that it does not point directly towards the symmetry related H1A atom. The freely refined position reported here for H1A may not be totally correct, but it does suggest the presence of such a bifurcated interaction; no attempt was made to restrain it further.

Compound 7, 60 sec frames (0.5° per frame)

Data was collected and integrated to a maximum resolution of 0.80 Å (θ_{max} = 26.44°). One reflection (-6 6 6) was removed from the final refinement because of poor agreement between F_{obs}^2 and F_{calc}^2.

The compound crystallized in the centrosymmetric Monoclinic space group $P2_1/c$ with one complete molecule in the asymmetric unit. The crystal was also found to be solvated, with disordered molecules of acetonitrile present in the lattice. Refinement of the structure gave the best results with each unit cell containing 4 molecules of compound and 3 molecules of acetonitrile. This was substantiated using the Squeeze routine in the program Platon[23] which calculated there to be 67 "solvent" electrons per unit cell; 3 molecules of acetonitrile would contribute 66 electrons.

The structure was found to be heavily disordered. In the molecule, the tetramethyl dioxaborolanyl rings are both disordered as is the solvent and one of the ethyl side groups. After modelling the disorder in only the one ethyl group, the Fourier map showed there to be disorder also in the 5-membered ring to which that ethyl group was bonded. Those carbon atoms not part of the central ring were also included in the disordered ethyl model. All of these disorders were each defined using two part models, with the total occupancy set to one in most cases; for the solvent, the total occupancy of the two parts was refined to 0.75 using a SUMP instruction. The occupancies of the two parts of the solvent model were first freely refined and found to total roughly 0.75.

In every model, the geometries of each part were restrained to be similar, and the atoms of the same type involved in each disordered group were restrained to have similar thermal parameters. Bonds from disordered parts to ordered parts of the molecules were restrained to be similar. Finally, a rigid bond restraint was placed over all of the atoms in both of the molecules. For the solvent, the occupancies of parts 1 and 2 refined to 0.444(5) and 0.306(5), respectively, for a total of 0.75 molecules of acetonitrile per molecule of compound. For the two tetramethyl dioxaborolanyl rings, the occupancies of the first ring (containing B2) refined to 57.1(4) % and 42.9 %, respectively, while the second ring (containing B3) had occupancies of 49.1(6) % and 50.9 %. Refinement of the occupancies of the atoms of the ethyl group gave 69(2) % and 31 % for parts 1 and 2, respectively.

Compound 3, 20 sec frames (0.75° per frame)

Data was collected and integrated to a maximum resolution of 0.65 Å (θ_{max} = 26.37°). All of this data was included in the refinement.

The compound crystallized in the centrosymmetric Triclinic space group *P-1* with one complete molecule in the asymmetric unit. There was also determined to be one molecule of acetonitrile solvent and one molecule of disordered water present in the asymmetric unit. The water molecule was found to occupy two quite distinct positions arising from its participation in the hydrogen bonding networks present in the structure.

There was considerable disorder observed in the main molecule. The fluorine atoms, the two ethyl groups on the 5-membered rings, and the entire chain on one side of the molecule (C1 to its terminal $B(OH)_2$ group) were treated as 3 distinct disordered regions in the refinement, with each assigned a different free variable to determine its occupancies. In addition, the $B(OH)_2$ group on the second arm of the molecule was found to be disordered, through its hydrogen bonding interactions with the other $B(OH)_2$ group. It was included in the same disordered group with that part of the molecule and the occupancies of its atoms refined under the same free variable. Each group was modelled with a two part disorder, in which the geometries were restrained to be similar. In addition, atoms of the same type in each part of the disorder were restrained to have similar anisotropic displacement parameters and the bond lengths from disordered to ordered parts of the molecule were restrained to be similar. For the fluorine atoms, the occupancies of the two parts refined to values of 70(5) % and 30% for parts A and B, respectively, and for the ethyl groups (which were first refined with two separate free variables and then one when they proved to be equal) these values were 93.4(3) and 6.6%, respectively.

The positions of the hydrogen atoms bonded to oxygen in Part A of the disordered $B(OH)_2$ groups were clearly visible in the Fourier difference map prior to their being added to the refinement. The occupancies of these hydrogen atoms were refined as a group (to total one with the contribution of Part B) to a final value of 88.6(2) %. The positions of the part A hydrogens could be freely refined with only a few weak restraints added to keep their geometries similar. This resulted in the first distinct hydrogen bonding system present in the solid-state structure (see the Table of hydrogen bond geometries and the included Figures).

The second, more minor, positions for the OH hydrogen atoms (11.4 %) were not always so clear. Based on evidence provided by Fourier peak positions, and the O..O and O…N distances in the unit cell, the OH hydrogen atoms of Part B were assigned. The positions of the hydrogen atoms on the second water molecule and for the second positions on O1B and O4B could be uniquely assigned. It then became apparent that there were two possible positions for the hydrogen atom on each of O2B and O3B. Assigning the positions in this way, leads to chains of hydrogen bonds that run in opposite directions through the part B molecules of the structure. The part B OH hydrogen atoms were included in the refinement in these geometrically calculated positions and allowed to ride on their parent oxygen atom, again with U_{iso}H equal to -1.5 U_{eq}O.

Table S3: Crystal data and structural refinement details.

Identification code	**5**	**6**	**2**	**7**	**3**
CCDC deposit number	2328990	2328989	2328988	2328991	2328992
Empirical formula	$C_{32}H_{31}BBr_2Cl_2F_2N_2$	$C_{43}H_{53}B_3F_2N_2O_4$	$C_{33}H_{36}B_3F_2N_3O_4$	$C_{44.50}H_{55.25}B_3F_2N_{2.75}O_4$	$C_{33}H_{38}B_3F_2N_3O_5$
Formula weight	723.12	732	609.08	763.09	627.09
Crystal system	Triclinic	Orthorhombic	Triclinic	Monoclinic	Triclinic
Space group	*P*-1	*P*ca2$_1$	*P-1*	*P2$_1$/c*	*P-1*
Unit cell dimensions (Å and º)	*a* = 10.9103(4) *b* = 12.9379(5) *c* = 13.0853(6) *α* = 109.188(2) *β* = 114.3958(14) *γ* = 95.445(15)	*a* =29.0246(8) *b* = 11.7719(3) *c* = 24.1756(6) *α* = 90 *β* = 90 *γ* = 90	*a* = 6.0544(3) *b* = 14.3219(7) *c* = 19.1147(11) *α* = 75.167(2) *β* = 87.342(2) *γ* = 81.353(2)	*a* = 13.7645(6) *b* = 26.9797(11) *c* = 11.5721(4) *α* = 90 *β* = 93.3297(15) *γ* = 90	*a* = 11.2401(4) *b* = 11.9427(5) *c* = 12.9055(5) *α* = 105.5226(14) *β* = 94.7259(13) *γ* = 104.8100(14)
Volume (Å^3)	1530.52(11)	8260.2(4)	1583.95(14)	4290.2(3)	1592.44(11)
Z	2	8	2	4	2
Density (calculated, Mg/m^3)	1.569	1.178	1.277	1.181	1.308
Absorption coefficient (mm^{-1})	2.861	0.079	0.090	0.080	0.094
F(000)	728	3120	640	1626	660
Crystal size (mm^3)	0.148x0.123x0.022	0.158x0.101x0.017	0.207x0.121x0.016	0.158x0.135x0.028	0.198x0.154x0.078
Theta range of data (º)	1.870 to 33.140	1.867 to 26.394	2.204 to 26.369	2.116 to 26.436	2.082 to 33.135
Index ranges (*h*, *k*, *l*)	-16/16, -19/19, -20/20	-34/36, -14/14, -27/30	-7/7, -17/17, -23/23	-17/16, -33/33, -14/13	-17/17, -18/18, -19/19
Reflections collected	114108	98626	83187	96901	158612
Independent reflections	11673	15965	6492	8797	12136
R(int)	0.0516	0.0858	0.0616	0.0577	0.0376
Completeness to 25.242º (%)	100	99.9	99.9	99.9	99.9
Max. and min. transmission	0.5676 and 0.4648	0.7454 and 0.6559	0.7457 and 0.6702	0.7454 and 0.6740	0.7465 and 0.7155
Data / restrains / parameters	11673 / 64 / 431	15965 / 2131 /1321	6492 / 91 / 486	8797 / 1298 / 762	12136 / 974 / 631
Goodness-of-fit on F^2	1.033	1.097	1.195	1.106	1.134
Final R indices [I>2sigma(I)]	R1 = 0.0356 wR2 = 0.0730	R1 = 0.0739 wR2 = 0.1585	R1 = 0.0663 wR2 = 0.11323	R1 = 0.0884 wR2 = 0.1956	R1 = 0.0581 wR2 = 0.1581
R indices (all data)	R1 = 0.0614 wR2 = 0.0835	R1 = 0.1087 wR2 = 0.1742	R1 = 0.0804 wR2 = 0.1397	R1 = 0.1137 wR2 = 0.2097	R1 = 0.0811 wR2 = 0.1905
Largest diff. peak and hole (e.Å^{-3})	0.891 and -1.27	0.323 and -0.313	0.318 and -0.219	0.271 and -0.248	0.529 and -0.364

Table S4: O-H…Acceptor hydrogen bonds in the structures studied [Å and °].

D-H...A	d(D-H)	d(H...A)	d(D...A)	<(DHA)
Compound 2				
O(1)-H(1A)...O(1)#1	0.87(3)	2.53(3)	3.359(4)	159(6)
O(1)-H(1A)...O(4)#2	0.87(3)	2.68(6)	2.931(3)	98(4)
O(1)-H(1B)...O(4)#3	0.87(3)	2.03(3)	2.898(3)	177(6)
O(2)-H(2B)...N(3B)	0.87(3)	1.99(4)	2.772(6)	149(6)
O(2)-H(2A)...O(3)#3	0.87(3)	1.84(3)	2.681(3)	161(8)
O(3)-H(3B)...O(2)#3	0.87(3)	1.82(3)	2.681(3)	171(7)
O(3)-H(3A)...N(3A)	0.87(3)	1.87(3)	2.699(5)	157(5)
O(4)-H(4B)...O(1)#4	0.87(3)	2.18(4)	2.931(3)	145(5)
O(4)-H(4A)...O(1)#3	0.86(3)	2.05(3)	2.898(3)	168(4)
Compound 3				
O(1A)-HO1A...O(2A)#5	0.912(16)	2.446(17)	3.356(3)	176(3)
O(2A)-HO2A...O(5A)	0.906(16)	2.059(17)	2.955(2)	170(3)
O(3A)-HO3A...O(5A)	0.927(16)	1.850(19)	2.741(2)	160(3)
O(4A)-HO4A...O(1A)#5	0.917(16)	1.929(17)	2.839(4)	171(3)
O(5A)-HO5A...N(3)	0.912(16)	2.152(18)	3.033(3)	162(3)
O(5A)-HO5B...F(2A)	0.921(16)	2.45(2)	3.288(7)	151(2)
O(5A)-HO5B...F(2A)#6	0.921(16)	2.10(2)	2.827(6)	135(3)
O(1B)-HO1C...O(2B)#5	0.86	1.72	2.55(3)	159.3
O(1B)-HO1C...O(3B)#5	0.86	2.44	2.96(2)	119.2
O(2B)-HO2D...O(3B)	0.90	2.04	2.764(19)	136.7
O(2B)-HO2C...O(1B)#5	0.90	1.96	2.55(3)	122.4
O(2B)-HO2C...O(2B)#5	0.90	1.72	2.58(2)	159.5
O(5B)-HO5C...F(1B)	0.91	1.74	2.52(3)	142.4
O(5B)-HO5D...N(3)	0.90	1.63	2.504(15)	162.7
O(3B)-HO3C...O(1B)#5	0.91	2.29	2.96(2)	130.2
O(3B)-HO3C...O(2B)	0.91	1.94	2.764(19)	148.8
O(3B)-HO3D...O(5B)	0.91	1.90	2.80(2)	174.1
O(4B)-HO4C...O(1B)#5	0.89	1.53	2.42(2)	174.2

Symmetry transformations used to generate equivalent atoms: #1 -x,-y,-z+1 #2 x,y-1,z #3 -x-1,-y+1,-z+1 #4 x,y+1,z #5 -x+1,-y+1,-z+2 #6 -x+1,-y+1,-z+1

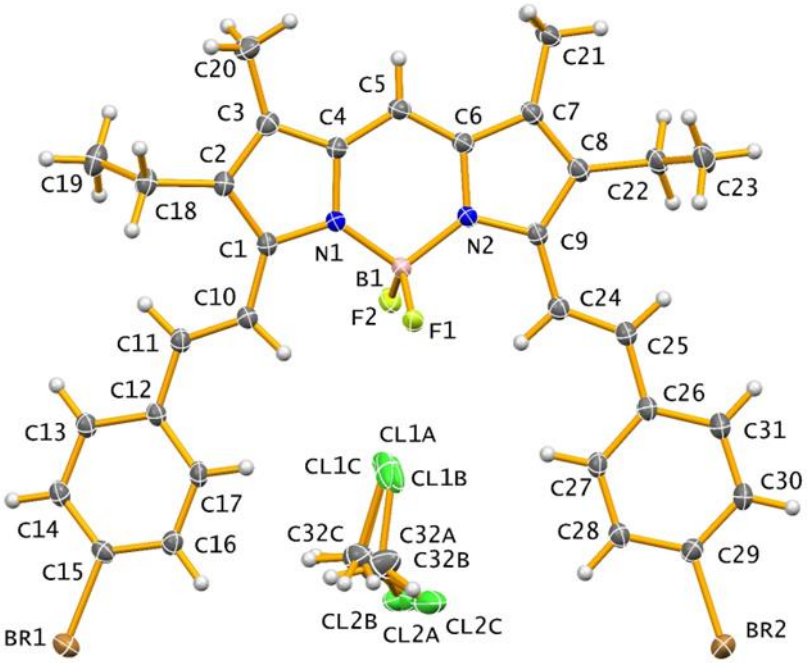

Figure S61: Structure of compound **5** with full labelling, including one molecule of disordered dichloromethane solvent. Thermal ellipsoids have been drawn at the 50% probability level. Hydrogen atoms are included but have not been labelled.

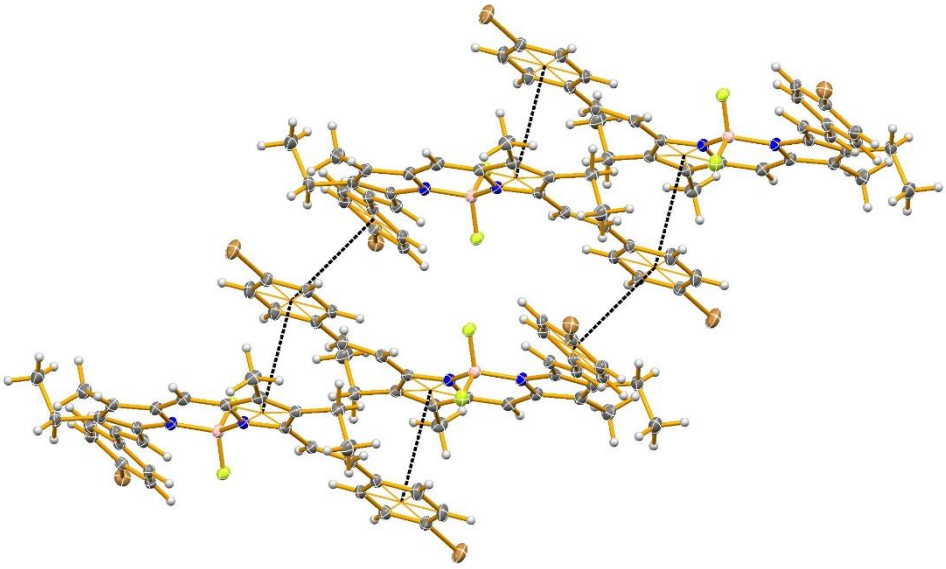

Figure S62: Intermolecular stacking contacts less than 3.8 Å (dashed lines) in compound **5**. Thermal ellipsoids have been drawn with 50% probability.

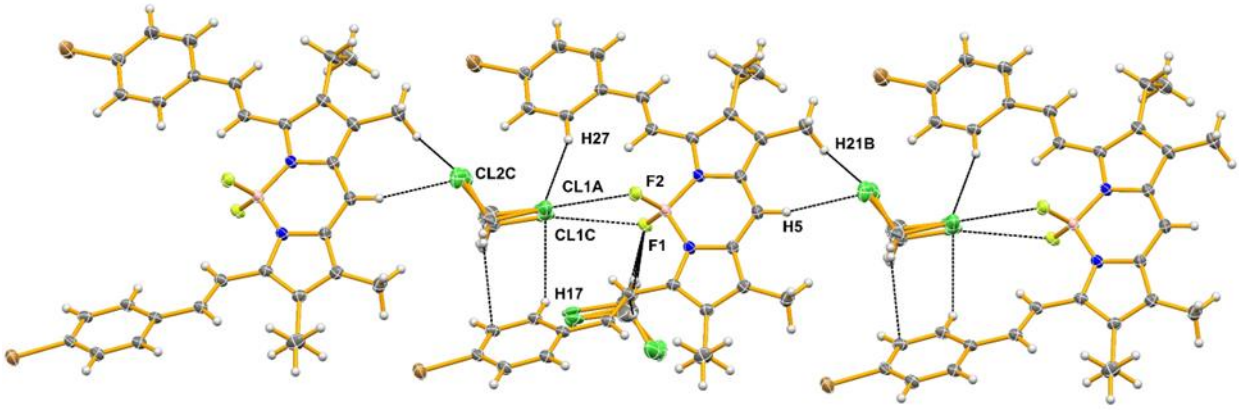

Figure S63: Intermolecular contacts involving the solvent (dashed lines – less than the sum of the van der Waals radii) in compound **5**. Thermal ellipsoids have been drawn with 50% probability. Only selected atoms have been labelled.

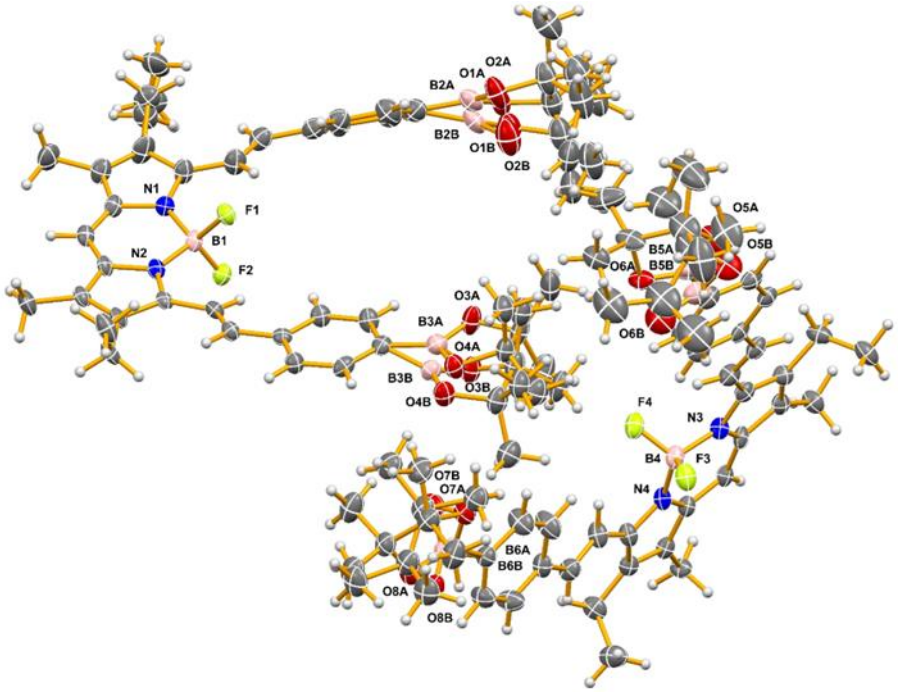

Figure S64: Structure of compound **6** with only the non-carbon atoms labelled. Disorder has not been removed. Thermal ellipsoids have been drawn at the 50% probability level. Hydrogen atoms are included but have not been labelled.

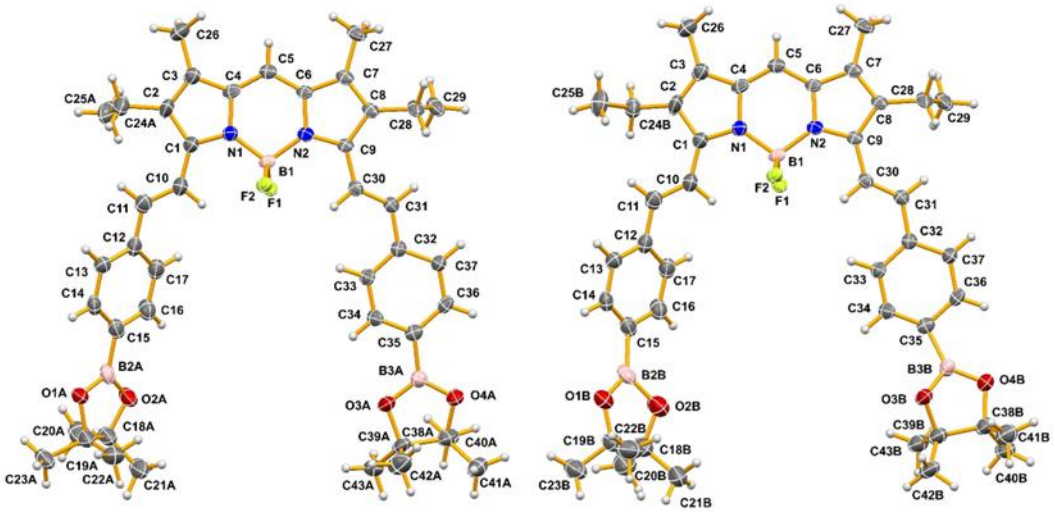

Figure S65: Composite diagram showing the two components of the disordered model used to refine molecule 1 in compound **6** with full labelling. In the center is the disordered molecule, while on the left is the contribution of part A (major) and on the right is part B (minor). Thermal ellipsoids have been drawn at the 50% probability level. Hydrogen atoms are included but have not been labelled.

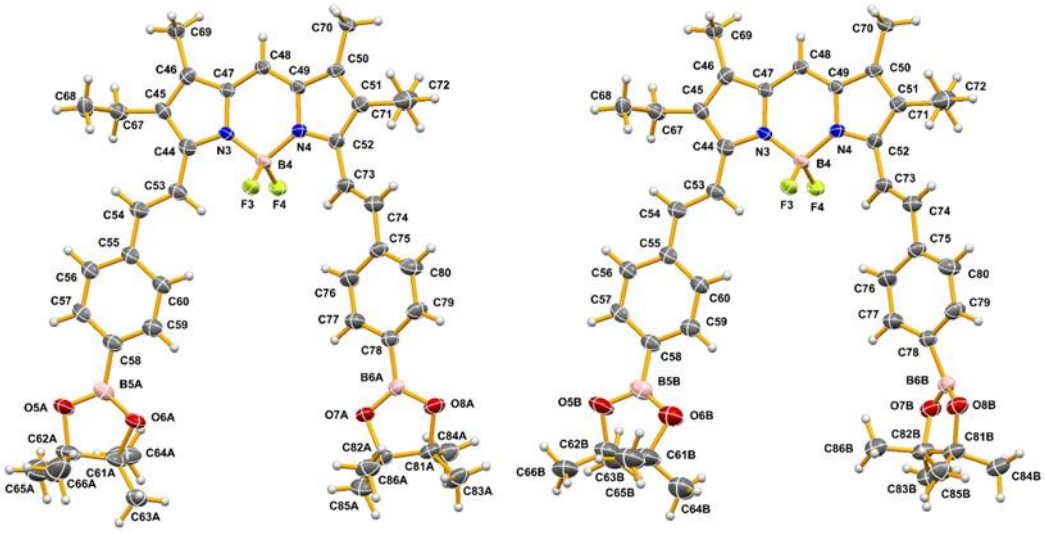

Figure S66: Composite diagram showing the two components of the disordered model used to refine molecule 2 in compound **6** with full labelling. In the center is the disordered molecule, while on the left is the contribution of part A (major) and on the right is part B (minor). Thermal ellipsoids have been drawn at the 50% probability level. Hydrogen atoms are included but have not been labelled.

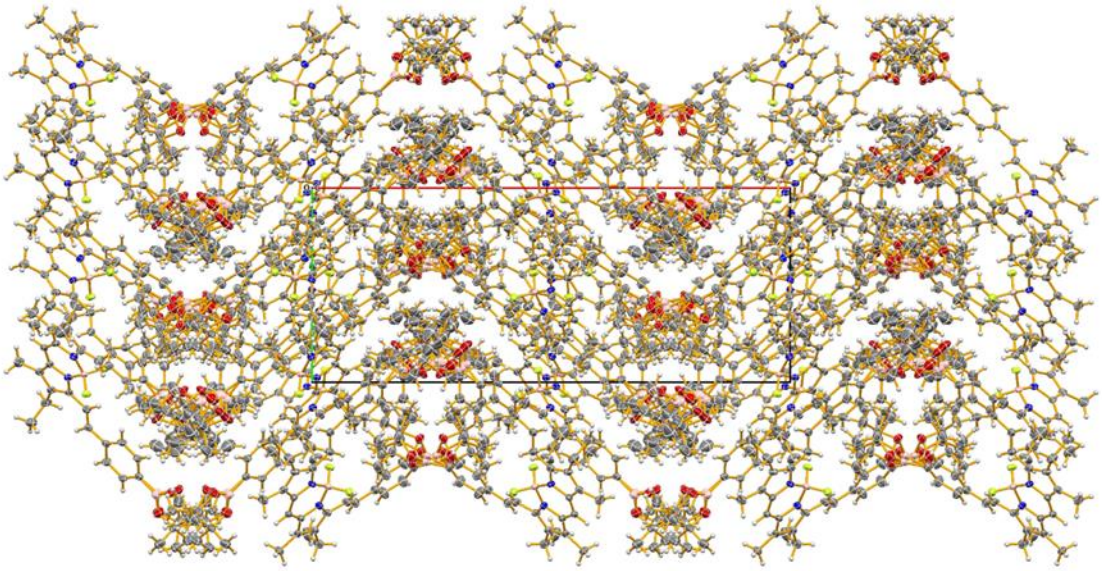

Figure S67: Packing diagram of compound **6** viewed down the C-axis.

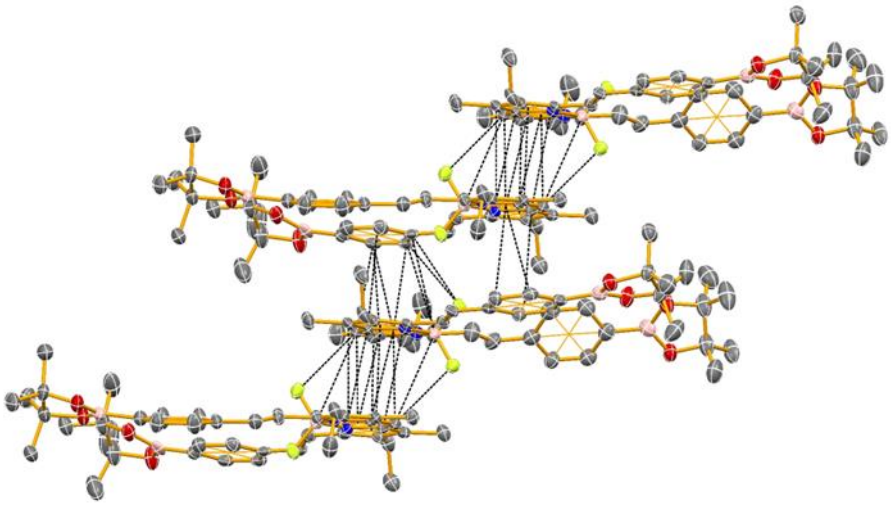

Figure S68: Intermolecular stacking contacts less than 3.8 Å (dashed lines) for part A of compound **6**. Intermolecular interactions less then the sum of the van der Waals radii plus 0.2 Å between these molecules are also shown. Thermal ellipsoids have been drawn with 50% probability. Atoms have not been labelled. Hydrogen atoms have been omitted for clarity.

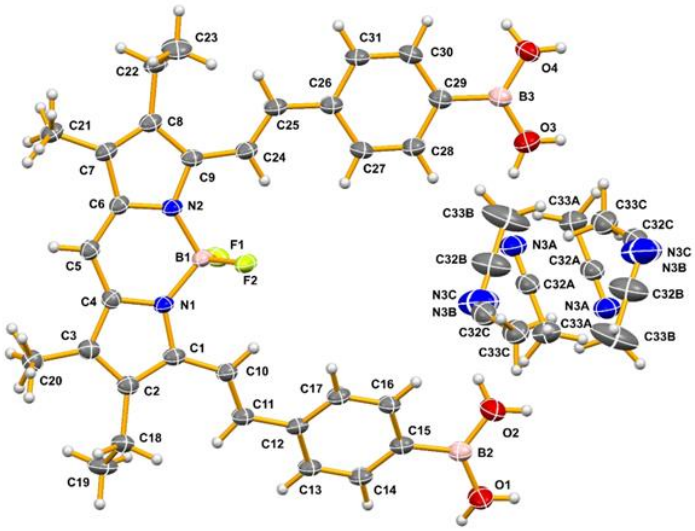

Figure S69: Structure of compound **2** with full labelling, including two molecules of disordered acetonitrile solvent. The hydrogen atoms bonded to oxygen are also disordered over two positions with partial occupancies. Thermal ellipsoids have been drawn at the 50% probability level. Hydrogen atoms are included but have not been labelled.

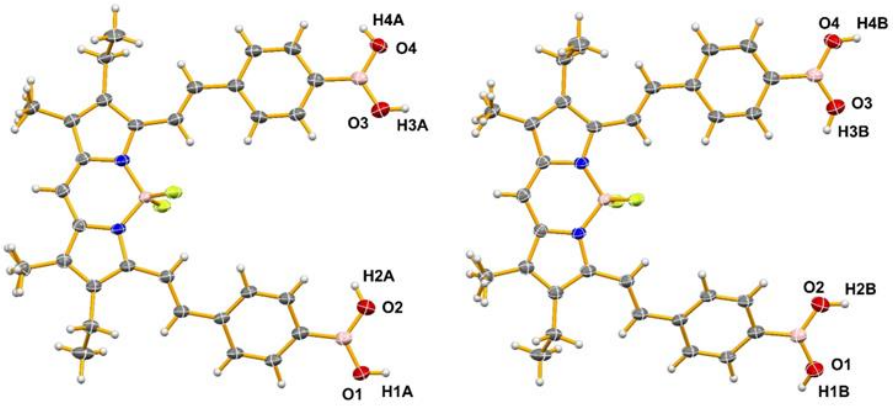

Figure S70: Composite diagram showing the two components of the disordered model used to refine the $B(OH)_2$ groups in compound **2**, part A(left) and part B (right). Thermal ellipsoids have been drawn at the 50% probability level. Other hydrogen atoms are included but have not been labelled.

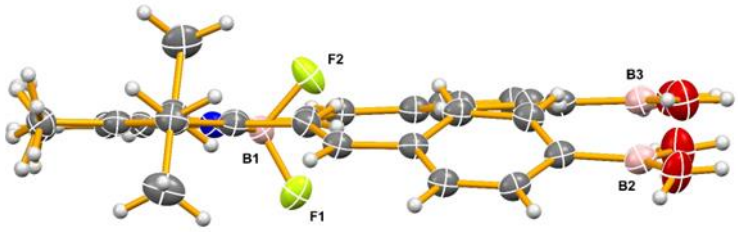

Figure S71: Perpendicular view of compound **2** with selected atoms labelled. Note the twisting of one ring relative to the rest of the atoms in the plane. Thermal ellipsoids have been drawn at the 50% probability level. Hydrogen atoms are included but have not been labelled.

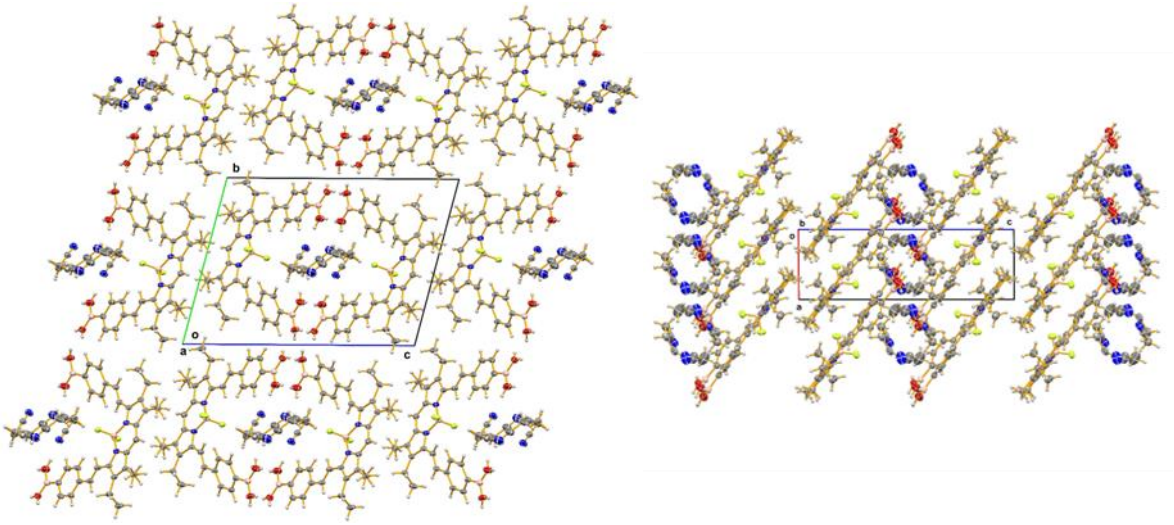

Figure S72: Packing diagrams of compound **2** viewed down the A-axis (left) and B-axis (right).

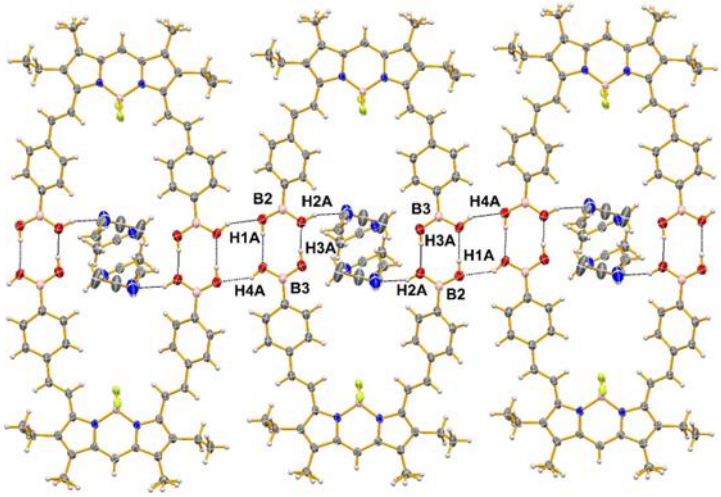

Figure S73: An overall view of the network of hydrogen bonds (dashed lines – less than the sum of the van der Waals radii + 0.2 Å) in Part A of compound **2**. Thermal ellipsoids have been drawn with 50% probability. Only selected atoms have been labelled.

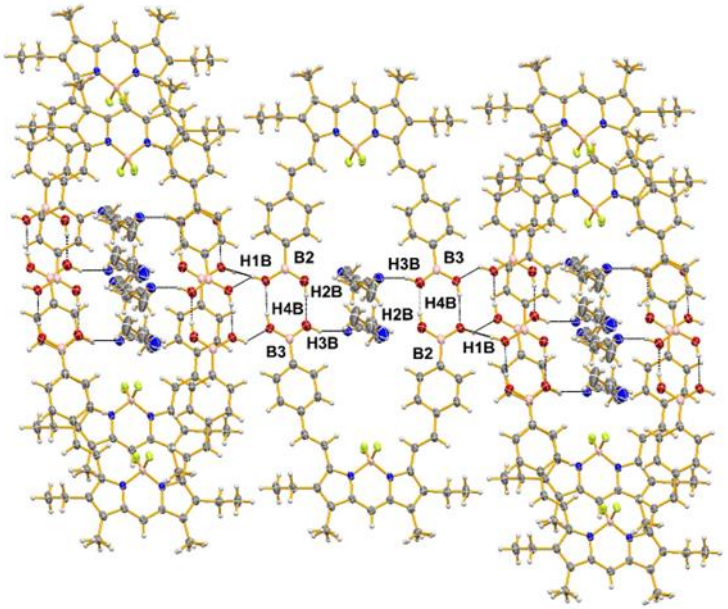

Figure S74: An overall view of the network of hydrogen bonds (dashed lines – less than the sum of the van der Waals radii + 0.2 Å) in Part B of compound **2**. Thermal ellipsoids have been drawn with 50% probability. Only selected atoms have been labelled.

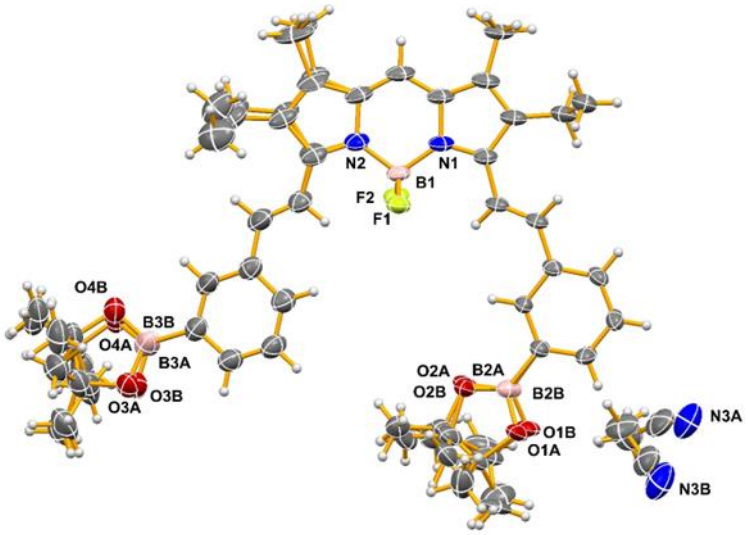

Figure S75: The disordered structure of compound **7** with only the non-carbon atoms labelled. There are 3 molecules of disordered acetonitrile solvent for every four molecules of **7**. Thermal ellipsoids have been drawn at the 50% probability level. Hydrogen atoms are included but have not been labelled.

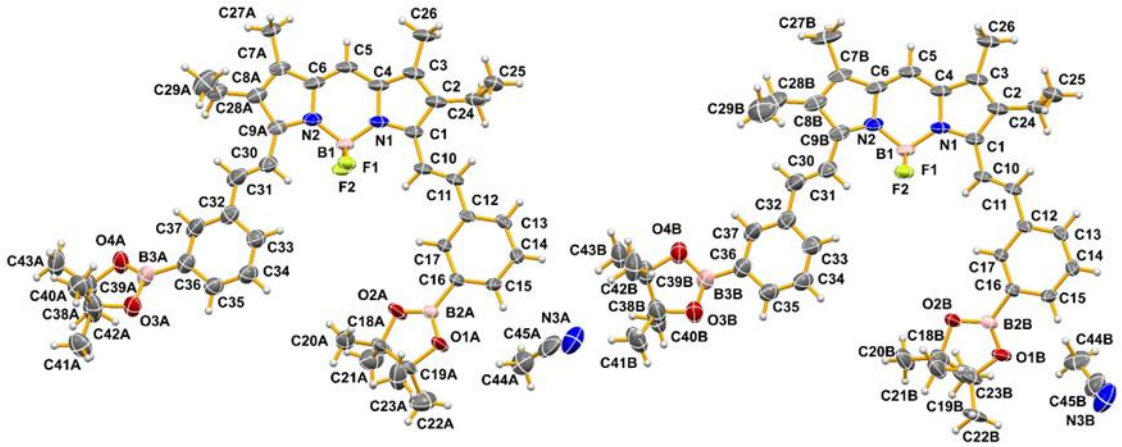

Figure S76: Composite diagram showing the two components of the disordered model used to refine compound **7**, part A(left) and part B (right). Thermal ellipsoids have been drawn at the 50% probability level. Hydrogen atoms are included but have not been labelled.

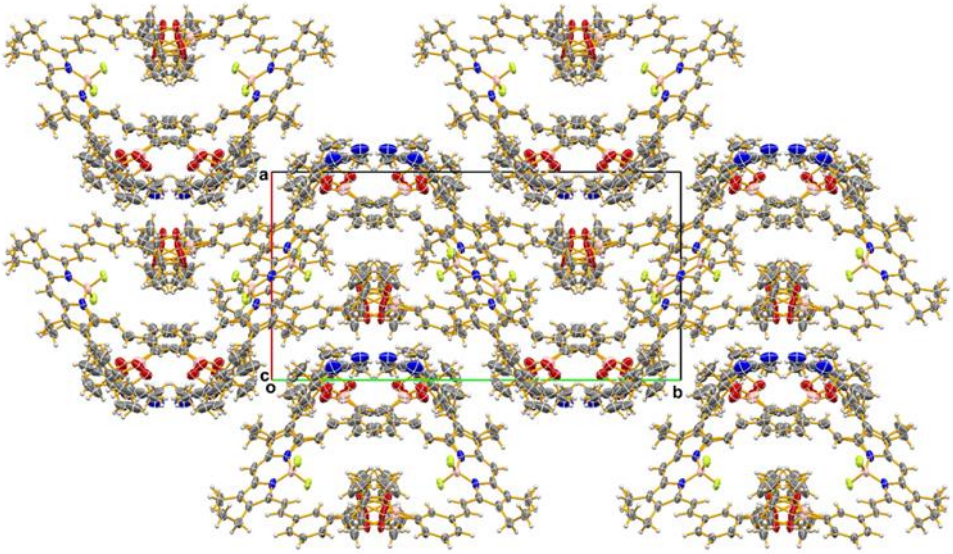

Figure S77: Packing diagram of compound **7** viewed down the C-axis.

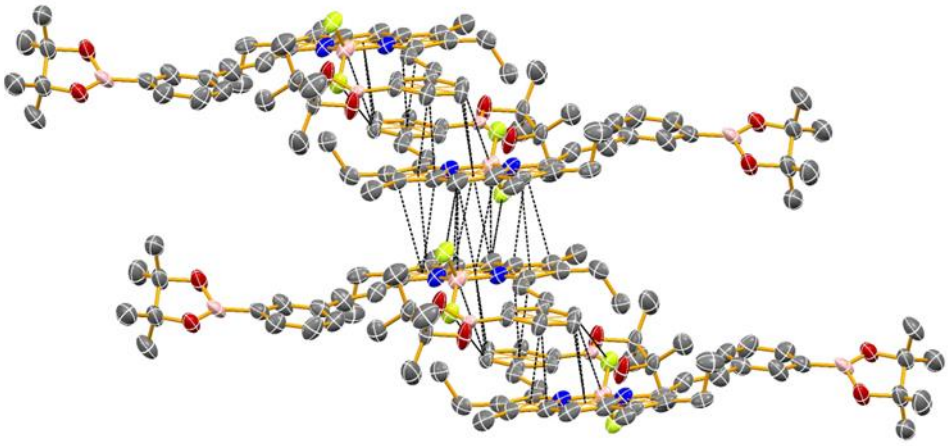

Figure S78: Intermolecular stacking contacts less than 3.8 Å (dashed lines) for part A of compound **7**. Intermolecular interactions less then the sum of the van der Waals radii plus 0.2 Å between these molecules are also shown. Thermal ellipsoids have been drawn with 50% probability. Atoms have not been labelled. Hydrogen atoms have been omitted for clarity.

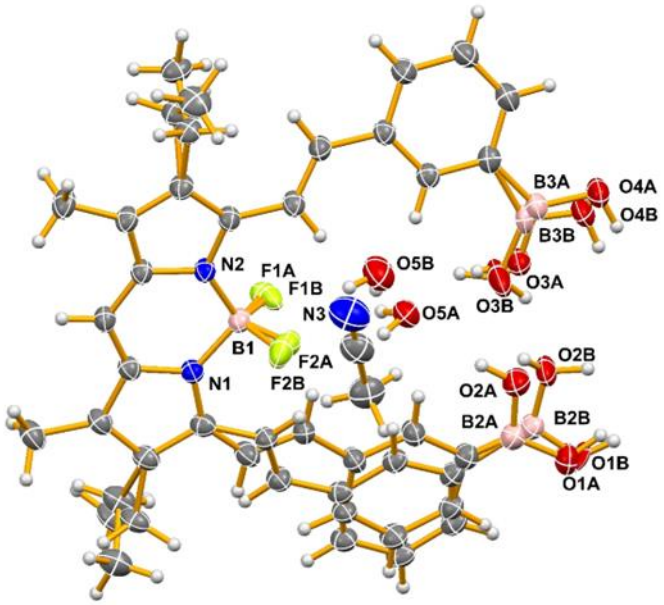

Figure S79: The disordered structure of compound **3** with only the non-carbon atoms labelled. There is one molecule of disordered water and one molecule of acetonitrile for every molecule of **3**. Thermal ellipsoids have been drawn at the 50% probability level. Hydrogen atoms are included but have not been labelled.

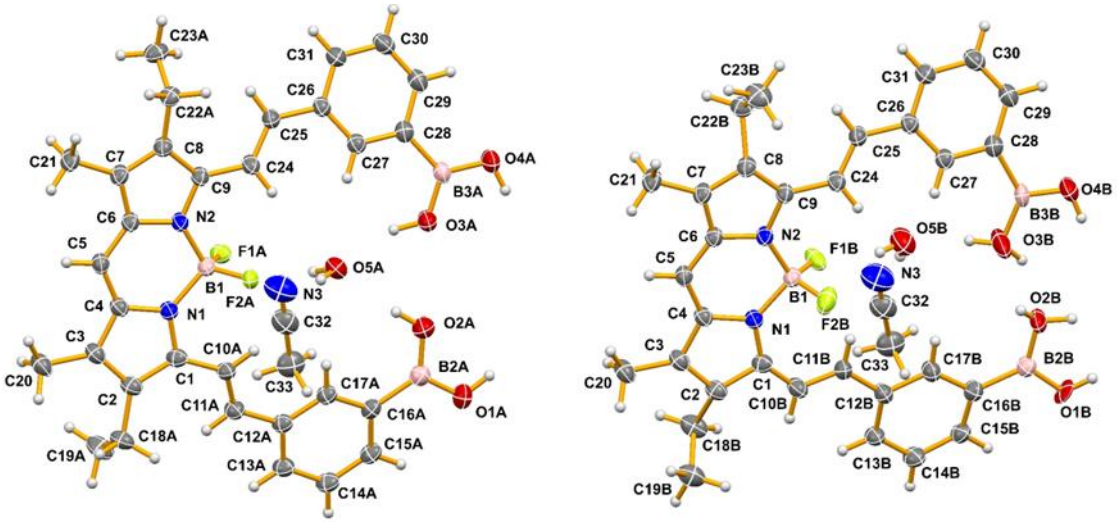

Figure S80: Composite diagram showing the two components of the disordered model used to refine compound **3**, part A(left) and part B (right). Note that in part B, the hydrogen atoms on O2B and O3B are still disordered; the total occupancy is one hydrogen on each oxygen. Thermal ellipsoids have been drawn at the 50% probability level. Hydrogen atoms are included but have not been labelled.

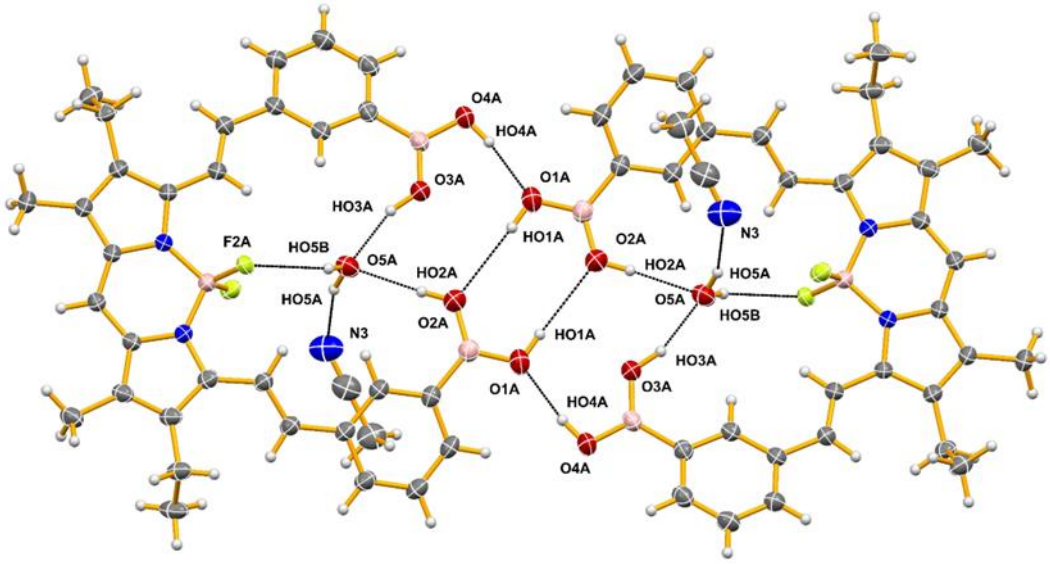

Figure S81: An overall view of the ordered network of hydrogen bonds (dashed lines – less than the sum of the van der Waals radii + 0.2 Å) formed by Part A of compound **3**. Thermal ellipsoids have been drawn with 50% probability. Only selected atoms have been labelled.

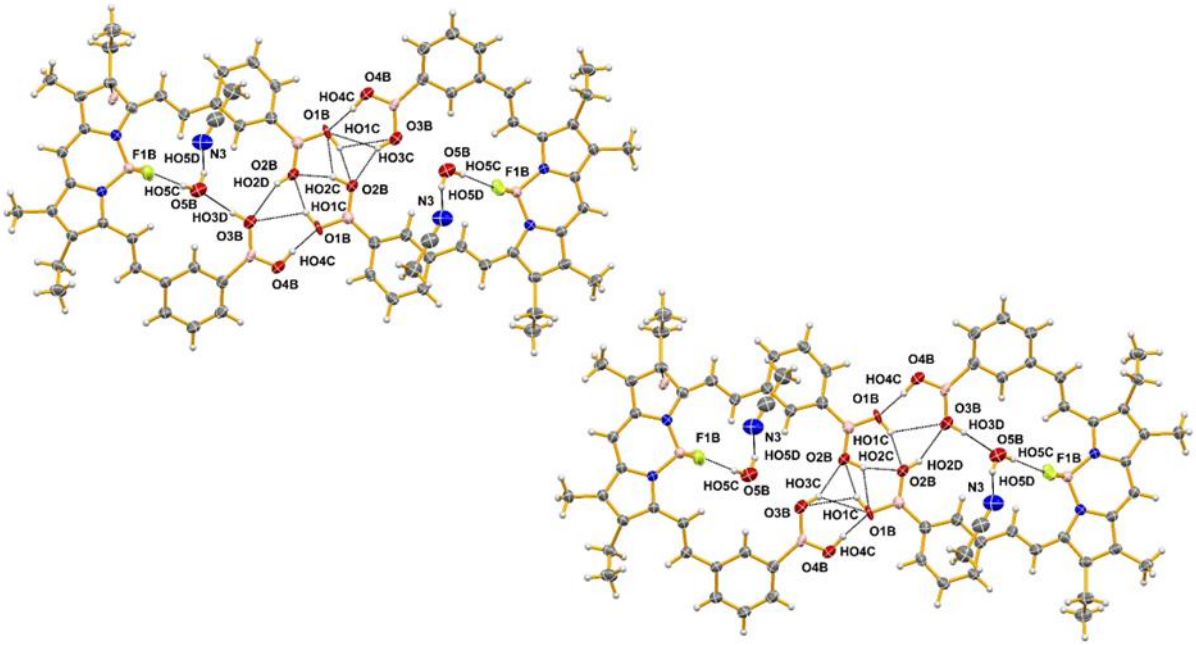

Figure S82: Composite view of the disordered network of hydrogen bonds (dashed lines – less than the sum of the van der Waals radii + 0.2 Å) formed by Part B of compound **3**. Thermal ellipsoids have been drawn with 50% probability. Only selected atoms have been labelled.

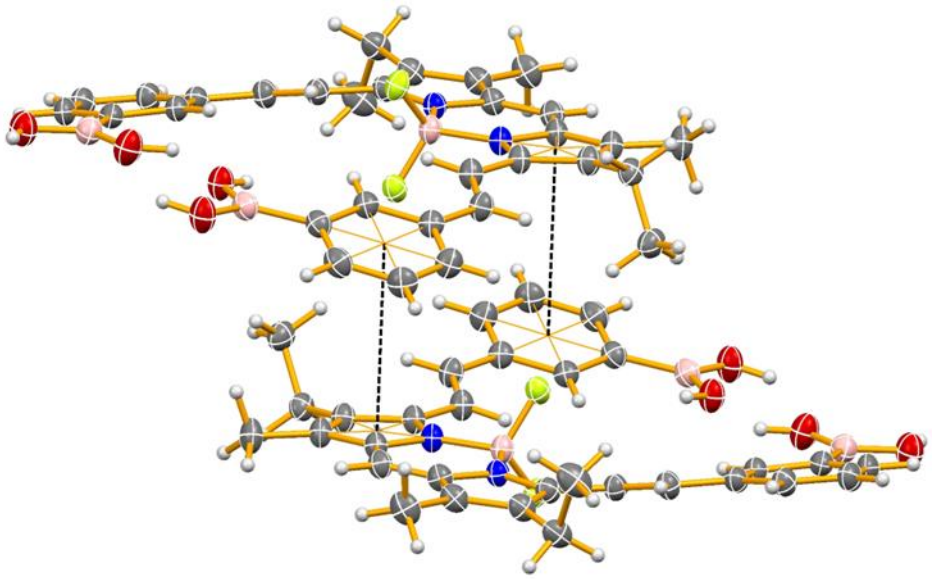

Figure S83: Intermolecular stacking contacts less than 3.9 Å (dashed lines) for part A of compound **3**. Thermal ellipsoids have been drawn with 50% probability. Atoms have not been labelled. Hydrogen atoms have been omitted for clarity.

NMR spectra

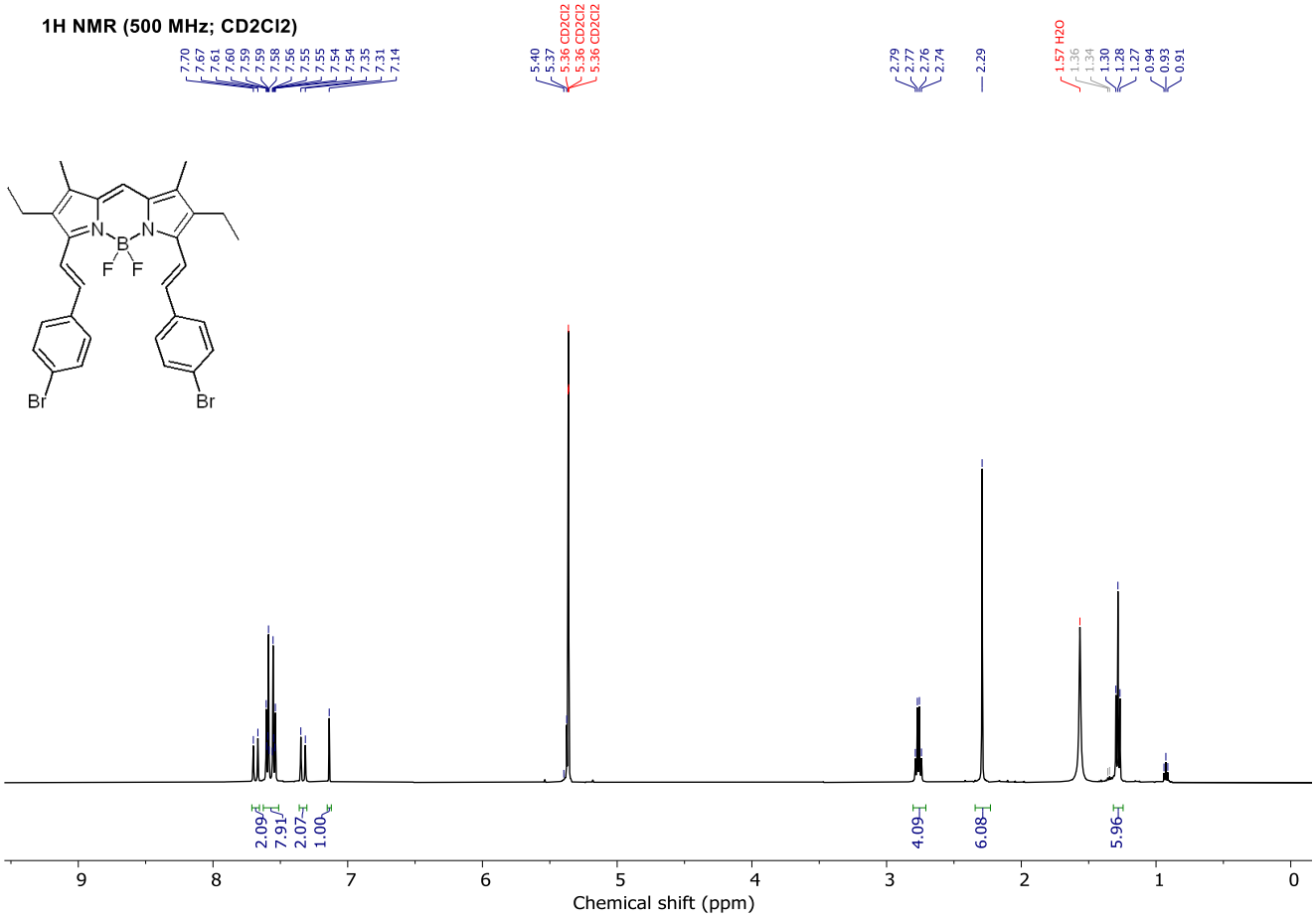

Figure S84: ^{1}H NMR spectrum of compound **5** in CD_2Cl_2.

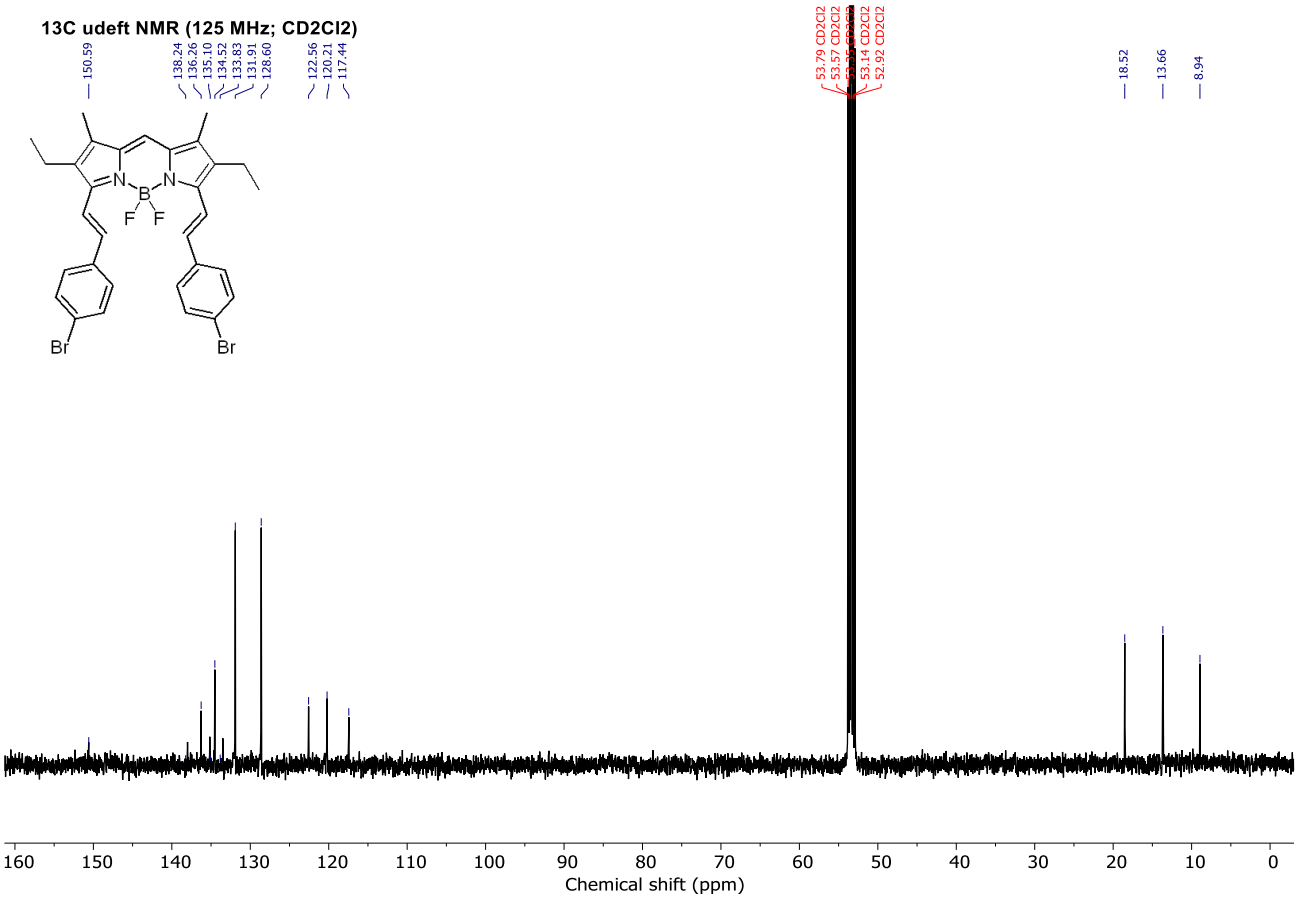

Figure S85: ^{13}C udeft NMR spectrum of compound **5** in CD_2Cl_2.

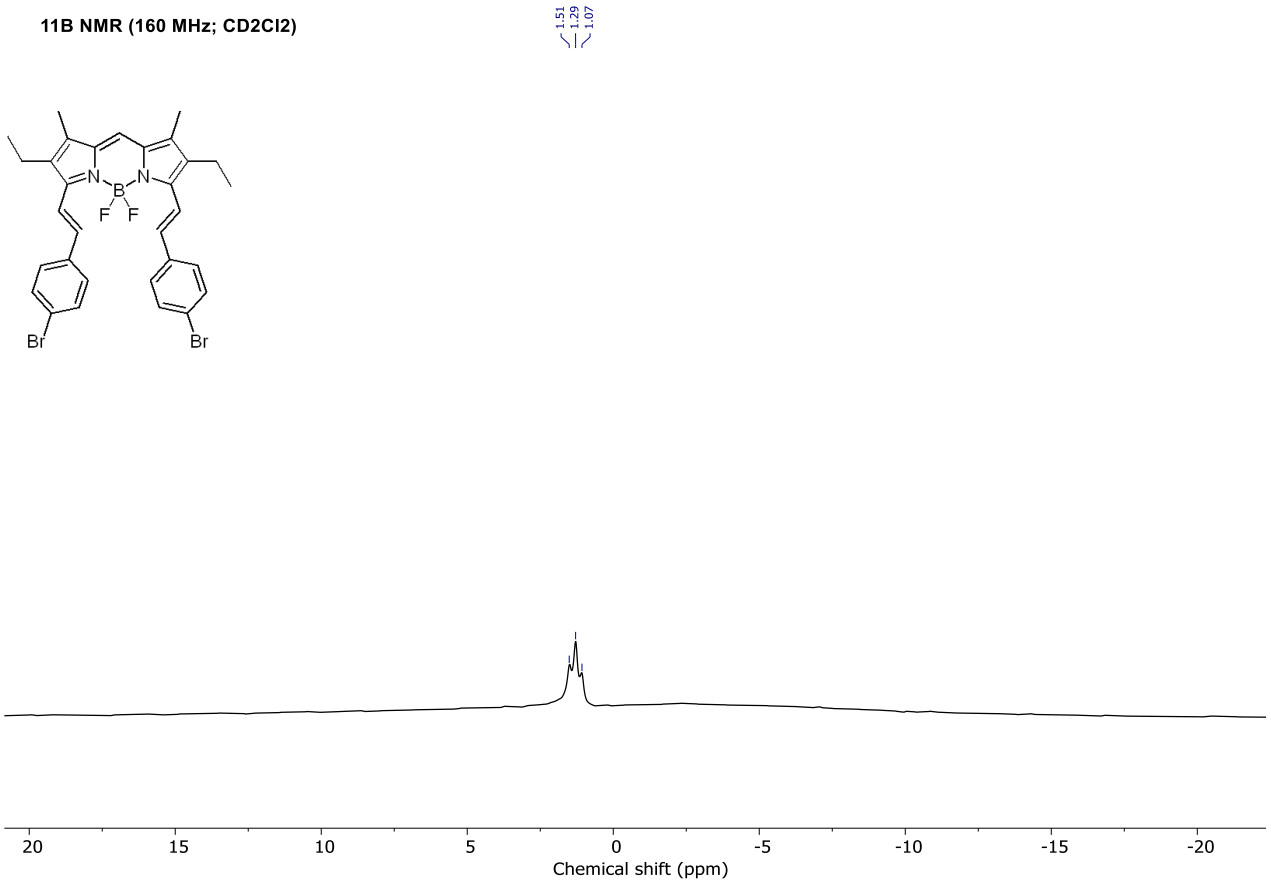

Figure S86: ^{11}B NMR spectrum of compound **5** in CD_2Cl_2.

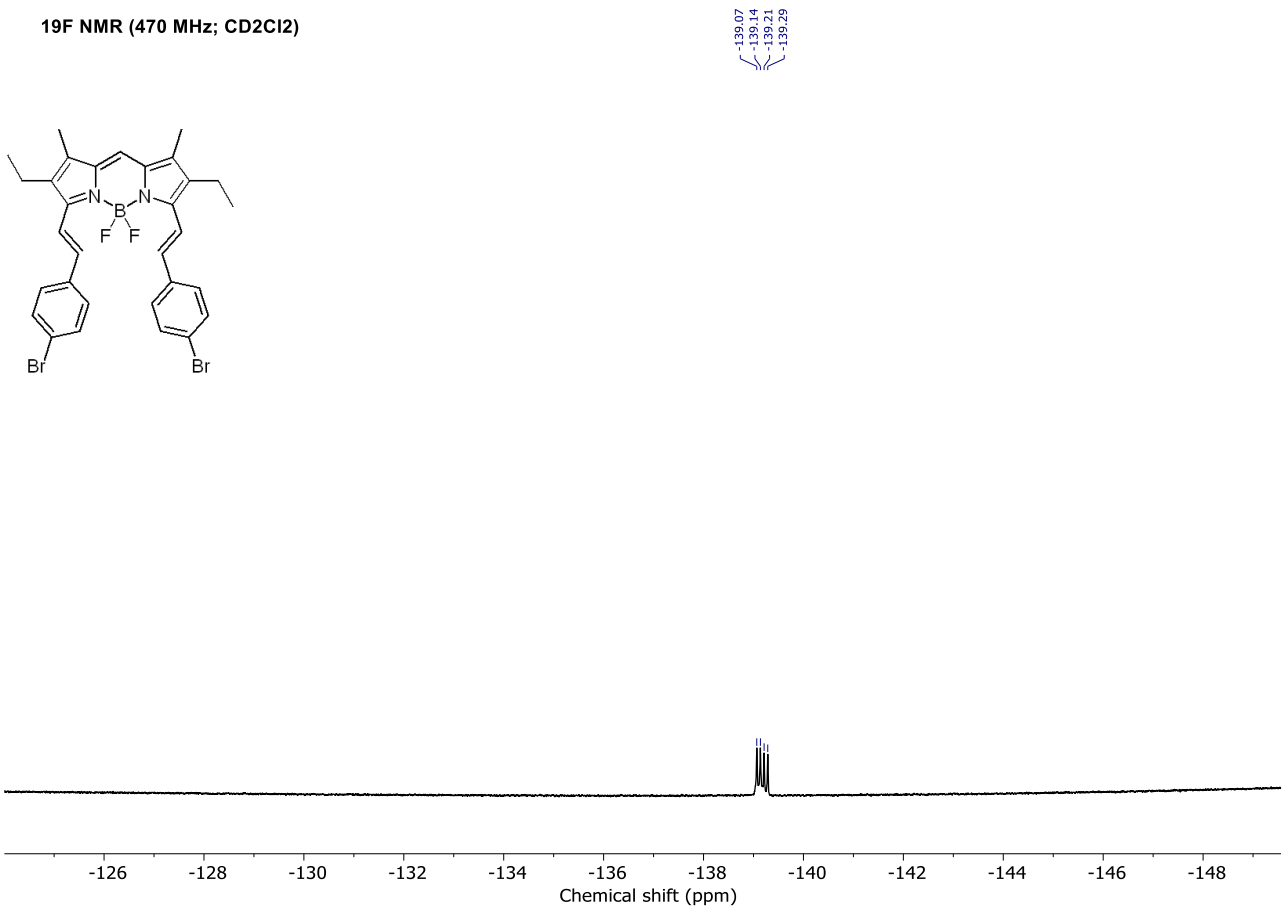

Figure S87: ^{19}F NMR spectrum of compound **5** in CD_2Cl_2.

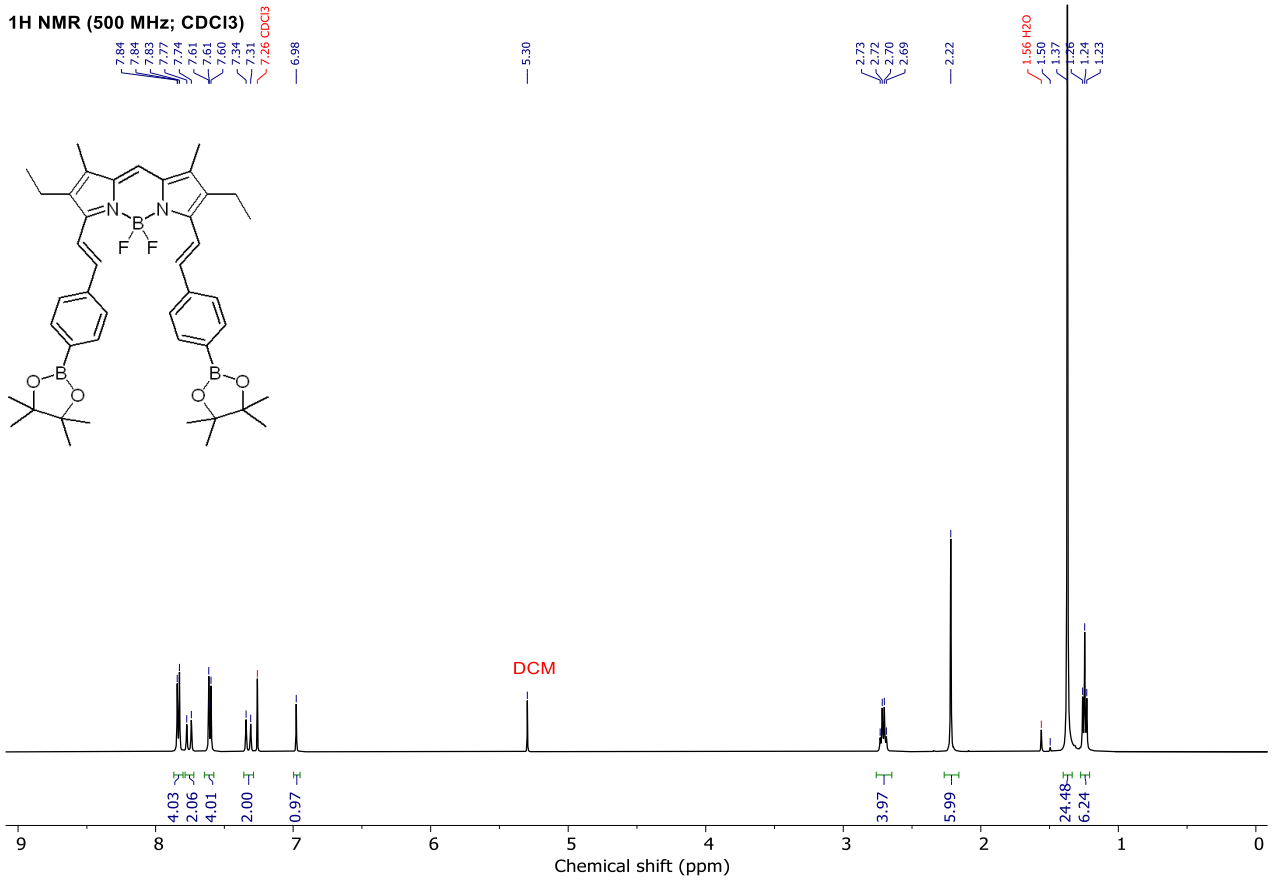

Figure S88: ^{1}H NMR spectrum of compound **6** in $CDCl_3$.

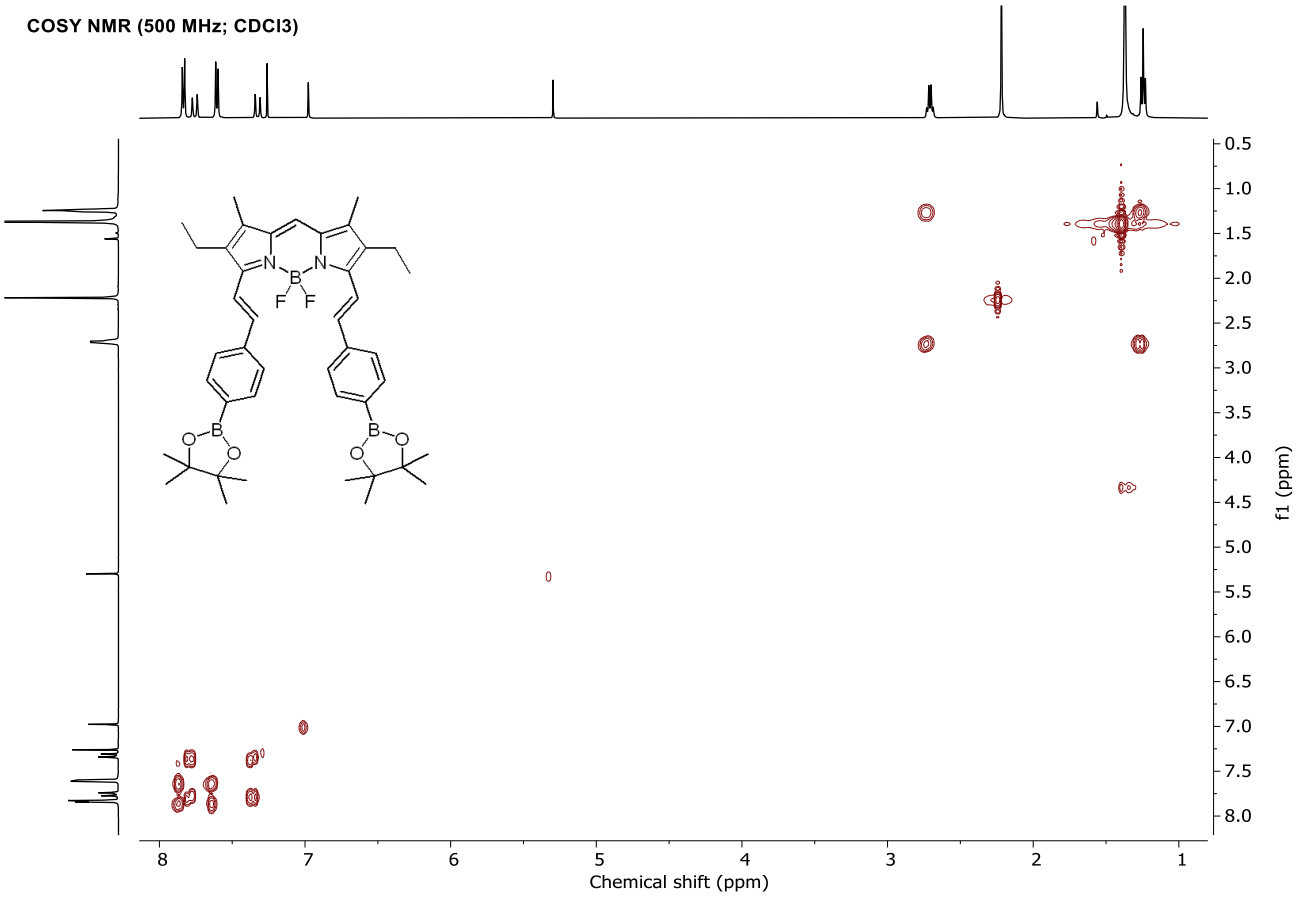

Figure S89: COSY NMR spectrum of compound **6** in $CDCl_3$.

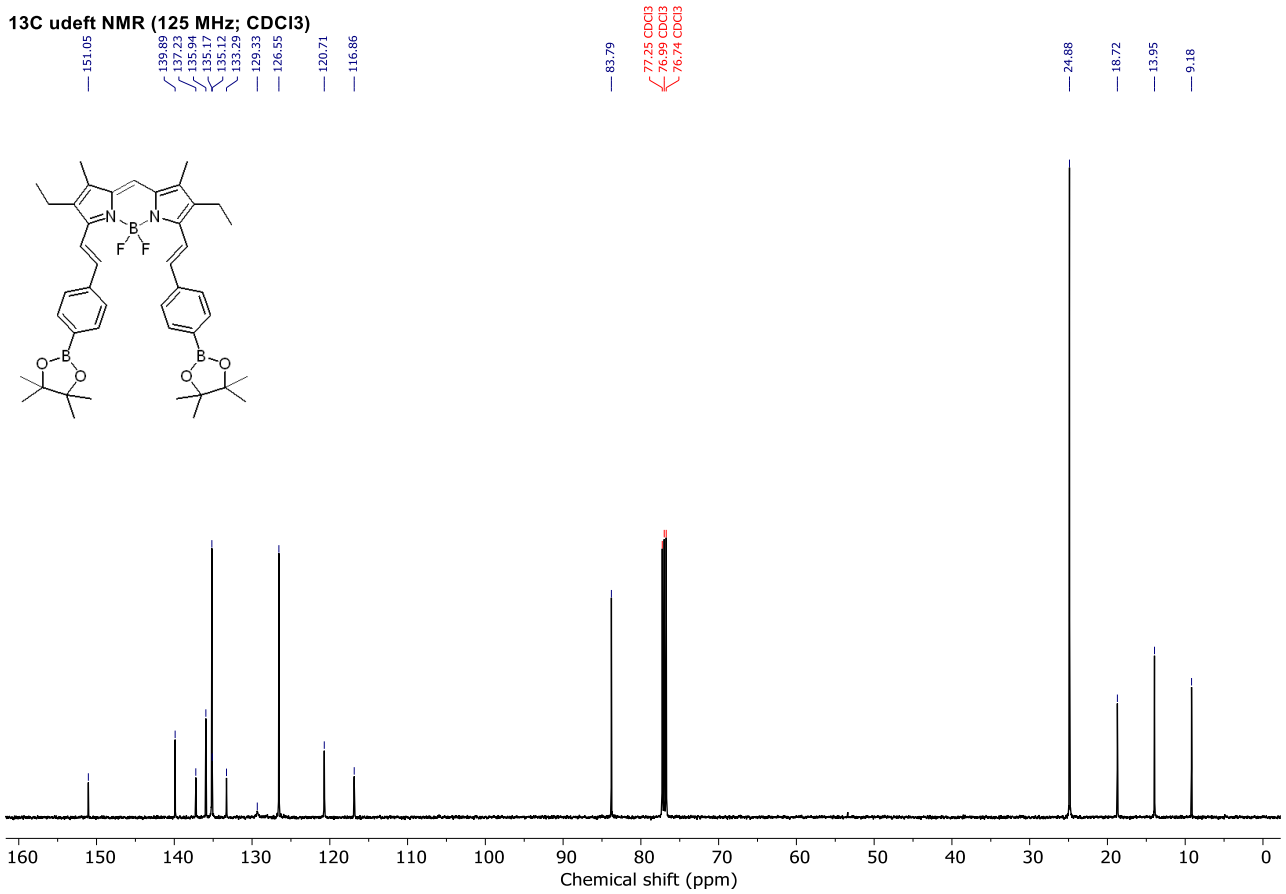

Figure S90: ^{13}C udeft NMR spectrum of compound **6** in $CDCl_3$.

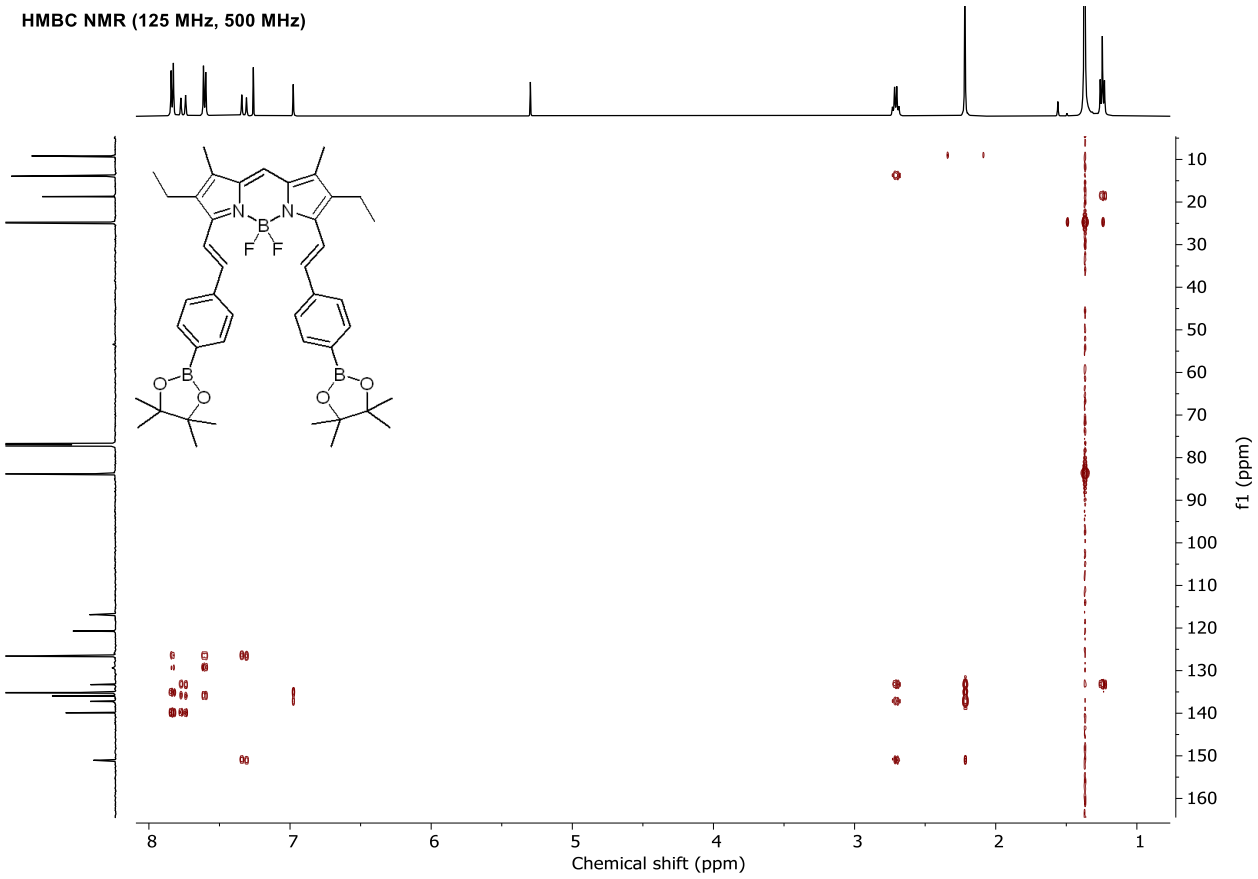

Figure S91: HMBC NMR spectrum of compound **6** in $CDCl_3$.

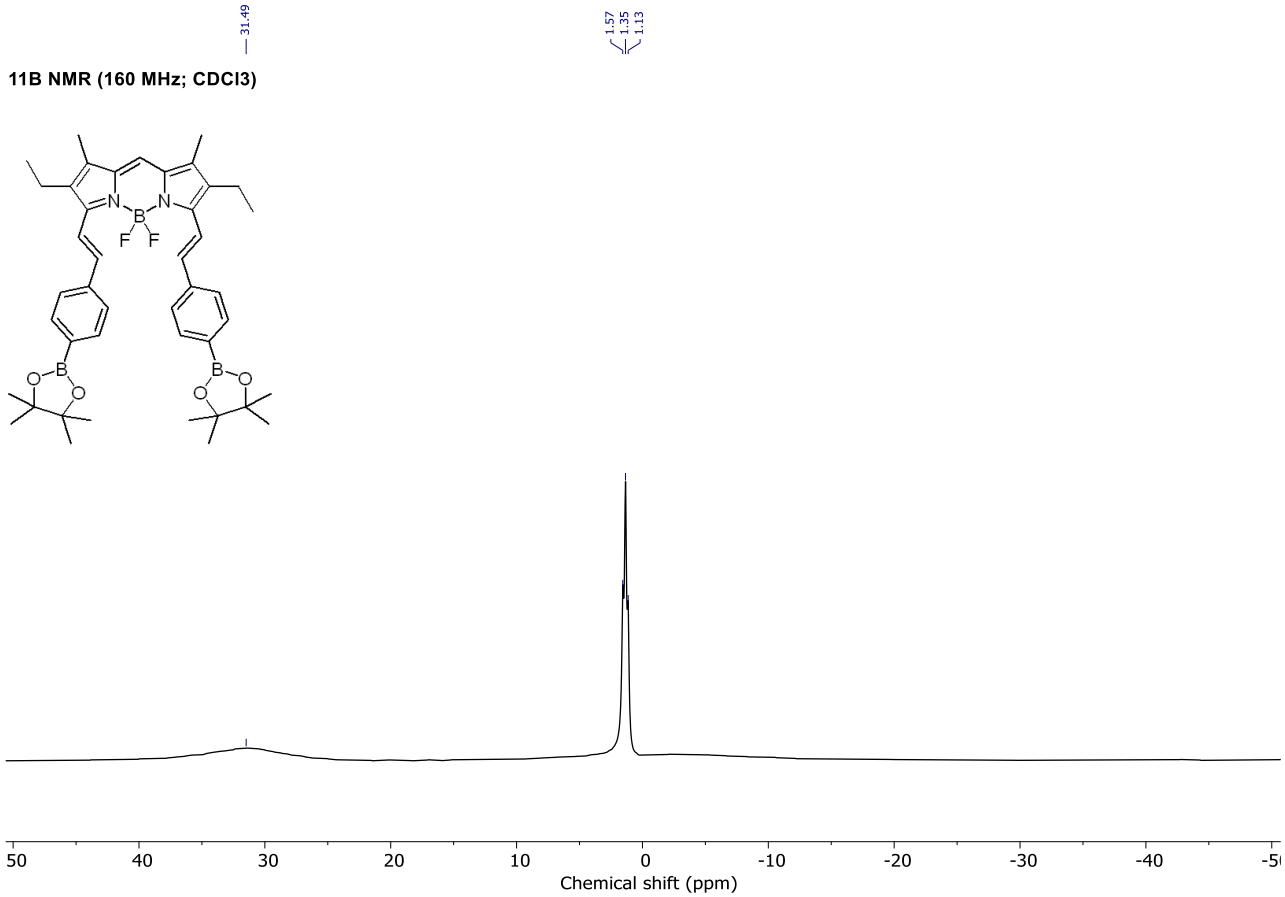

Figure S92: ^{11}B NMR spectrum of compound **6** in $CDCl_3$.

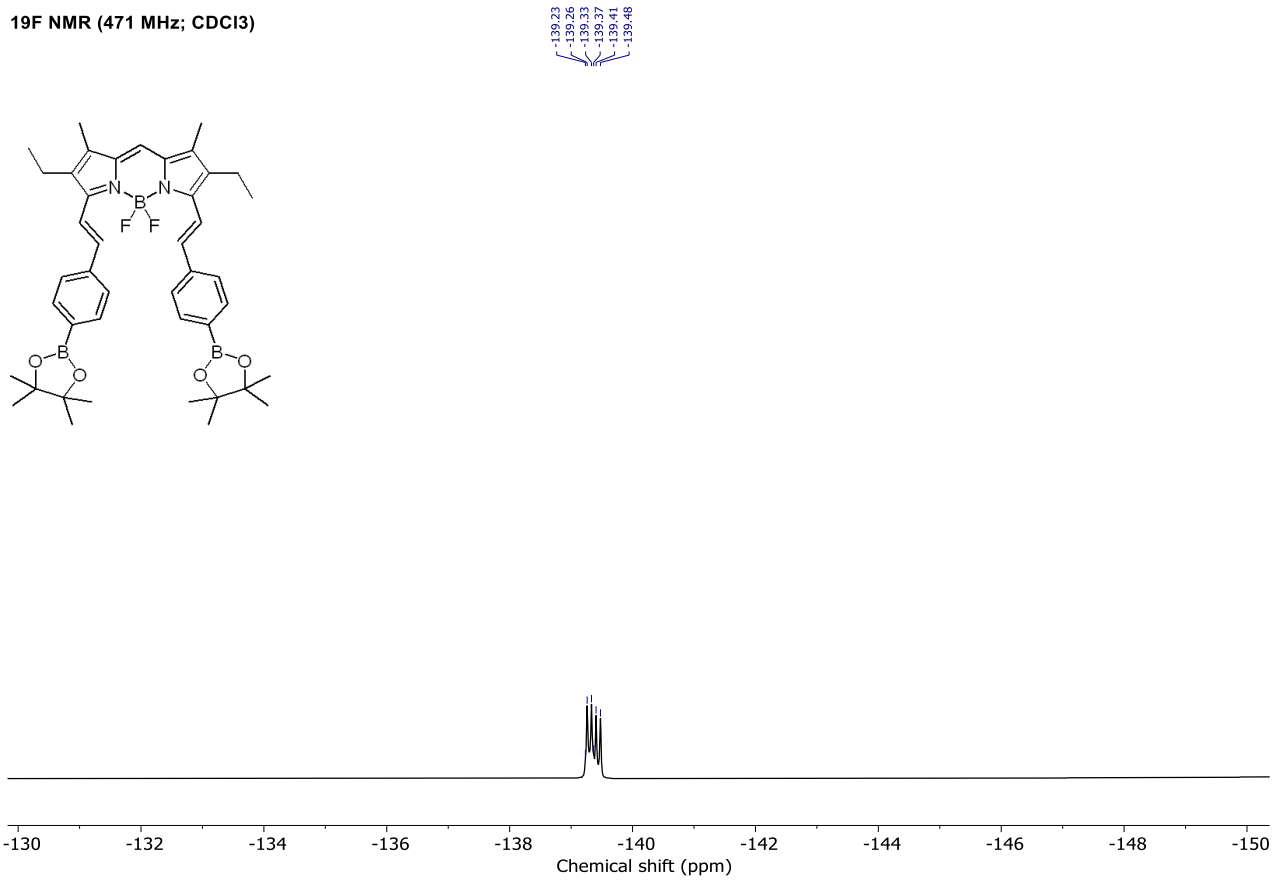

Figure S93: ^{19}F NMR spectrum of compound **6** in $CDCl_3$.

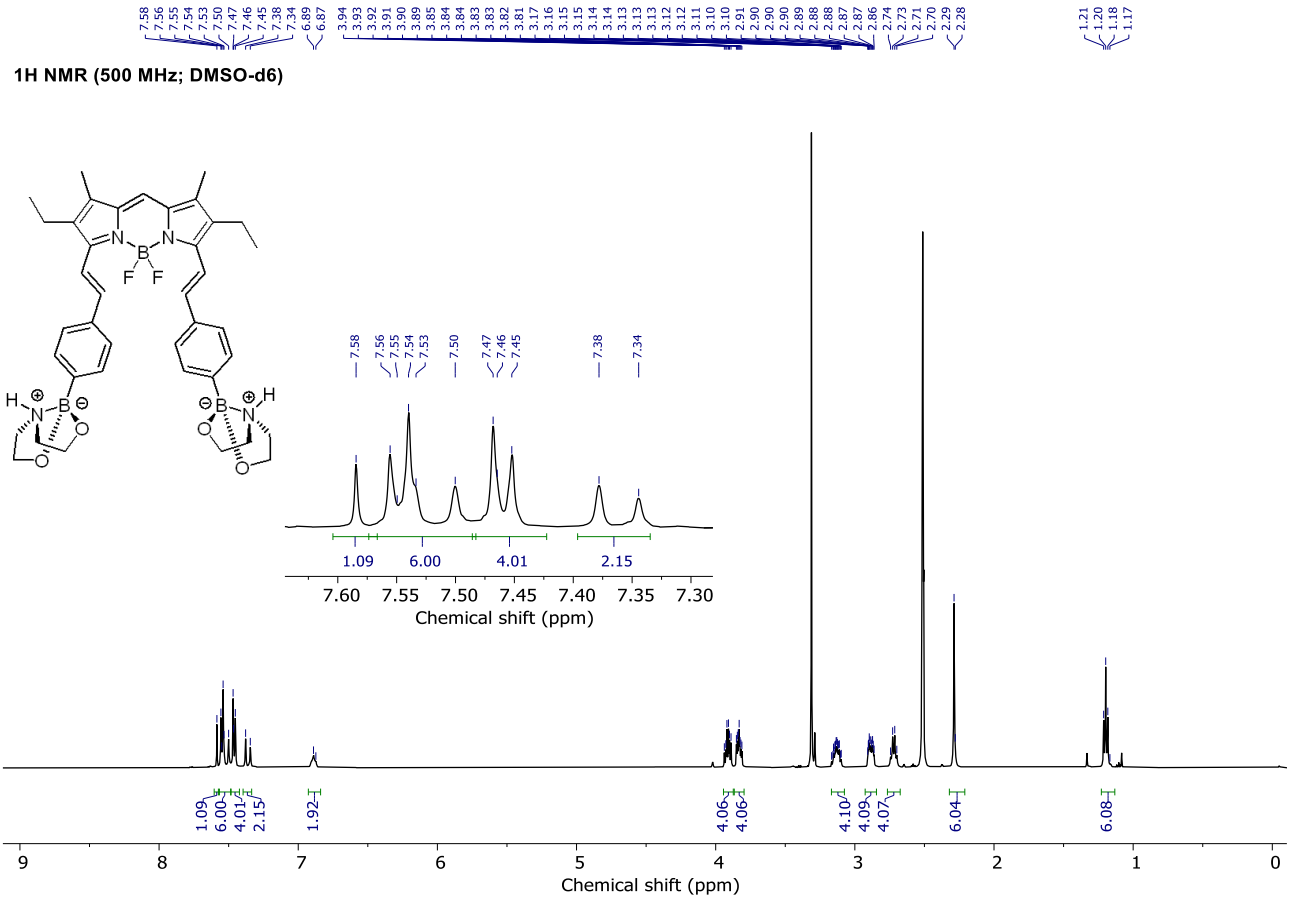

Figure S94: ^{1}H NMR spectrum of compound **8** in DMSO-d$_6$.

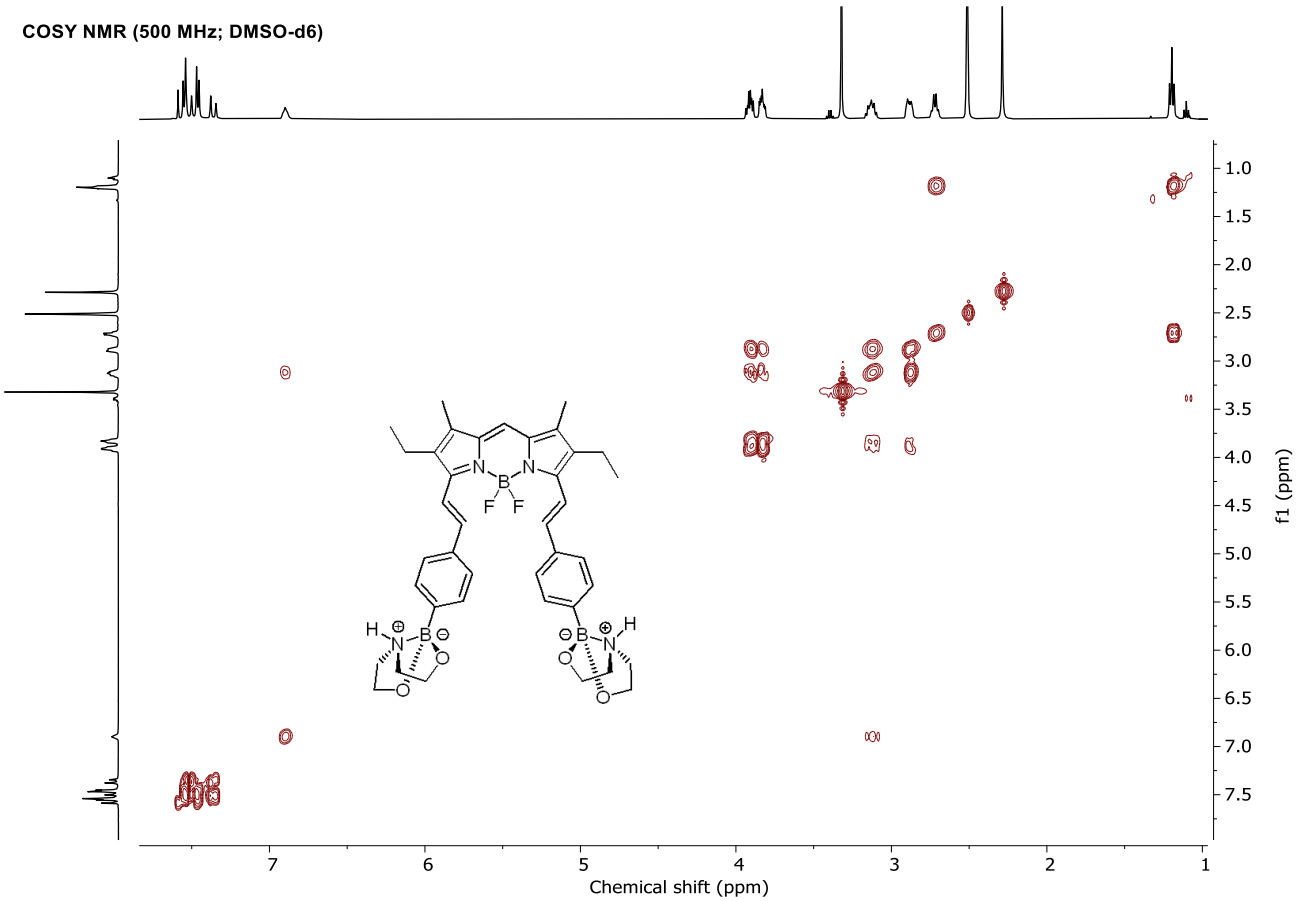

Figure S95: COSY NMR spectrum of compound **8** in DMSO-d_6.

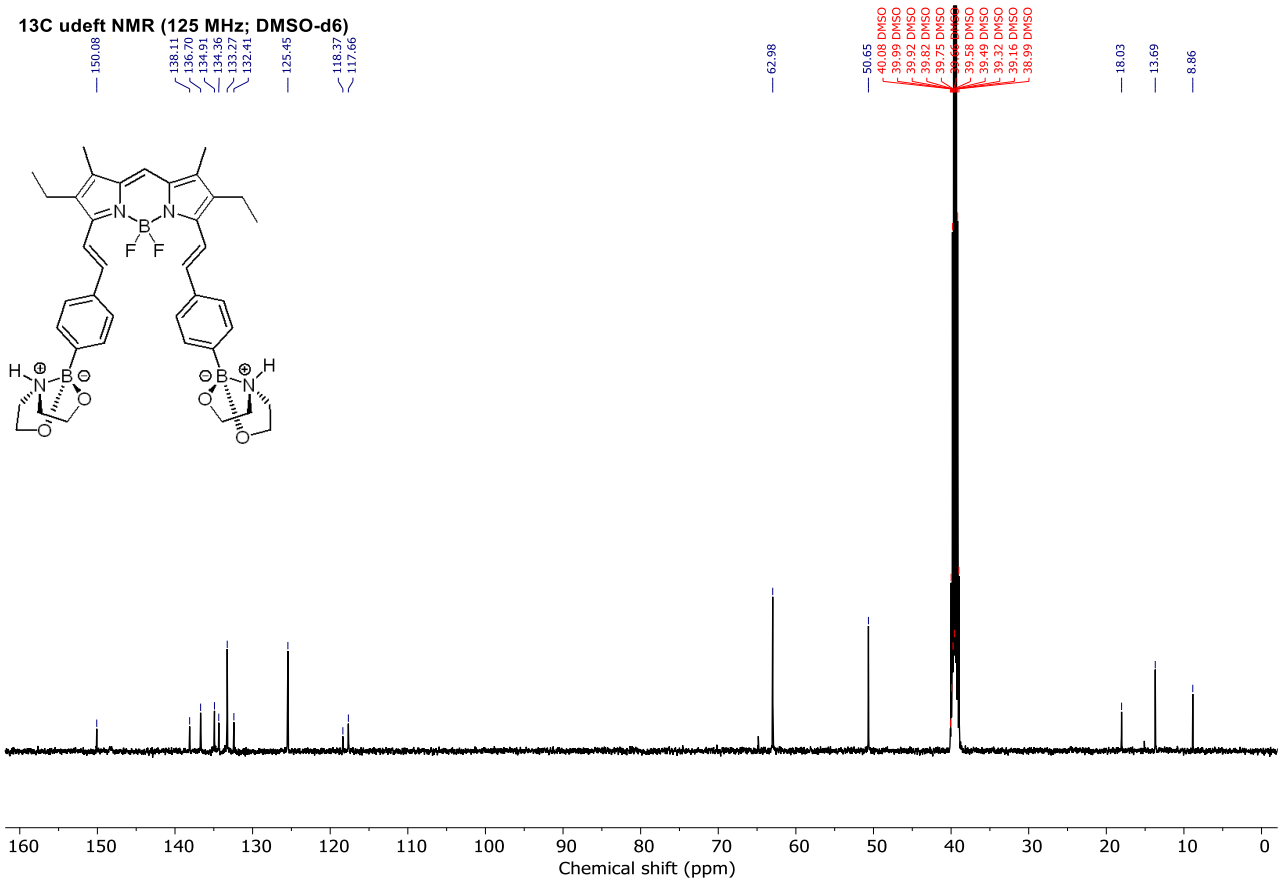

Figure S96: ^{13}C udeft NMR spectrum of compound **8** in DMSO-d_6.

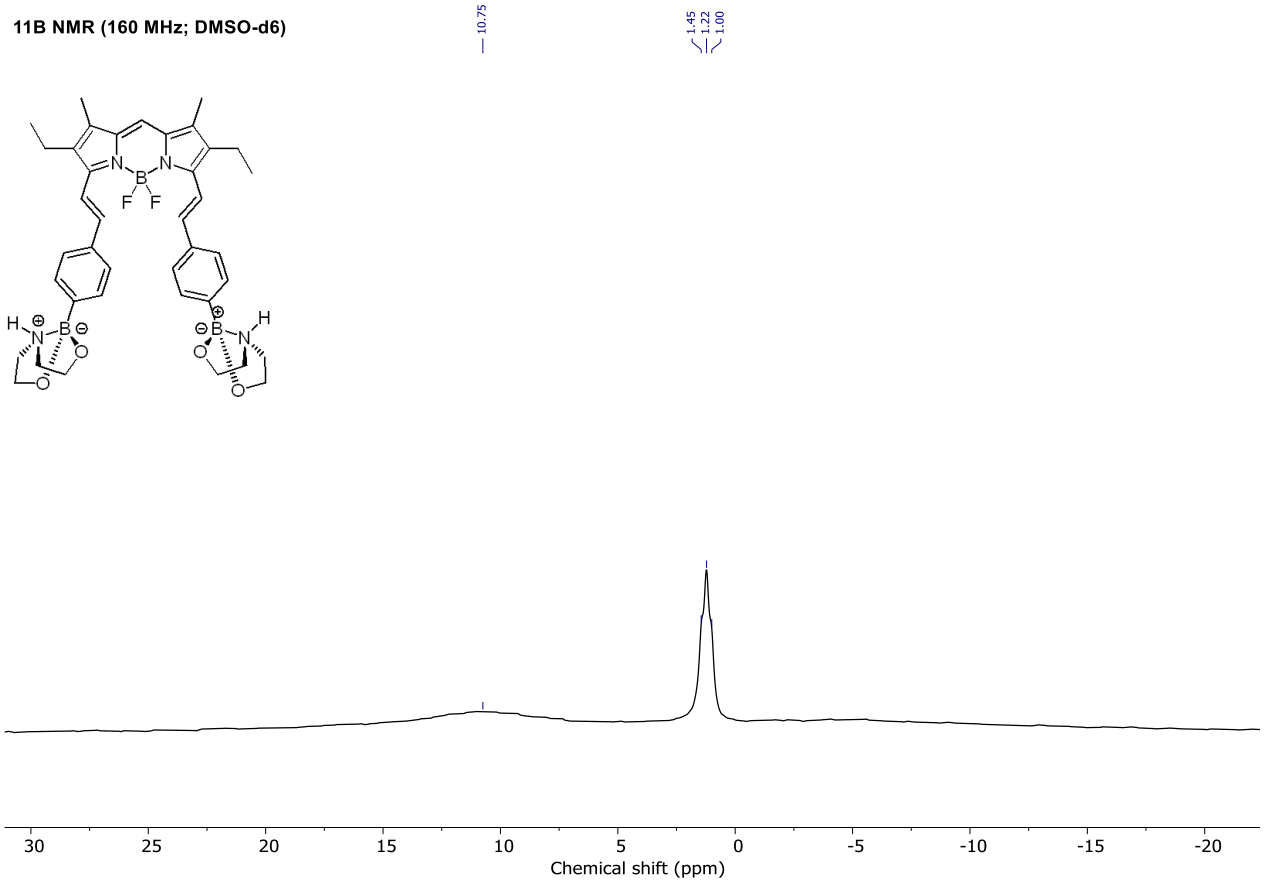

Figure S97: ^{11}B NMR spectrum of compound **8** in DMSO-d$_6$.

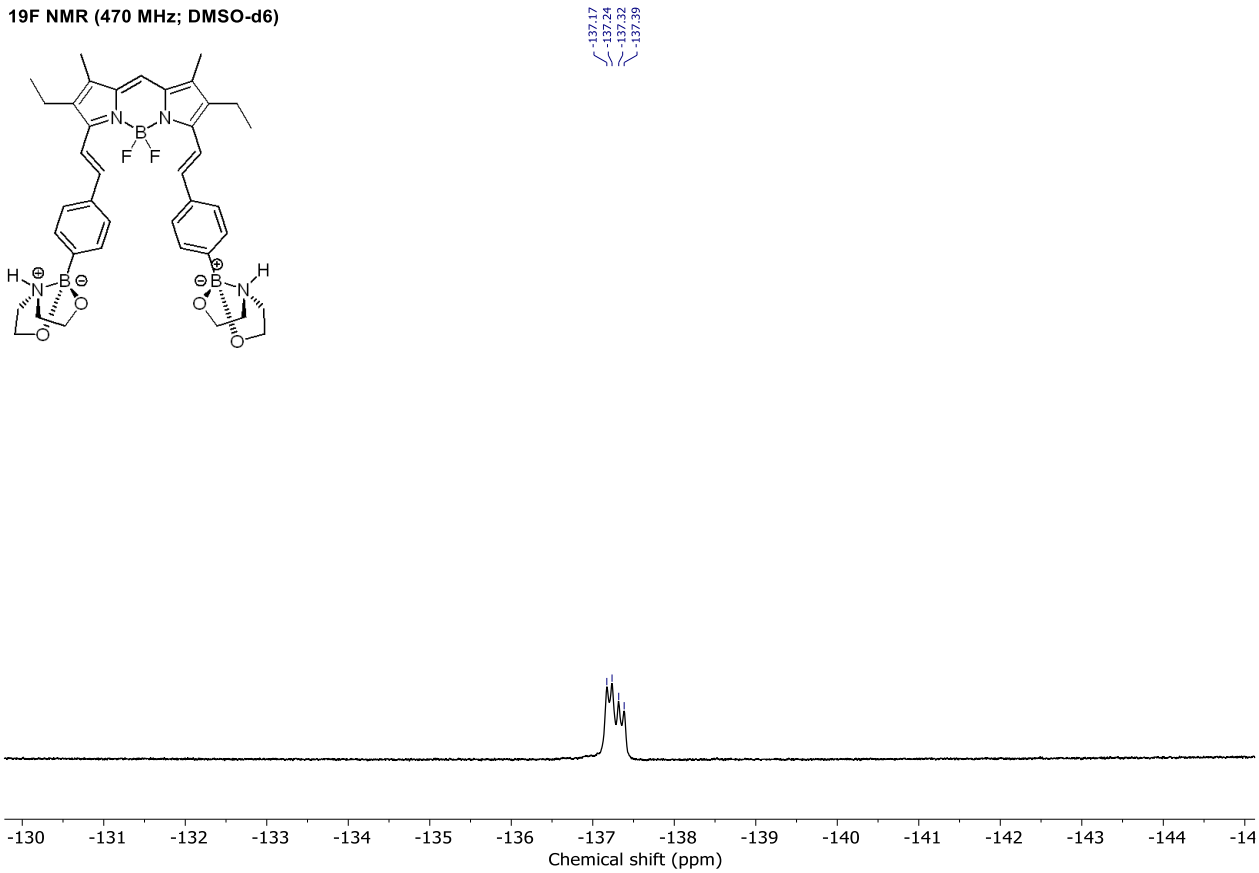

Figure S98: ^{19}F NMR spectrum of compound **8** in DMSO-d_6.

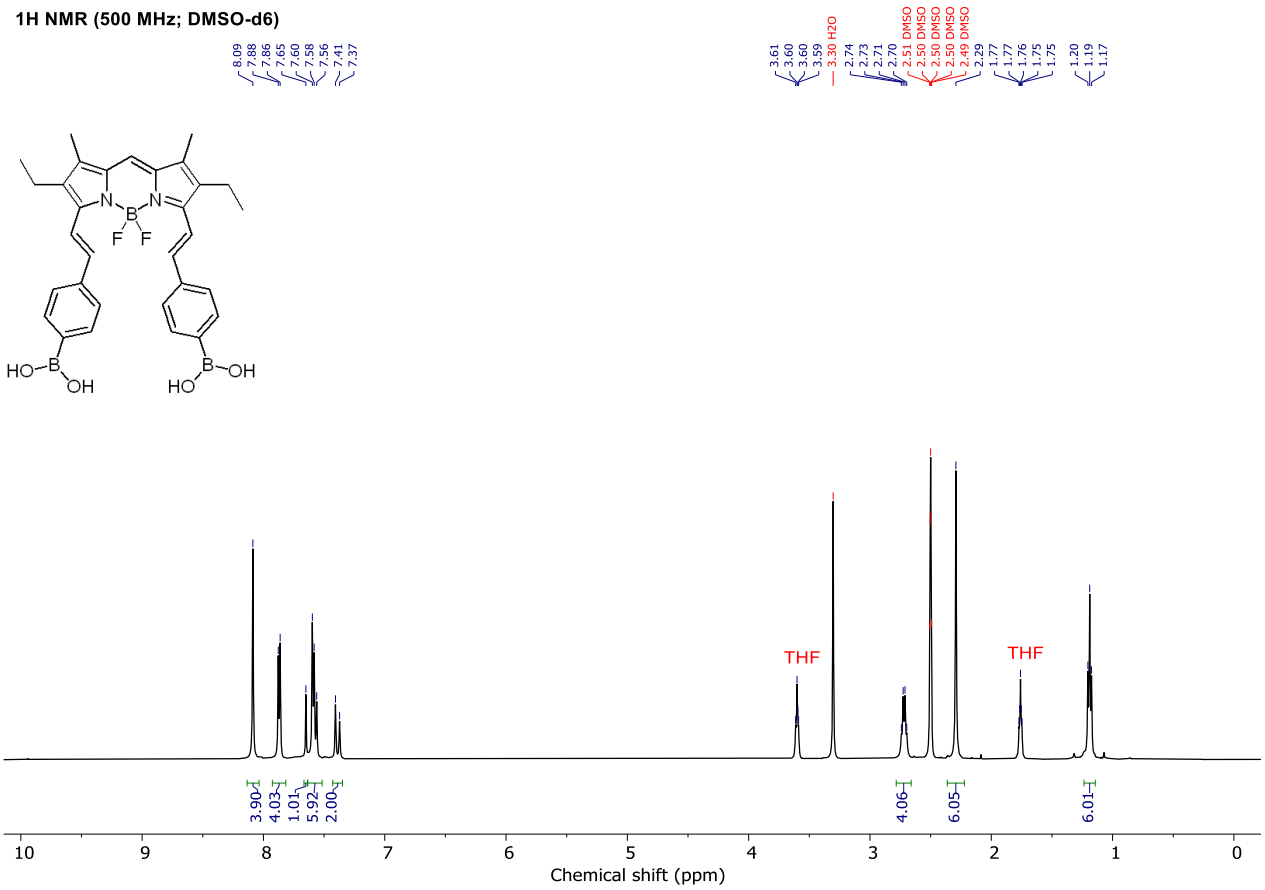

Figure S99: ^{1}H NMR spectrum of compound **2** in DMSO-d_6.

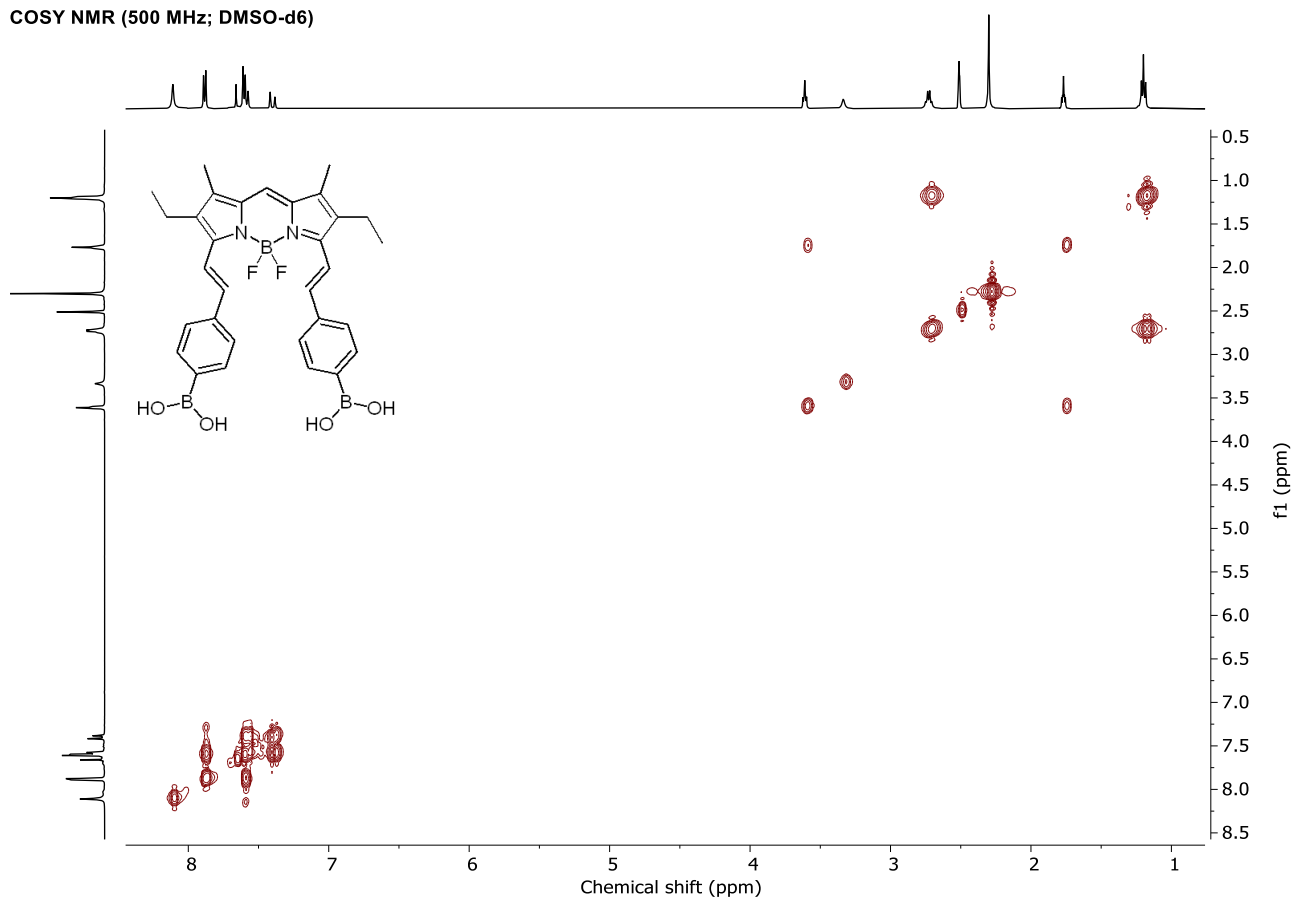

Figure S100: COSY NMR spectrum of compound **2** in DMSO-d_6.

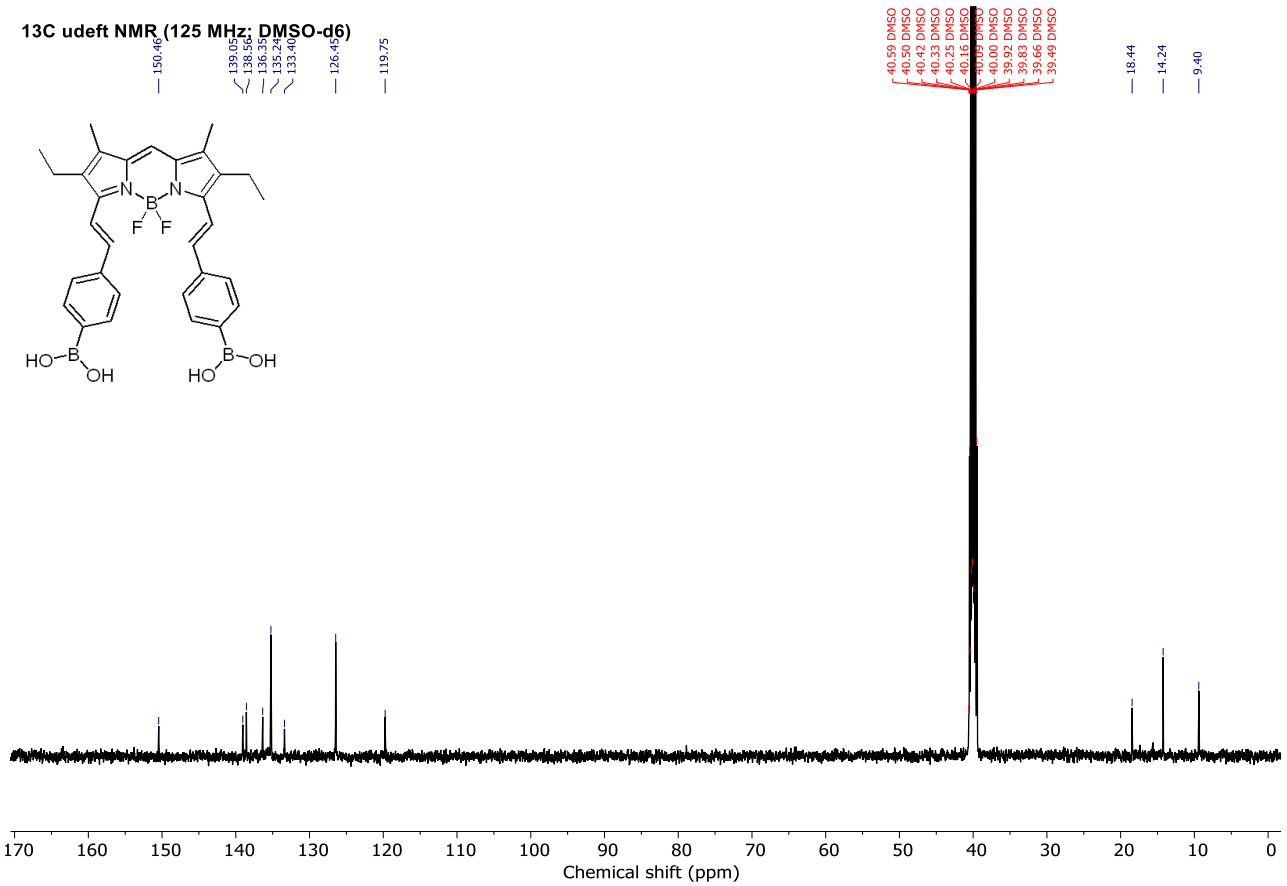

Figure S101: ^{13}C NMR spectrum of compound **2** in DMSO-d$_6$.

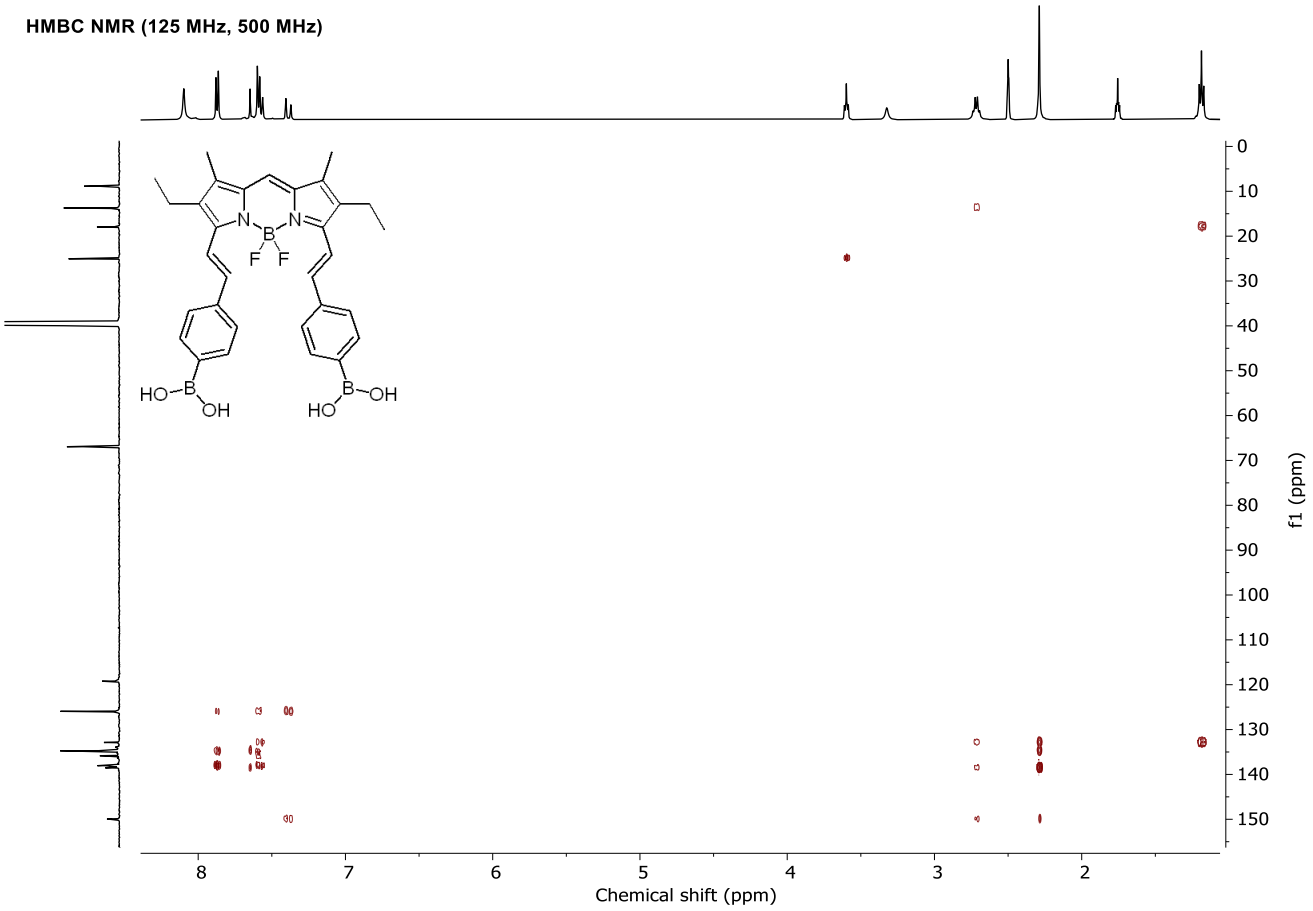

Figure S102: HMBC NMR spectrum of compound **2** in DMSO-d_6.

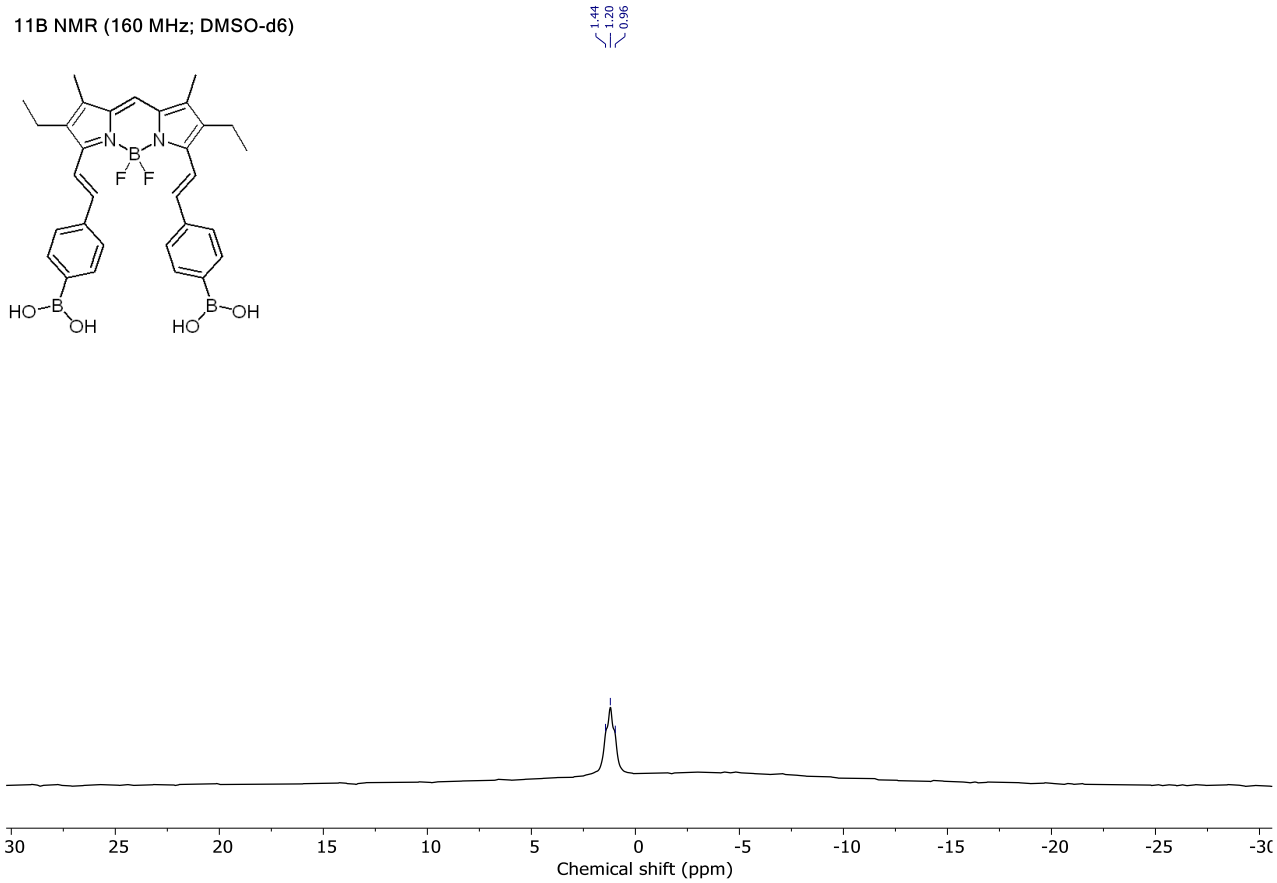

Figure S103: ^{11}B NMR spectrum of compound **2** in DMSO-d$_6$.

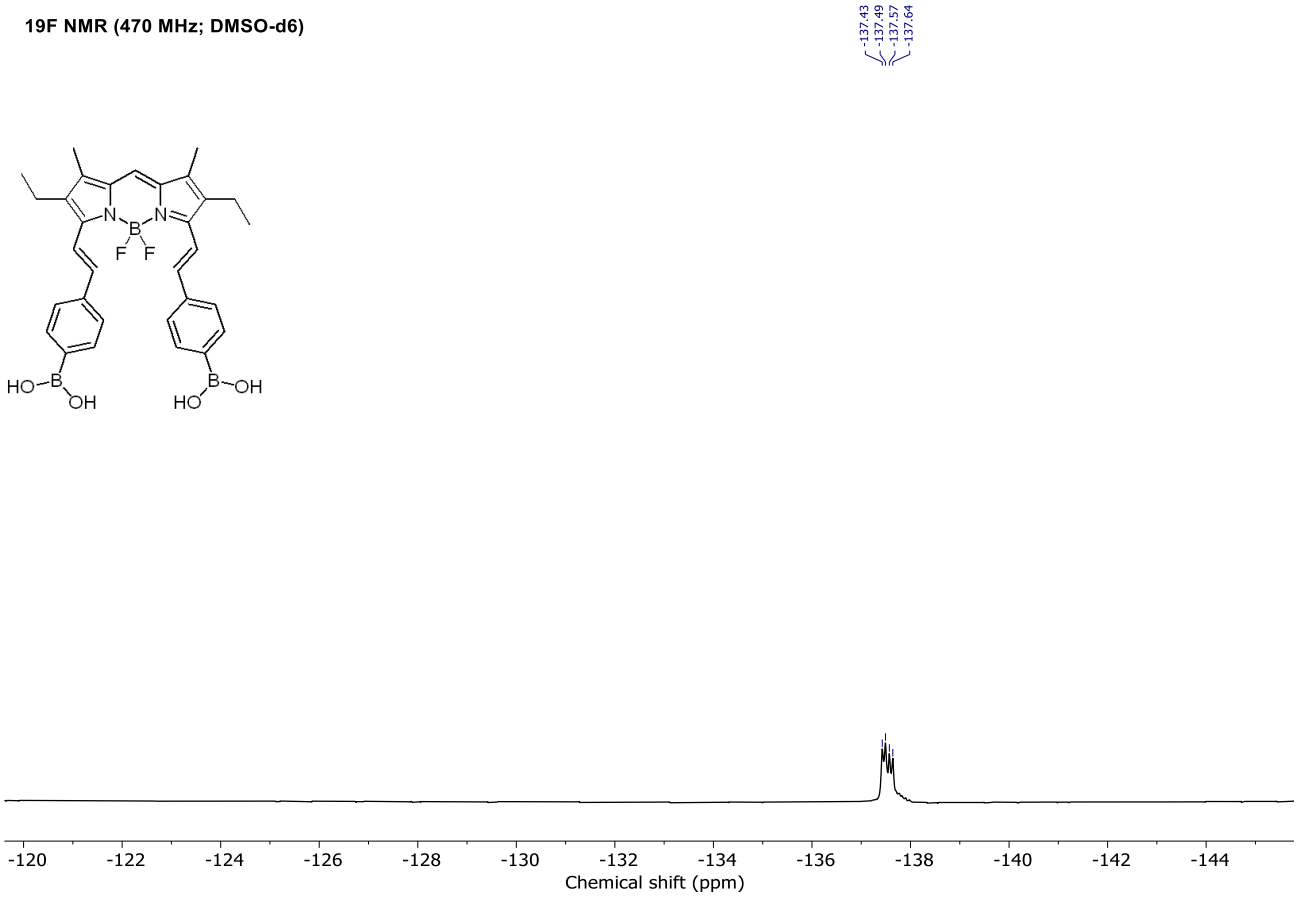

Figure S104: ^{19}F NMR spectrum of compound **2** in DMSO-d_6.

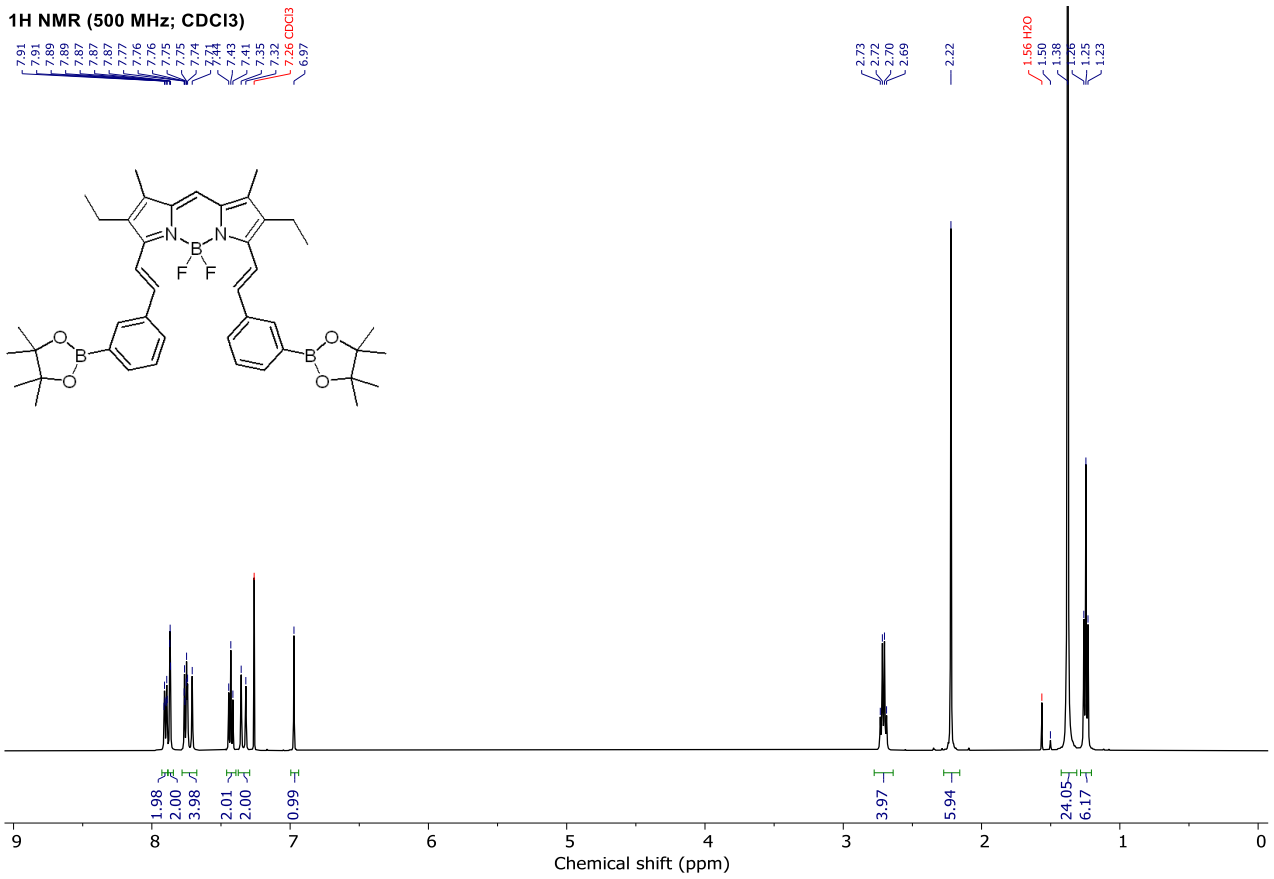

Figure S105: ^{1}H NMR spectrum of compound **7** in $CDCl_3$.

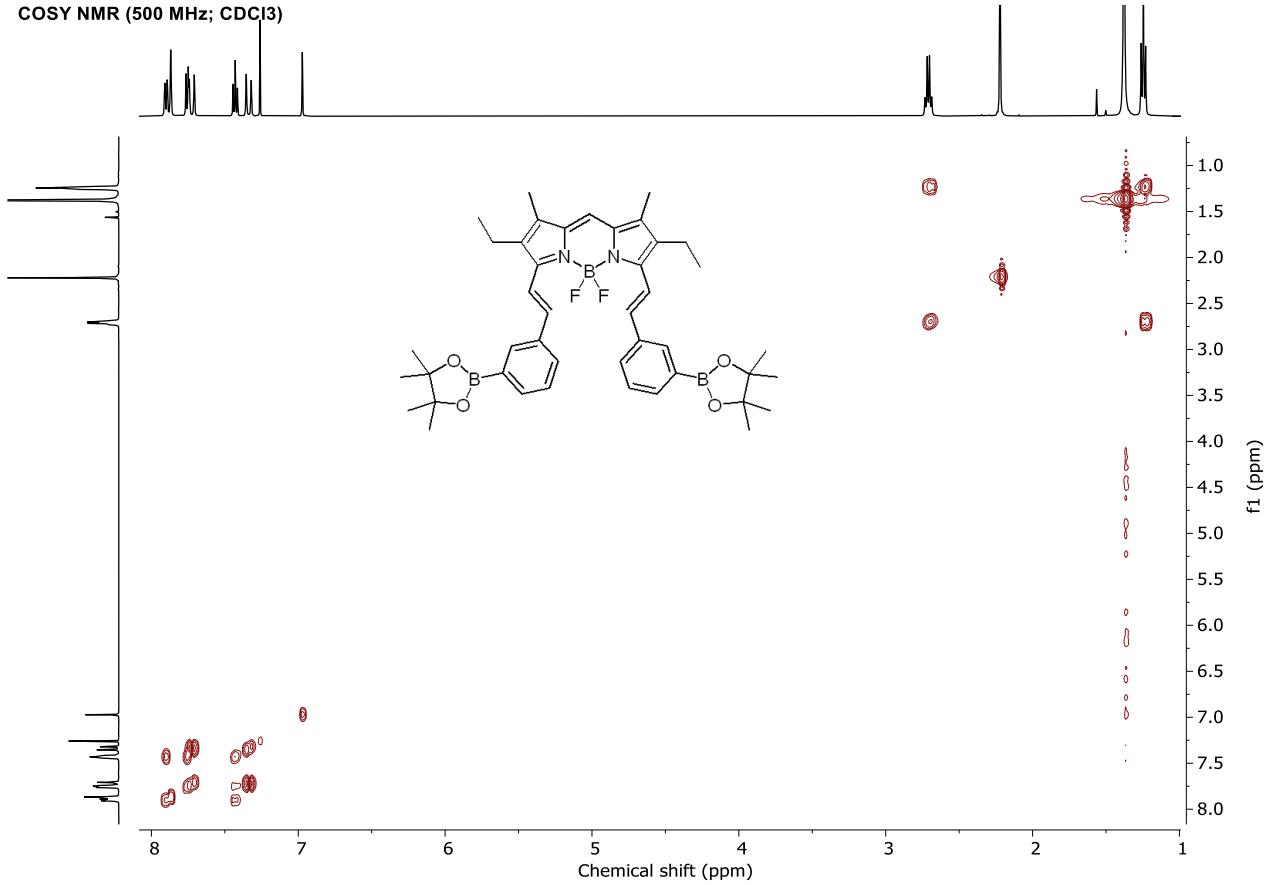

Figure S106: COSY NMR spectrum of compound **7** in $CDCl_3$.

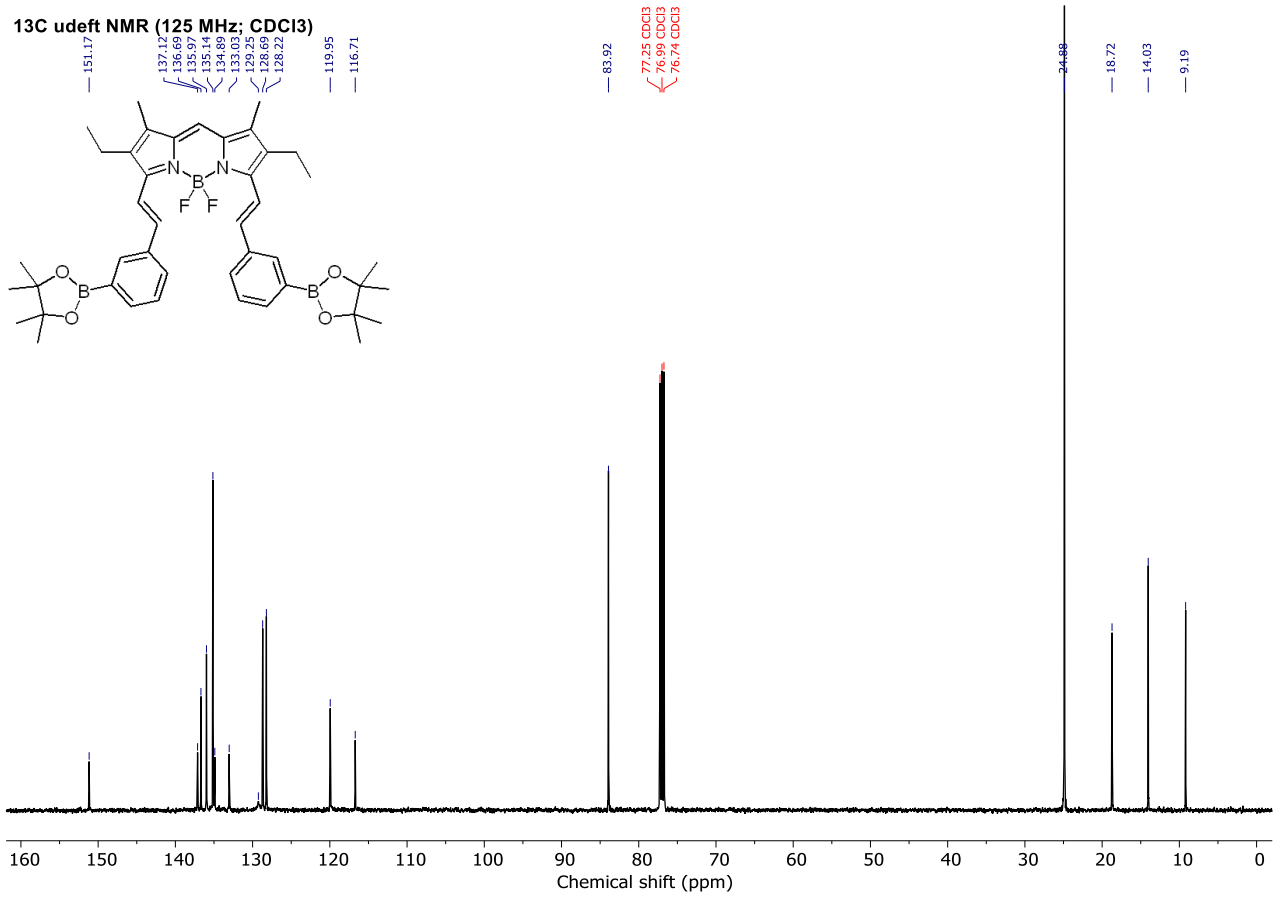

Figure S107: ^{13}C udeft NMR spectrum of compound **7** in $CDCl_3$.

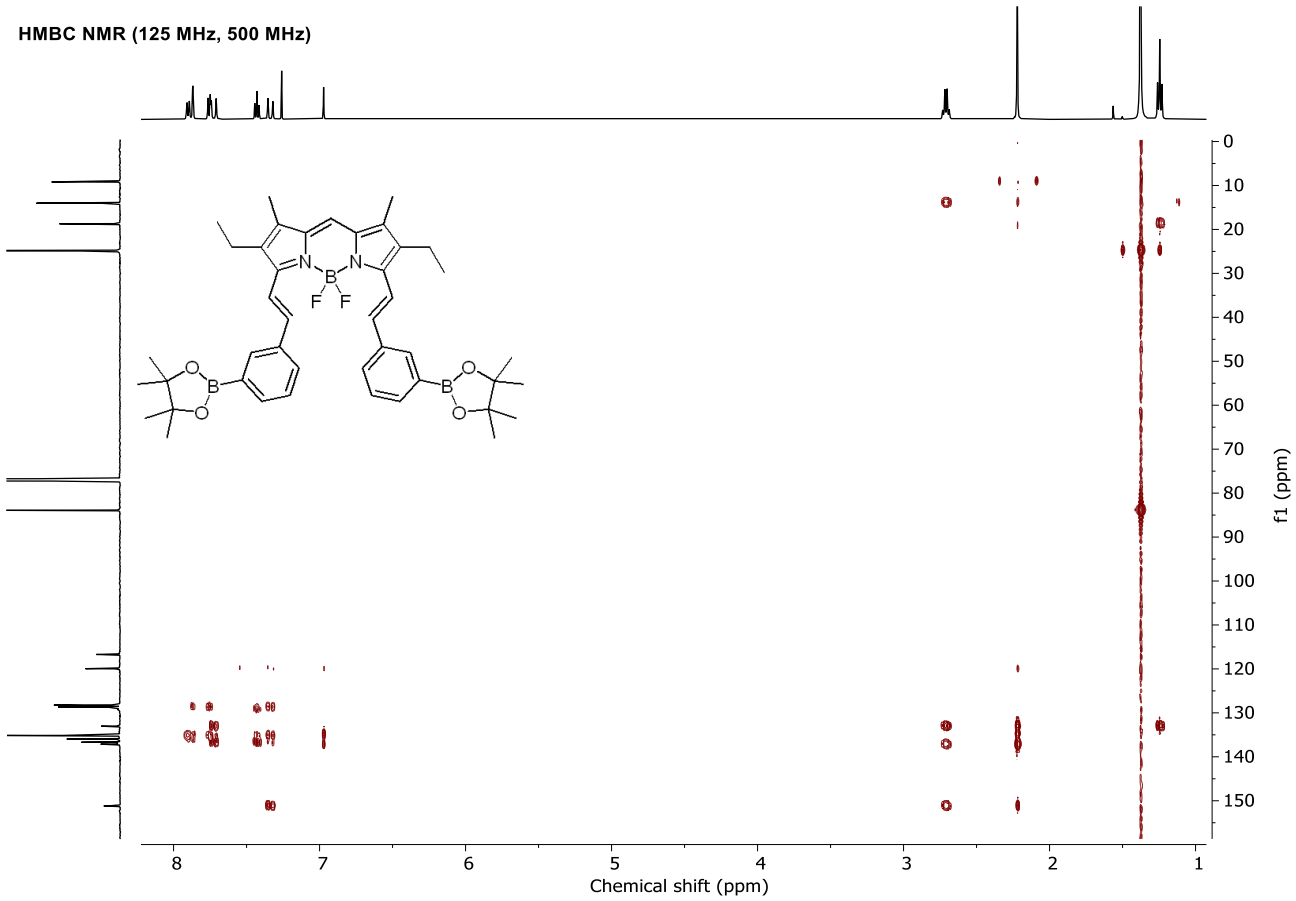

Figure S108: HMBC NMR spectrum of compound **7** in $CDCl_3$.

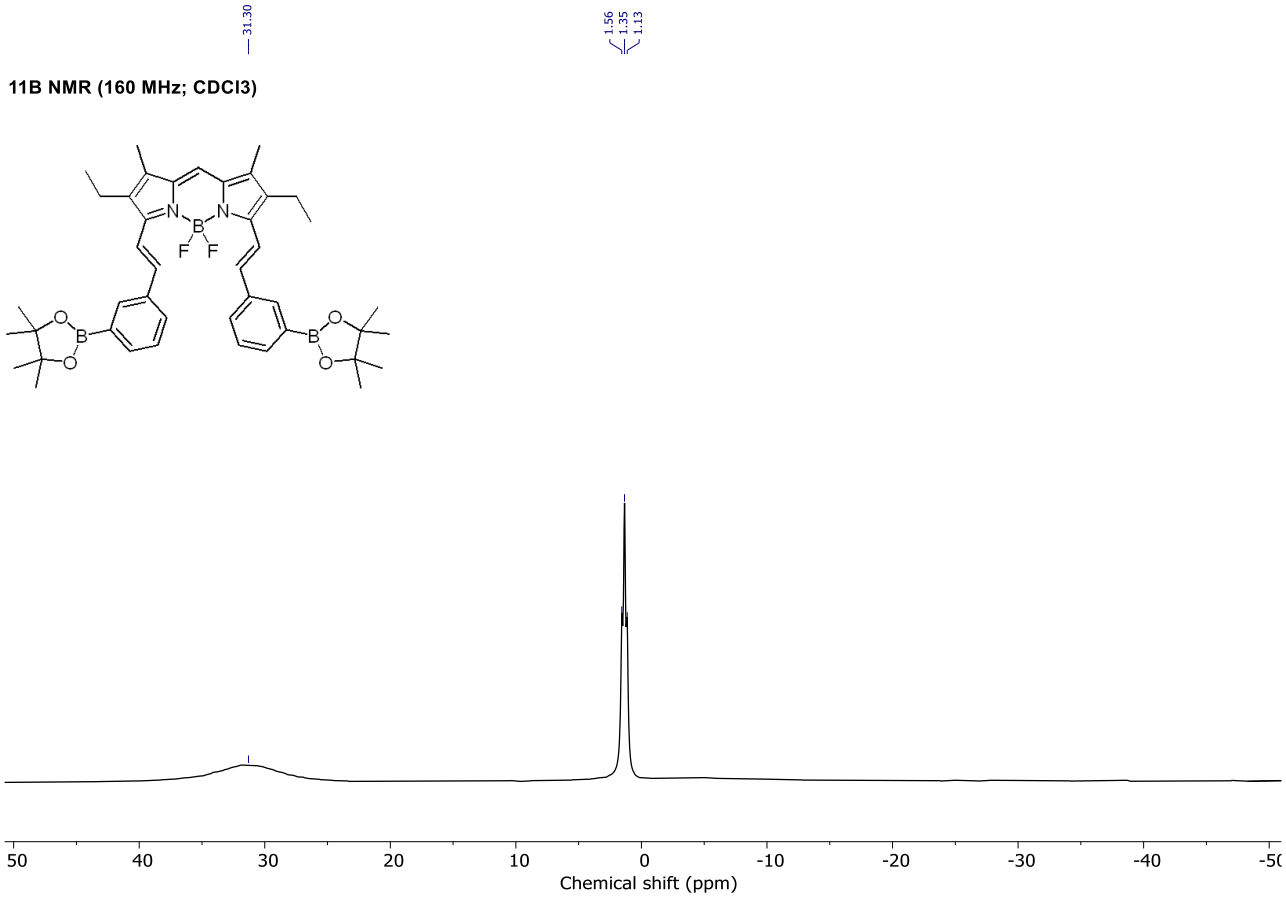

Figure S109: ^{11}B NMR spectrum of compound **7** in $CDCl_3$.

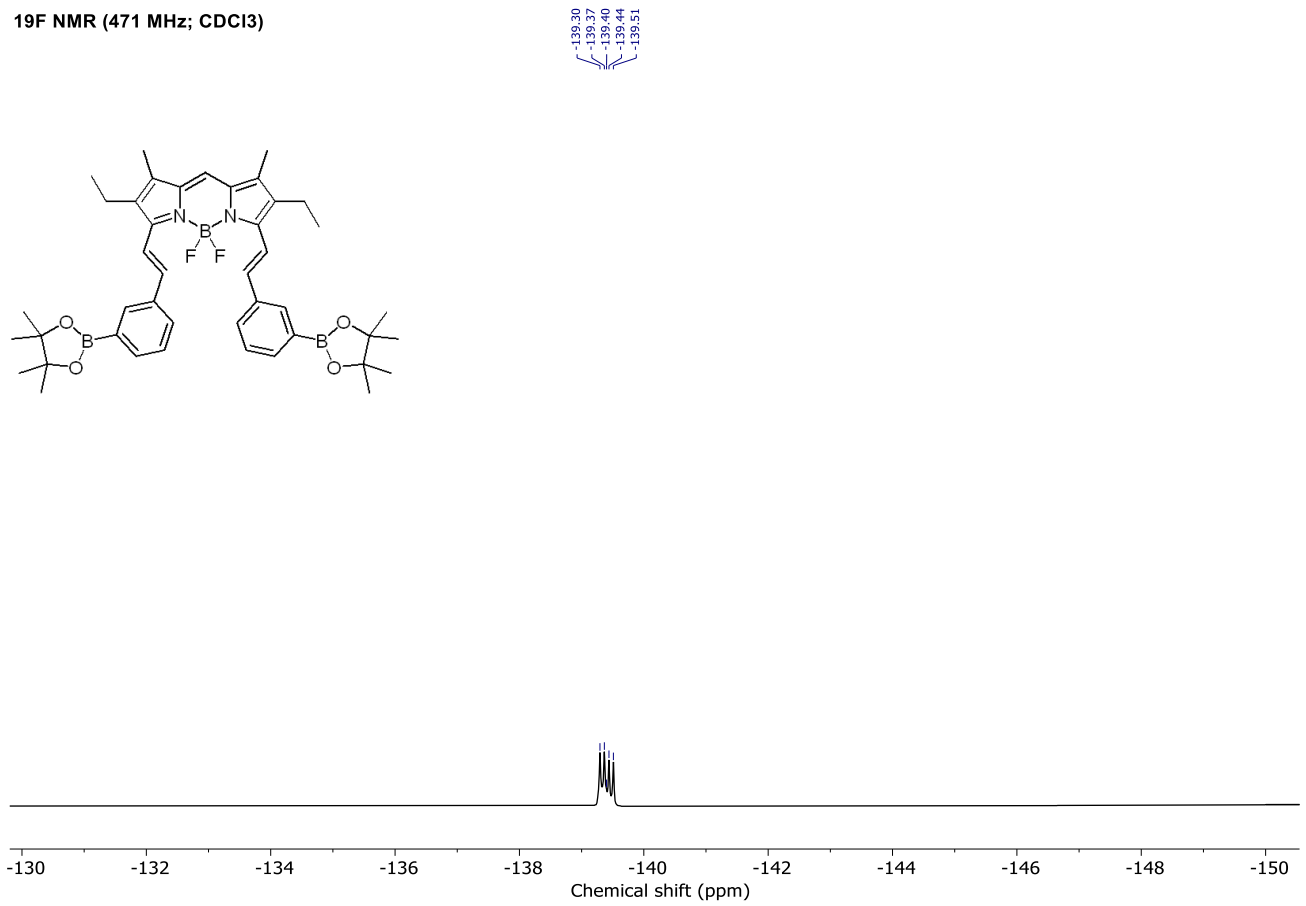

Figure S110: ^{19}F NMR spectrum of compound **7** in $CDCl_3$.

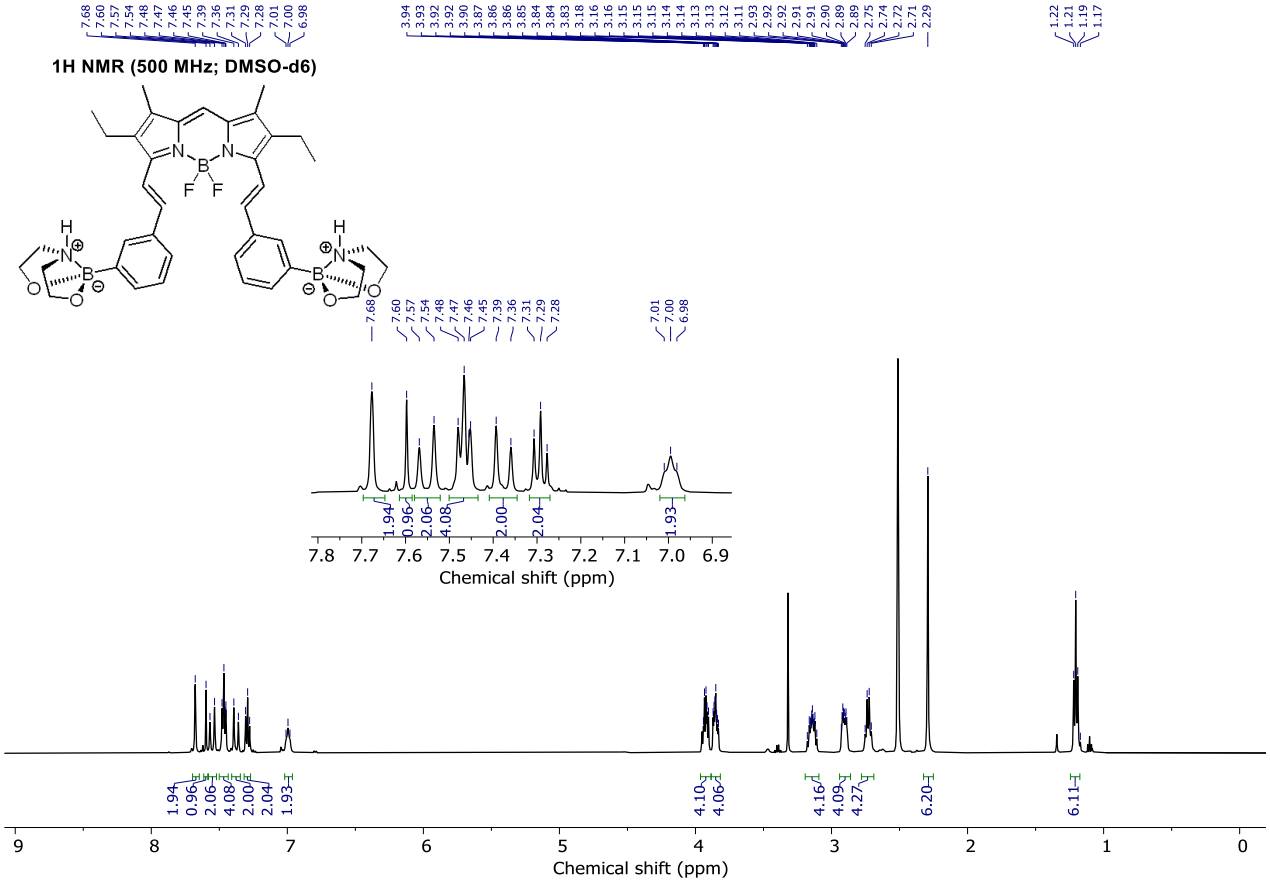

Figure S111: ^{1}H NMR spectrum of compound **9** in DMSO-d$_6$.

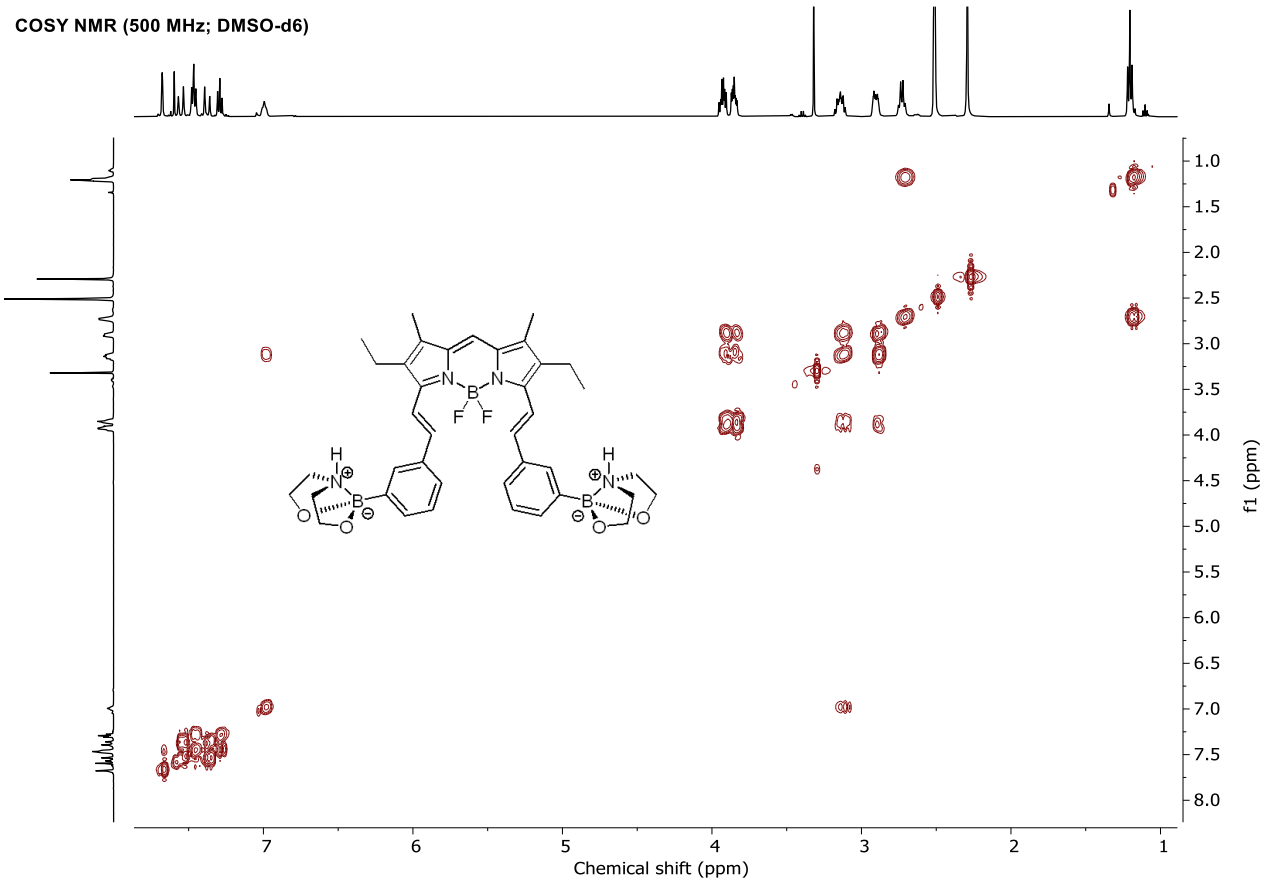

Figure S112: COSY NMR spectrum of compound **9** in DMSO-d_6.

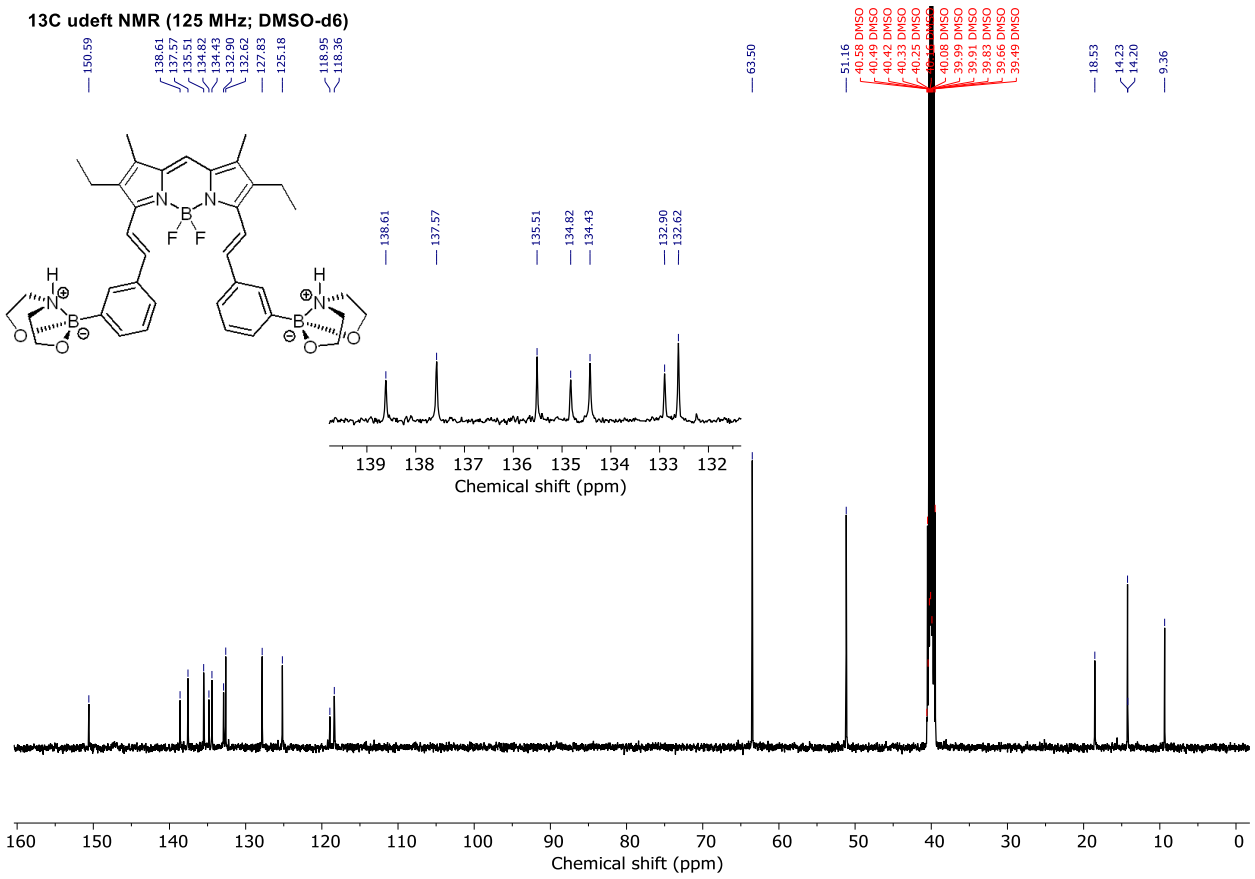

Figure S113: ^{13}C udeft NMR spectrum of compound **9** in DMSO-d$_6$.

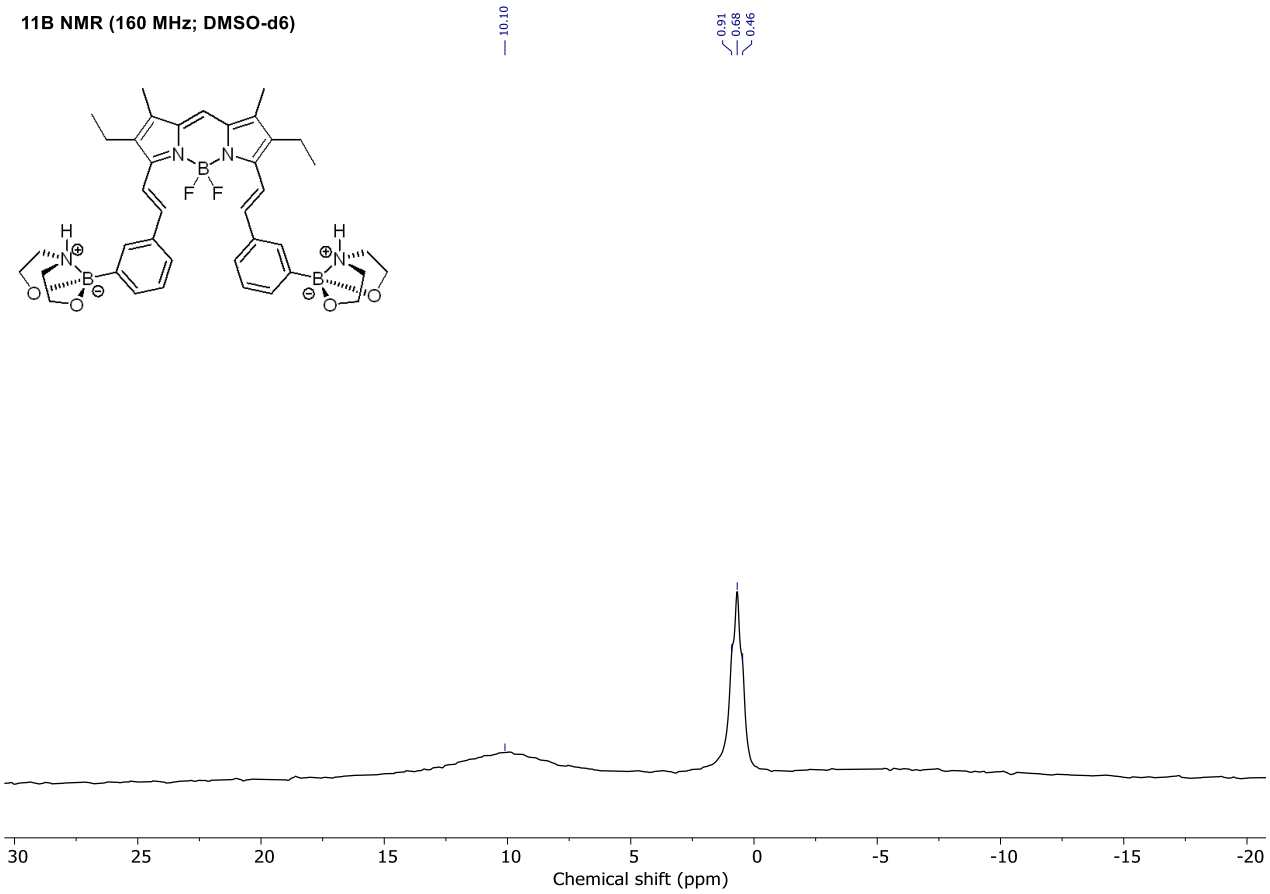

Figure S114: ^{11}B NMR spectrum of compound **9** in DMSO-d_6.

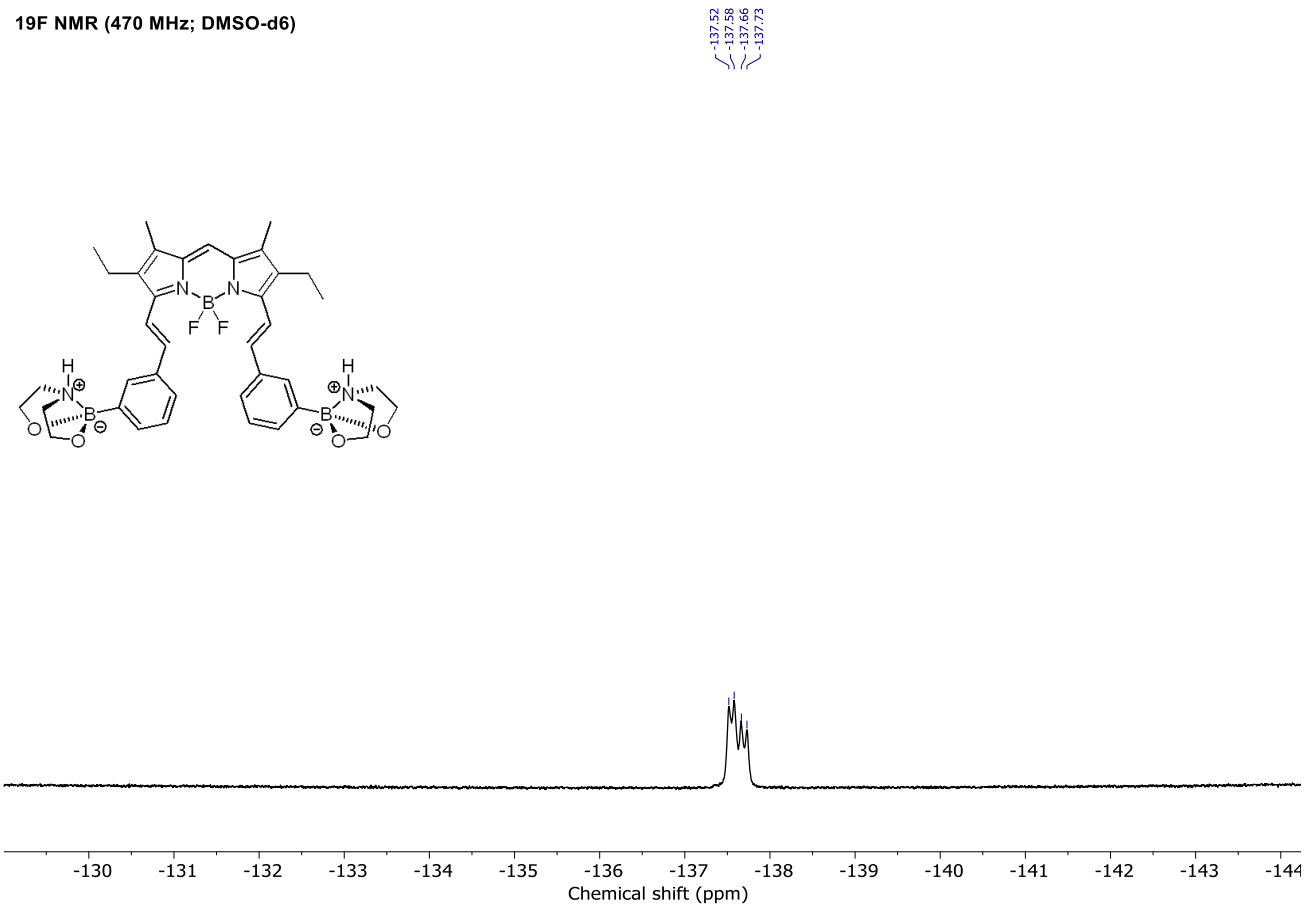

Figure S115: ^{19}F NMR spectrum of compound **9** in DMSO-d_6.

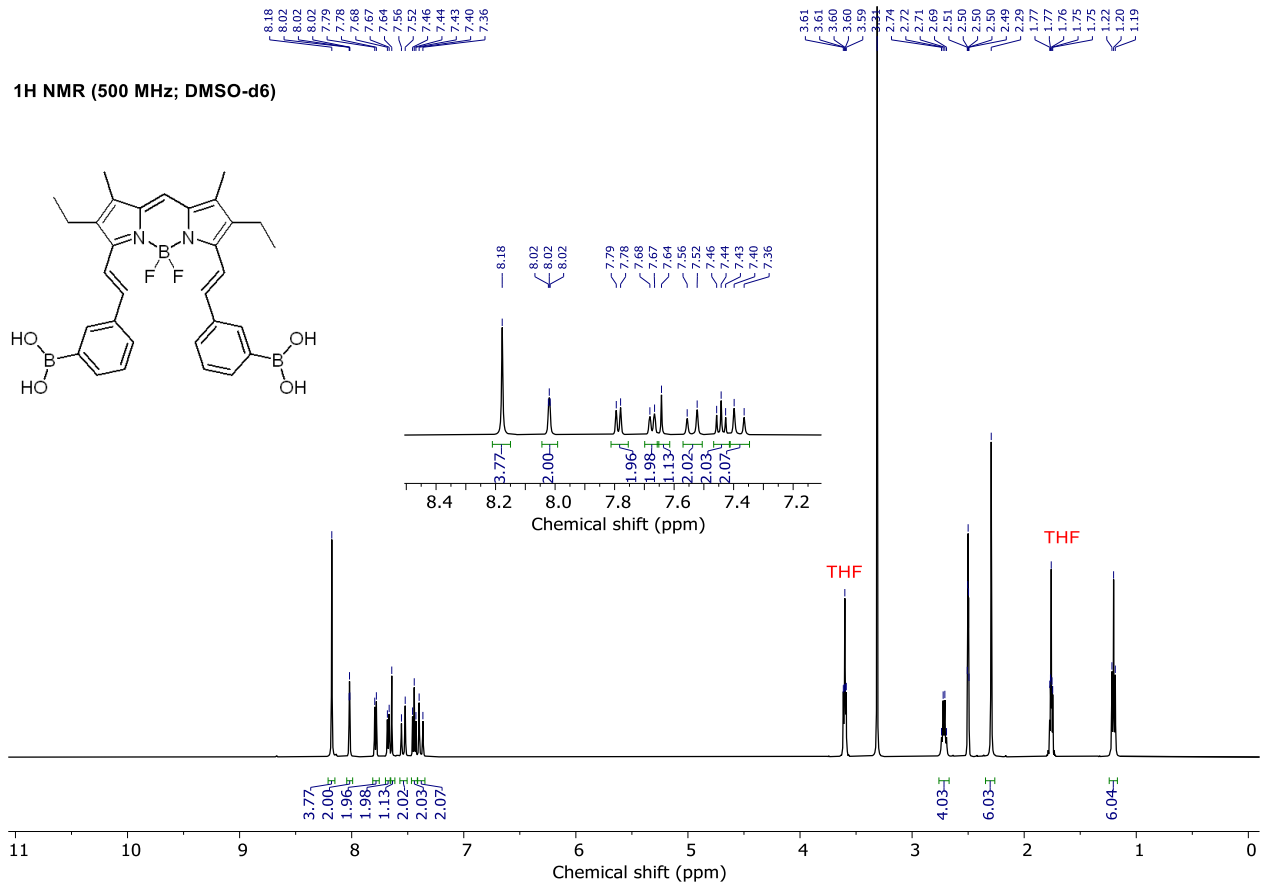

Figure S116: ^{1}H NMR spectrum of compound **3** in DMSO-d$_6$.

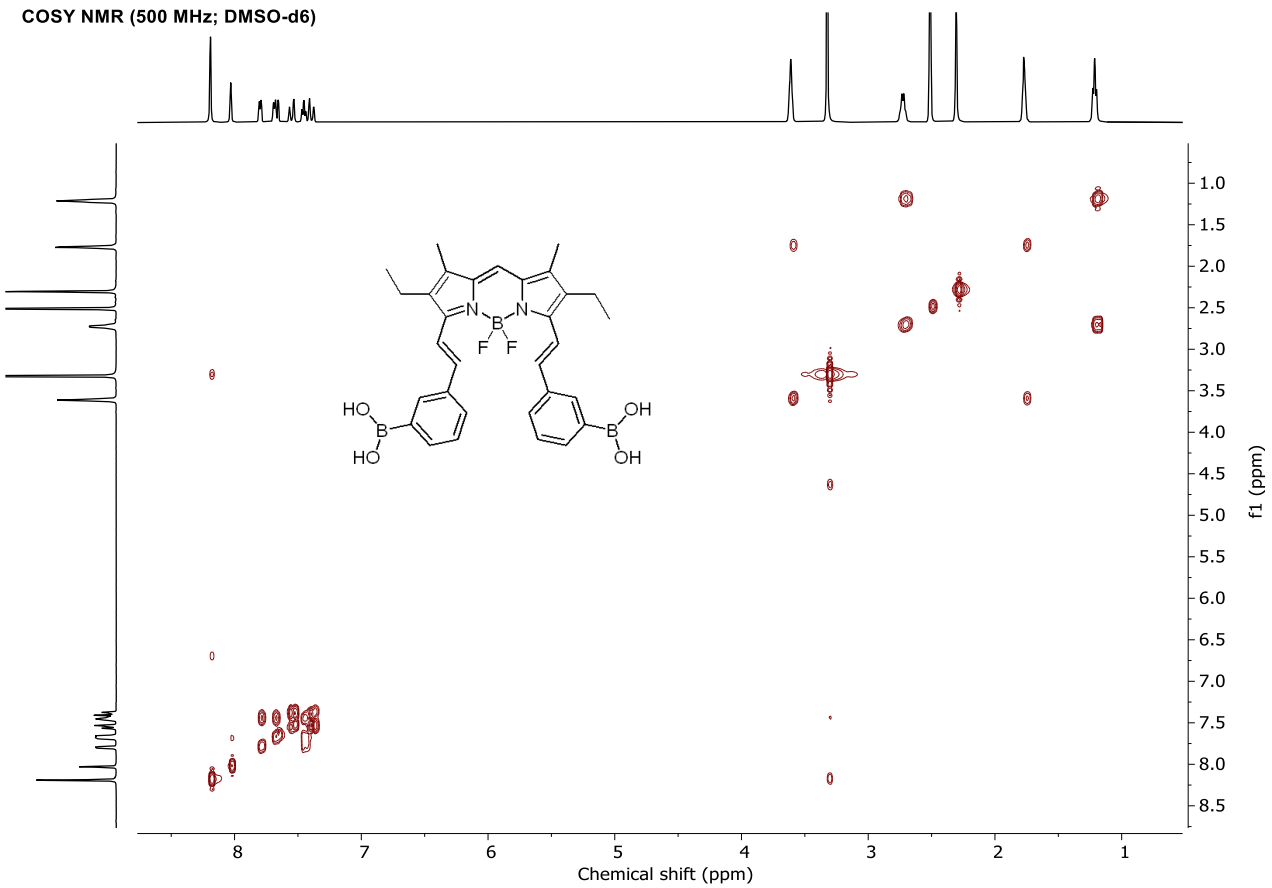

Figure S117: COSY NMR spectrum of compound **3** in DMSO-d_6.

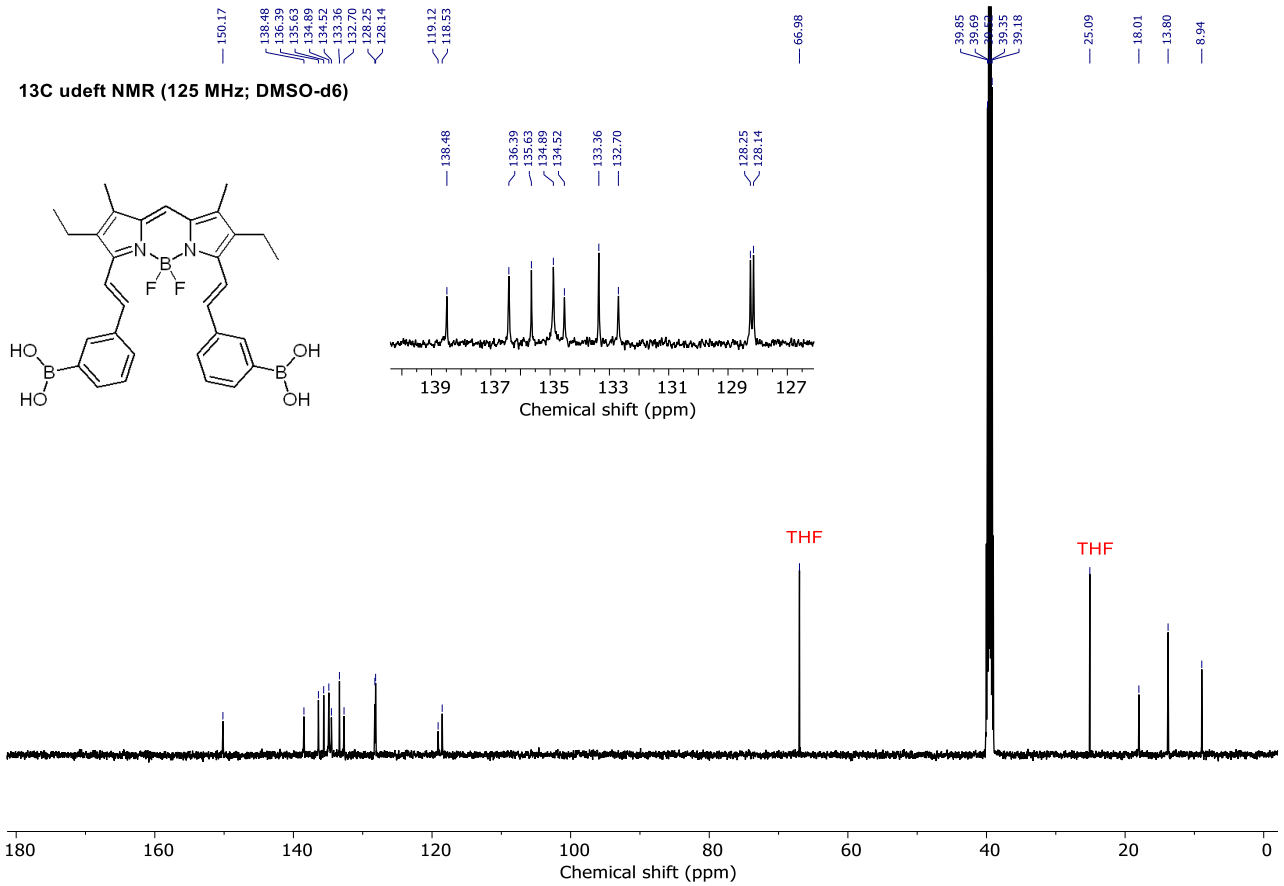

Figure S118: ^{13}C udeft NMR spectrum of compound **3** in DMSO-d$_6$.

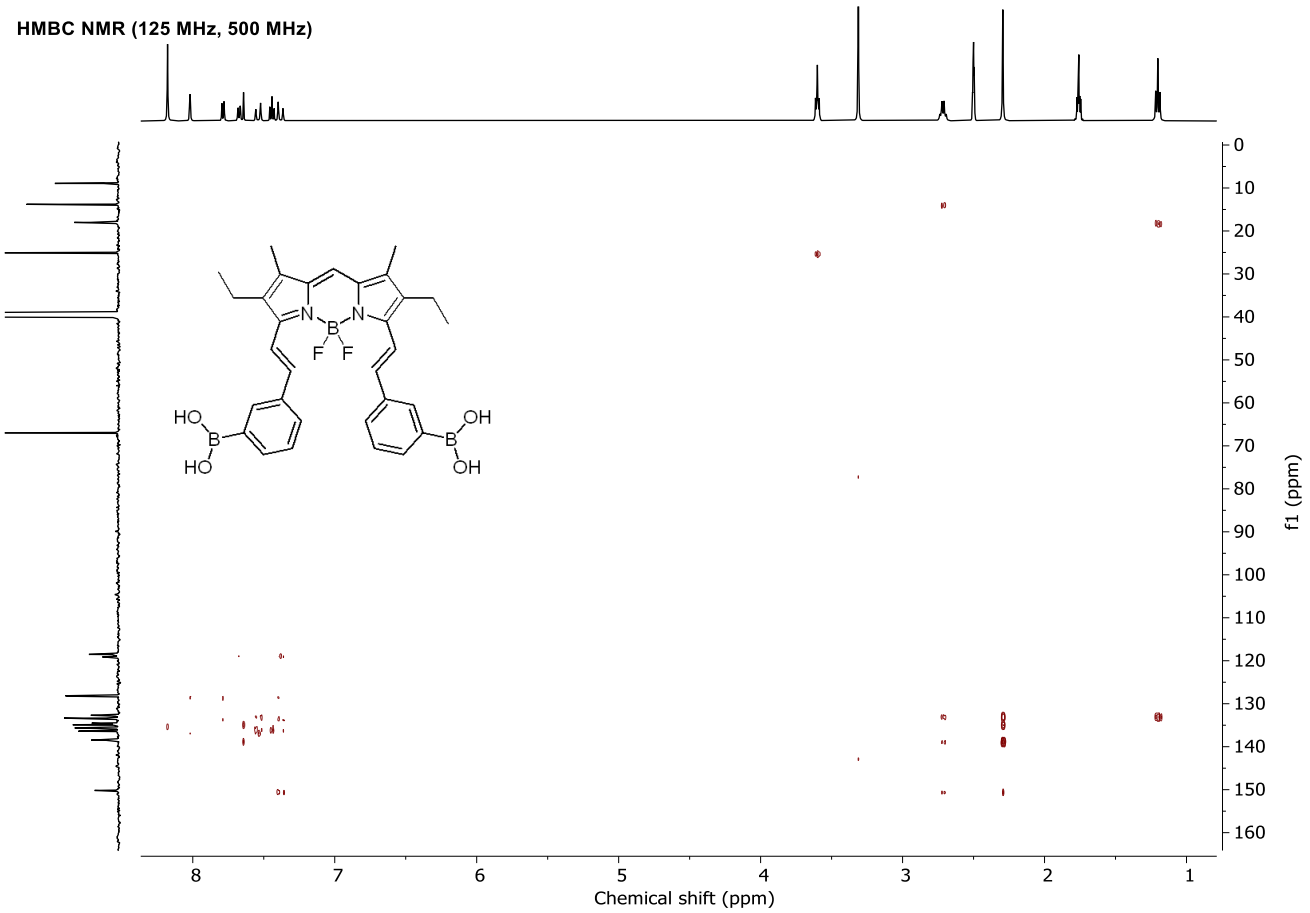

Figure S119: HMBC NMR spectrum of compound **3** in DMSO-d_6.

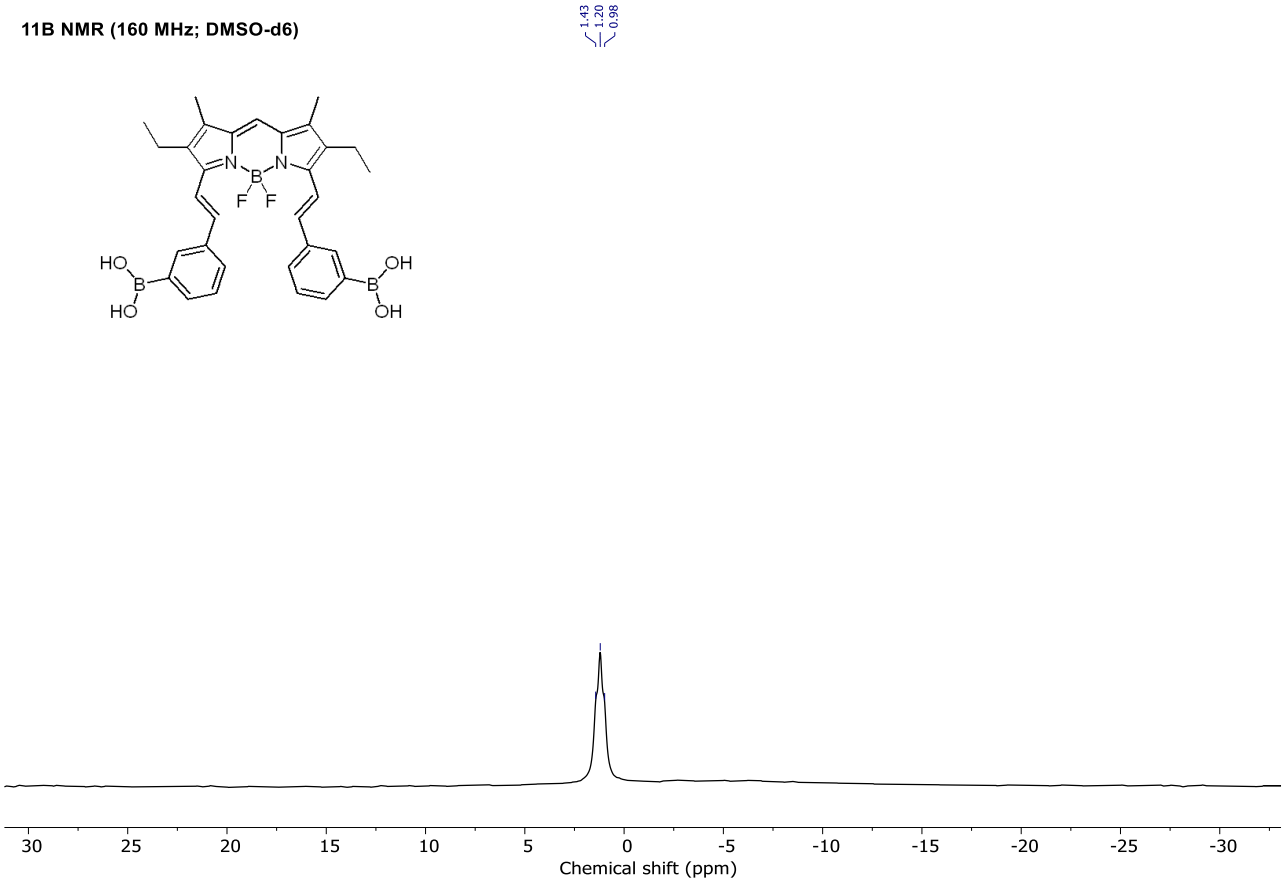

Figure S120: ^{11}B NMR spectrum of compound **3** in DMSO-d$_6$.

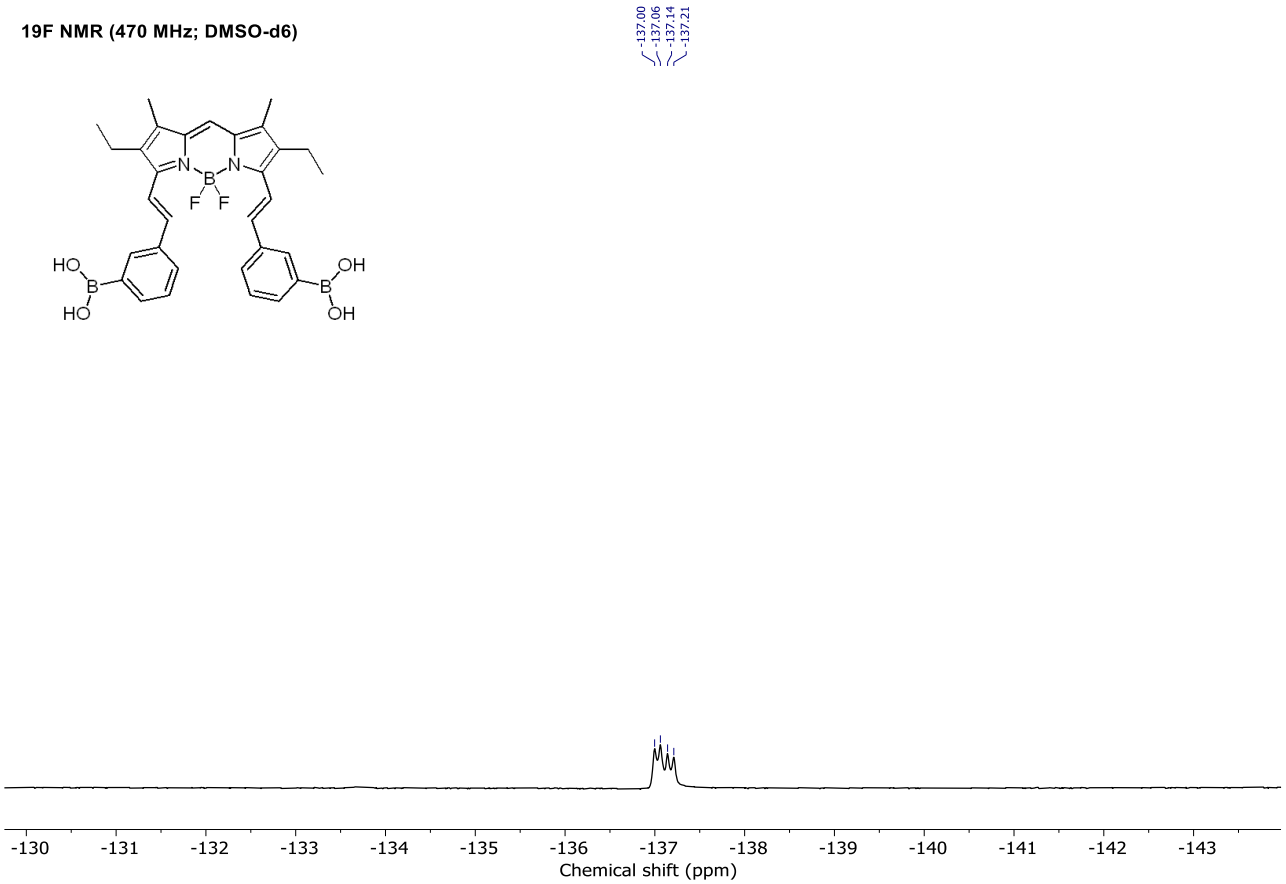

Figure S121: ^{19}F NMR spectrum of compound **3** in DMSO-d_6.

References

(1) V'yugin, A. I. Thermal Oxidative Degradation of the Functionally Substituted 2,2′-Dipyrrolylmethenes Hydrobromides and Difluoroborates. *Russ. J. Gen. Chem.* **2013**, *83* (3), 545–551.

(2) Beh, M. H. R.; Douglas, K. I. B.; House, K. T. E.; Murphy, A. C.; Sinclair, J. S. T.; Thompson, A. Robust Synthesis of F-BODIPYs. *Org. Biomol. Chem.* **2016**, *14* (48), 11473–11479.

(3) Taniguchi, M.; Lindsey, J. S. Database of Absorption and Fluorescence Spectra of >300 Common Compounds for Use in PhotochemCAD. *Photochem. Photobiol.* **2018**, *94* (2), 290–327.

(4) Brouwer, A. M. Standards for Photoluminescence Quantum Yield Measurements in Solution (IUPAC Technical Report). *Pure Appl. Chem.* **2011**, *83* (12), 2213–2228.

(5) Vydrov, O. A.; Scuseria, G. E. Assessment of a Long-Range Corrected Hybrid Functional. *J. Chem. Phys.* **2006**, *125* (23), 234109.

(6) Johnson, E. R.; Otero-de-la-Roza, A.; Dale, S. G.; DiLabio, G. A. Efficient Basis Sets for Non-Covalent Interactions in XDM-Corrected Density-Functional Theory. *J. Chem. Phys.* **2013**, *139* (21), 214109.

(7) Becke, A. D.; Johnson, E. R. Exchange-Hole Dipole Moment and the Dispersion Interaction Revisited. *J. Chem. Phys.* **2007**, *127* (15), 154108.

(8) Johnson, E. R. Chapter 5 - The Exchange-Hole Dipole Moment Dispersion Model. In *Non-Covalent Interactions in Quantum Chemistry and Physics*; Otero de la Roza, A., DiLabio, G. A., Eds.; Elsevier, 2017; pp 169–194.

(9) Scalmani, G.; Frisch, M. J. Continuous Surface Charge Polarizable Continuum Models of Solvation. I. General Formalism. *J. Chem. Phys.* **2010**, *132* (11), 114110.

(10) Brooks, W. L. A.; Deng, C. C.; Sumerlin, B. S. Structure–Reactivity Relationships in Boronic Acid–Diol Complexation. *ACS Omega* **2018**, *3* (12), 17863–17870.

(11) Thordarson, P. Binding Constants and Their Measurement. In *Supramolecular Chemistry*; 2012.

(12) Thordarson, P. Determining Association Constants from Titration Experiments in Supramolecular Chemistry. *Chem. Soc. Rev.* **2011**, *40* (3), 1305–1323.

(13) Ellis, G. A.; Palte, M. J.; Raines, R. T. Boronate-Mediated Biologic Delivery. *J. Am. Chem. Soc.* **2012**, *134* (8), 3631–3634. https://doi.org/10.1021/ja210719s.

(14) Dowlut, M.; Hall, D. G. An Improved Class of Sugar-Binding Boronic Acids, Soluble and Capable of Complexing Glycosides in Neutral Water. *J. Am. Chem. Soc.* **2006**, *128* (13), 4226–4227.

(15) APEX 4 (Bruker, 2018) Bruker AXS Inc., Madison, Wisconsin, USA.

(16) SAINT (Bruker, 2019) Bruker AXS Inc., Madison, Wisconsin, USA.

(17) SADABS (Bruker, 2016) Bruker AXS Inc., Madison, Wisconsin, USA.

(18) Sheldrick, G. M. SHELXT – Integrated Space-Group and Crystal-Structure Determination. *Acta Cryst. A* **2015**, *71* (1), 3–8.

(19) Sheldrick, G. M. Crystal Structure Refinement with SHELXL. *Acta Cryst. C* **2015**, *71* (1), 3–8.

(20) Mercury CSD 4.3 (2008).

(21) Macrae, C. F.; Bruno, I. J.; Chisholm, J. A.; Edgington, P. R.; McCabe, P.; Pidcock, E.; Rodriguez-Monge, L.; Taylor, R.; van de Streek, J.; Wood, P. A. Mercury CSD 2.0 – New Features for the Visualization and Investigation of Crystal Structures. *J. Appl. Cryst.* **2008**, *41* (2), 466–470.

(22) Sheldrick, G. M. (2008) CELL_NOW, University of Göttingen, Germany.

(23) Spek, A. L. Structure Validation in Chemical Crystallography. *Acta Cryst.* **2009**, *65* (2), 148–155.